The protective role of transcription factor NRF2 against liver injury in human and mouse models of Hereditary Hemochromatosis

Andreia dos Santos Gonçalves
Mestrado em Biologia Celular e Molecular
Departamento de Biologia
2015

Orientador
Doutor Tiago Duarte, Investigador no Grupo Basic and Clinical Research on Iron Biology, Instituto de Biologia Molecular e Celular, Universidade do Porto

Co-orientadora
Doutora Maria da Graça Beça Gonçalves Porto, Professora Catedrática no Instituto de Ciências Biomédicas Abel Salazar, Universidade do Porto

Todas as correções determinadas pelo júri, e só essas, foram efetuadas.

O Presidente do Júri,

Porto, _____/_____/_____

Agradecimentos

Antes de mais gostaria de agradecer ao Doutor Tiago Duarte e à Doutora Graça Porto a oportunidade que me proporcionaram em trabalhar no grupo *Basic and Clinical Research on Iron Biology*. Ao Doutor Tiago Duarte agradeço ainda a orientação prestada ao longo de todo o trabalho, principalmente na parte animal, e toda a paciência e apoio que foram essenciais para a realização desta tese. À Doutora Graça Porto agradeço toda a ajuda prestada na parte humana, uma vez que seria impossível realizar esta componente sem a sua orientação.

Agradeço ao staff do Corelab do Centro Hospitalar do Porto - Hospital Geral de Santo António, pela análise de soro e sangue de ratinhos, à Professora Maria João Martins a ajuda indispensável na realização do ensaio de TBARS e quantificação da glutationa e ao Engenheiro Paulo Limão a assistência prestada na quantificação dos níveis de "cytokines/chemokines" no soro de ratinho.

Gostaria ainda de agradecer à Ana Santos, Mónica Costa e Sílvia Chambel, que mais do que colegas de grupo, foram verdadeiras amigas que me proporcionaram momentos muito felizes no laboratório. À Ana agradeço a dissecção dos ratinhos, a ajuda indispensável que me prestou em todas as técnicas laboratoriais e o apoio que sempre me deu. À Mónica agradeço a ajuda que me deu na análise das sequenciações e as respostas a todas as dúvidas que lhe coloquei. À Sílvia gostaria de agradecer também toda a ajuda que nunca hesitou prestar, mesmo tendo uma tese para escrever, e toda a amizade que já vem desde o 1º ano de licenciatura. Sem elas e sem a Gina não haveria tanta boa disposição e tantas gargalhadas no laboratório. Agradeço também aos restantes membros do BCRIB, III e MP, que permitiram que este ano fosse tão agradável.

Agradeço ainda a todos os meus coleguinhas de Mestrado, que fizeram com que estes dois anos passassem a voar. Um agradecimento especial ao Steeve, ao Rui, à Ana e à Patrícia, que entre momentos de brincadeira e amizade, sempre me apoiaram. Obrigada ainda aos meus “amigos da Maia”, por toda a amizade e carinho.

Finalmente, gostaria de fazer um agradecimento muito especial aos meus pais, avós e padrinhos, à Raquel e ao Francisco, por todo o apoio que me deram e pela paciência que tiveram comigo. Sem vocês nada disto teria sido possível.

This work was funded by FEDER funds through the Operational Competitiveness Programme – COMPETE and by National Funds through FCT – Fundação para a Ciência e a Tecnologia under the project FCOMP-01-0124-FEDER-028447 (PTDC/BIM-MET/0739/2012).

UNIÃO EUROPEIA
Fundo Social Europeu

Abstract

Hereditary hemochromatosis (HH) is a group of primary genetic disorders of iron homeostasis. *HFE*-HH, the most common form of HH in populations of northern European ancestry, is mainly caused by a C282Y mutation in the *HFE* gene. HH is characterized by hyperabsorption of dietary iron, which is delivered to plasma leading to increased transferrin saturation and tissue iron accumulation. The liver accumulates large amounts of iron and the excess free iron is capable of generating reactive oxygen species, which damage the tissue. NRF2 is the key transcription factor involved in the antioxidant response, so we hypothesized that it can act as a modifier of the clinical expression of HH. In this study, we aimed to: i) determine the effect of *Nrf2* suppression in a model of chronic iron overload that mimics HH, the *Hfe*$^{-/-}$ mouse; ii) identify polymorphisms/genotypes in the human *NRF2* gene promoter that may influence HH penetrance in HFE C282Y$^{+/+}$ patients. Female WT, *Nrf2*$^{-/-}$, *Hfe*$^{-/-}$ and *Nrf2/Hfe*$^{-/-}$ mice on a C57BL/6J background at 24 months of age were fasted overnight for blood and organ collection. Aged *Nrf2/Hfe*$^{-/-}$ mice presented lower body weight, mild anemia and hypoglycemia at starvation. Mild liver inflammation was detected in mice of the four genotypes, possibly as a consequence of aging. NRF2 proved to be essential in the antioxidant defense, as *Nrf2*$^{-/-}$ and *Nrf2/Hfe*$^{-/-}$ mice presented decreased levels of *Nqo1* transcript and the GSH/GSSG ratio was significantly decreased in *Nrf2*$^{-/-}$ livers. Despite the similar amount of non-heme iron in *Hfe*$^{-/-}$ and *Nrf2/Hfe*$^{-/-}$ livers, we observed a shift in the local deposition of iron from the liver parenchyma (in *Hfe*$^{-/-}$ mice) to sinusoidal cells (in *Nrf2/Hfe*$^{-/-}$ mice). Necrosis, fibrosis and the number of TUNEL-positive cells were augmented in *Nrf2/Hfe*$^{-/-}$ livers. Overall, we conclude that the suppression of NRF2 leads to spontaneous liver damage in *Hfe*$^{-/-}$ mice, the mouse model of HH. In the human study, DNAs of patients *HFE* C282Y$^{+/+}$ were genotyped for Rs35652124, Rs670664, Rs150648896 and Rs6721961 SNPs in the *NRF2* promoter region. Our results indicate that none of the SNPs alone prompts the patients to develop a specific clinical manifestation, but patients carrying the allele C in Rs35652124 SNP are somehow protected from clinical manifestations of HH. In conclusion, the current study shows that NRF2 has an important hepatoprotective role in the animal model of HH and suggests that gene variants may be also implicated in the clinical course of the human disease.

Keywords: Aging, Iron, Hereditary Hemochromatosis, *Hfe*, *Nrf2*.

Resumo

A hemocromatose hereditária (HH) é um grupo de doenças genéticas primárias de homeostasia do ferro. Na população originária do norte da Europa, a *HFE*-HH é a forma mais comum de HH, sendo principalmente causada pela mutação C282Y no gene *HFE*. A HH é caracterizada por hiperabsorção de ferro da dieta, que entra na corrente sanguínea e leva ao aumento da saturação da transferrina e da acumulação de ferro nos tecidos. O fígado acumula grandes quantidades de ferro, capaz de gerar espécies reactivas de oxigénio que danificam o tecido. Como o NRF2 é o fator de transcrição chave da resposta antioxidante, pensámos que este pode ser um modificador da expressão clínica da HH. Os objetivos do nosso estudo foram: i) determinar o efeito da supressão do *Nrf2* num modelo de sobrecarga de ferro crónica que imita a HH, o murganho *Hfe*$^{-/-}$; ii) identificar polimorfismos/genótipos no promotor do gene *NRF2* humano, que possam influenciar a penetrância da HH em pacientes C282Y$^{+/+}$. Foram recolhidos órgãos e sangue de murganhos fêmea WT, *Nrf2*$^{-/-}$, *Hfe*$^{-/-}$ and *Nrf2/Hfe*$^{-/-}$ com 24 meses de idade. Os murganhos *Nrf2/Hfe*$^{-/-}$ velhos tinham baixo peso corporal, anemia ligeira e hipoglicemia em jejum. Nos murganhos dos quatro genótipos observou-se inflamação hepática ligeira, possivelmente devida ao envelhecimento. O NRF2 provou ser essencial na defesa antioxidante, uma vez que os murganhos *Nrf2*$^{-/-}$ e *Nrf2/Hfe*$^{-/-}$ apresentaram níveis diminuídos de transcrito do gene *Nqo1* e que a razão GSH/GSSG se encontrou significativamente diminuída nos fígados *Nrf2*$^{-/-}$. Apesar da semelhante quantidade de ferro não-heme em fígados *Hfe*$^{-/-}$ e *Nrf2/Hfe*$^{-/-}$, observámos uma alteração no local de deposição do ferro do parênquima do fígado (em murganhos *Hfe*$^{-/-}$) para as células sinusoidais (em murganhos *Nrf2/Hfe*$^{-/-}$). A necrose, a fibrose e o número de células TUNEL-positivas estavam aumentados nos fígados *Nrf2/Hfe*$^{-/-}$. Concluímos que a supressão do NRF2 leva a um dano hepático espontâneo no murganho *Hfe*$^{-/-}$, o modelo animal da HH. No estudo humano, DNAs de pacientes *HFE* C282Y$^{+/+}$ foram genotipados para os SNPs Rs35652124, Rs670664, Rs150648896 e Rs6721961 na região promotora do *NRF2*. Os nossos resultados indicam que nenhum SNP, por si só, leva ao desenvolvimento de uma manifestação clínica, mas pacientes portadores do alelo C no SNP Rs35652124 estão de alguma forma protegidos das manifestações da HH. Concluindo, o presente estudo mostra que o NRF2 tem um papel hepatoprotetor importante no modelo animal da HH e que as variantes genéticas podem estar implicadas no curso clínico da doença humana.

Palavras-chave: Envelhecimento, Ferro, Hemocromatose Hereditária, *Hfe*, *Nrf2*.

Table of contents

Agradecimentos I
Abstract III
Resumo V
Table of contents VII
List of figures XI
List of tables XIII
List of abbreviations XV

Introduction 1
1. Iron metabolism 1
1.1. Body iron distribution 1
1.2. Intestinal iron absorption 1
1.3. Iron storage 3
1.4. Iron export 4
1.5. Iron transport and uptake 5
1.5.1. Transferrin-dependent mechanisms 5
1.5.2. Transferrin-independent mechanisms 6
1.6. Iron consumption: erythropoiesis 6
1.7. Iron recycling: macrophages 7
1.8. Control of cellular iron homeostasis 7
1.9. Control of systemic iron homeostasis 8
1.9.1. Hepcidin regulation 9
2. Iron metabolism disorders 11
2.1. Hereditary Hemochromatosis 11
2.1.1. *HFE*-related HH 12
2.1.2. Non-HFE hereditary hemochromatosis 12
3. Oxidative stress 13
3.1. Antioxidant defense 14
3.2. NRF2 pathway 15
3.2.1. NRF2 target genes 16
3.2.2. NRF2, a key protector against liver iron toxicity 17
3.2.3. *Nrf2* polymorfisms 17
4. Aims 18

Material and Methods 19
1. Animal study 19
1.1. Animals 19
1.2. Hematological measurements 19
1.3. Serum analysis 19
1.4. RNA extraction and cDNA synthesis 20
1.5. Real-time reverse-transcription (RT)-PCR 21
1.6. Quantification of non-heme iron 21
1.7. Histological analysis 22
1.7.1. Hematoxylin and eosin staining 23
1.7.2. Sirius red staining 23
1.7.3. Perls' Prussian Blue staining 24
1.7.4. TUNEL assay 24
1.8. Evaluation of oxidative stress 25
1.8.1. Thiobarbituric Acid Reactive Substances (TBARS) assay 25
1.8.2. Quantification of the GSH/GSSG ratio 25
1.8.2.1. Quantification of the total gluthatione 25
1.8.2.2. Quantification of GSSG 26
1.9. Hydroxyproline Assay 26
2. Human study 26
2.1. Patients 26
2.2. *NRF2* genotyping 27
2.3. Datafile collection 28
3. Statistical analysis 28
3.1. Animal study 28
3.2. Human study 28

Results 31
Animal study 31
1. Body, liver and spleen weights 31
2. Hematological parameters 31
3. Characterization of the anemia of *Nrf2/Hfe*$^{-/-}$ mice 32
4. Serum analysis 35
5. Expression of glucogenesis genes 36
6. Iron metabolism 36
7. Oxidative stress 41
8. Liver fibrosis 43

9. Hepatic inflammation and steatosis 45
10. Liver damage 46
Human study 49

Discussion 55
Animal study 55
1. *Hfe* and *Nrf2* genes in erythropoiesis 55
2. *Hfe* and *Nrf2* genes in gluconeogenesis 57
3. *Hfe* and *Nrf2* genes in iron metabolism 58
4. *Hfe* and *Nrf2* genes and oxidative stress 60
5. *Hfe* and *Nrf2* genes in liver fibrosis 60
6. *Hfe* and *Nrf2* genes in liver inflammation and steatosis 61
7. *Hfe* and *Nrf2* genes and liver damage 62
Human study 62
Study limitations 64

Conclusions 65
Future perspectives 66
Publications 67
References 69

List of figures

Figure 1. Iron distribution in the human body. **3**
Figure 2. Heme and non-heme iron uptake, utilization and export by enterocytes. **4**
Figure 3. The Transferrin Cycle. **6**
Figure 4. Iron recycling in macrophages. **8**
Figure 5. Regulation of hepcidin transcription.. ..... **10**
Figure 6. Structural and functional zonation of the liver. **14**
Figure 7. Activation of the KEAP1-NRF2-ARE pathway by oxidants/electrophiles. **16**
Figure 8. Body weight and percentage of relative liver and spleen weights of WT, *Nrf2*$^{-/-}$, *Hfe*$^{-/-}$ and *Nrf2/Hfe*$^{-/-}$ mice. **31**
Figure 9. EPO levels and LDH activity in WT, *Nrf2*$^{-/-}$, *Hfe*$^{-/-}$ and *Nrf2/Hfe*$^{-/-}$ mice. **33**
Figure 10. Expression of macrophages-associated genes in liver and spleen of WT, *Nrf2*$^{-/-}$, *Hfe*$^{-/-}$ and *Nrf2/Hfe*$^{-/-}$ mice. **34**
Figure 11. Expression of gluconeogenesis genes in the liver of WT, *Nrf2*$^{-/-}$, *Hfe*$^{-/-}$ and *Nrf2/Hfe*$^{-/-}$ mice. **36**
Figure 12. Iron levels and percentage of transferrin saturation in the serum of WT, *Nrf2*$^{-/-}$, *Hfe*$^{-/-}$ and *Nrf2/Hfe*$^{-/-}$ mice. **36**
Figure 13. Tissue non-heme iron content and *Hamp* gene expression in the liver of WT, *Nrf2*$^{-/-}$, *Hfe*$^{-/-}$ and *Nrf2/Hfe*$^{-/-}$ mice. **38**
Figure 14. Representative images of H&E and Perls' Prussian Blue staining of spleen, kidney, heart and pancreas sections of WT, *Nrf2*$^{-/-}$, *Hfe*$^{-/-}$ and *Nrf2/Hfe*$^{-/-}$ *mice*.. ..... **39**
Figure 15. H&E, Perls' Prussian Blue and Sirius Red stained liver sections of WT, *Nrf2*$^{-/-}$, *Hfe*$^{-/-}$ and *Nrf2/Hfe*$^{-/-}$ mice.. ..... **40**
Figure 16. Histological grades of iron storage in WT, *Nrf2*$^{-/-}$, *Hfe*$^{-/-}$ and *Nrf2/Hfe*$^{-/-}$ livers.. ..... **41**
Figure 17. MDA concentration and *Nqo1* gene expression in the livers of WT, *Nrf2*$^{-/-}$, *Hfe*$^{-/-}$ and *Nrf2/Hfe*$^{-/-}$ mice. **42**
Figure 18. Hepatic fibrosis and expression of fibrogenic genes in the livers of WT, *Nrf2*$^{-/-}$, *Hfe*$^{-/-}$ and *Nrf2/Hfe*$^{-/-}$ mice. **44**
Figure 19. Fibrosis degree of WT, *Nrf2*$^{-/-}$, *Hfe*$^{-/-}$ and *Nrf2/Hfe*$^{-/-}$ livers. **44**
Figure 20. Expression of proinflammatory genes in the liver of WT, *Nrf2*$^{-/-}$, *Hfe*$^{-/-}$ and *Nrf2/Hfe*$^{-/-}$ mice. **45**
Figure 21. H&E grading of lobular inflammation and steatosis in WT, *Nrf2*$^{-/-}$, *Hfe*$^{-/-}$ and *Nrf2/Hfe*$^{-/-}$ liver sections. **46**

Figure 22. Levels of serum ALT and TUNEL-positive cells in the liver of WT, *Nrf2*$^{-/-}$, *Hfe*$^{-/-}$ and *Nrf2/Hfe*$^{-/-}$ mice. **46**
Figure 23. TUNEL assay. **47**
Figure 24. Representative H&E stained liver sections of *Nrf2/Hfe*$^{-/-}$ mice **48**
Figure 25. PCR amplification of a 284 bp fragment of the *NRF2* promoter region. **49**
Figure 26. Representative elecropherogram. **50**

List of tables

Table 1. Sequences of the oligonucleotide primers used in qRT-PCR and the respective annealing temperatures. **22**

Table 2. Patients' general characteristics and frequency of clinical manifestations. **27**

Table 3. Hematological parameters of WT, *Nrf2*$^{-/-}$, *Hfe*$^{-/-}$ and *Nrf2/Hfe*$^{-/-}$ mice. **32**

Table 4. Levels of cytokines and chemokines in the serum of WT, *Nrf2*$^{-/-}$, *Hfe*$^{-/-}$ and *Nrf2/Hfe*$^{-/-}$ mice. **35**

Table 5. Levels of glucose, triglycerides and insulin in the serum of WT, *Nrf2*$^{-/-}$, *Hfe*$^{-/-}$ and *Nrf2/Hfe*$^{-/-}$ mice. **35**

Table 6. Levels of GSX, GSSG and GSH and GSH/GSSG ratio, in the serum of WT, *Nrf2*$^{-/-}$, *Hfe*$^{-/-}$ and *Nrf2/Hfe*$^{-/-}$ mice. **42**

Table 7. Actual sample and reference allele frequencies. **50**

Table 8. Allele frequencies in patients stratified according to the clinical manifestations of disease. **50**

Table 9. Frequencies of the several genotypes in 97 patients. **51**

Table 10. Genotype frequencies in patients with or without cirrhosis, arthropathy and symptoms **52**

Table 11. Clinical characterization of the genotypes groups. **52**

List of abbreviations

ALT	alanine aminotransferase
Acta2	alpha-smooth muscle actin gene
AI	anemia of inflammation
Apo-Tf	apo-transferrin
ARE	antioxidant response elements
AST	aspartate aminotransferase
BMP	bone morphogenic protein
BMPR	bone morphogenic protein receptor
BMP-RE	bone morphogenic protein responsive element
BTB	tramtrack and bric-à-brac domain
C/EBPα	CCAAT/enhancer-binding protein alpha
CAT	catalase
cDNA	complementary deoxyribonucleic acid
CGPP	’Centro de Genética Preditiva e Preventiva’
CHP	’Centro Hospitalar do Porto’
Col1a1	type I collagen gene
Cul3	cullin 3
Cys	cysteine
DAPI	4',6-diamidino-2-phenylindole
DCYTB	duodenal cytochrome b
DEPC	diethylpyrocarbonate
DGR	double glycine repeats
DMT1	divalent metal transporter 1
DNA	deoxyribonucleic acid
dNTP	deoxyribonucleotide triphosphate
DTT	dithiothreitol
ECM	extracellular matrix
EDTA	ethylenediaminetetraacetic acid
ELISA	enzyme-linked immunosorbent assay
EPO	erythropoietin
FA	fatty acid
FAC	ferric ammonium citrate
Fe	iron
Fe^{2+}	ferrous iron

Fe_2-Tf	diferric transferrin
Fe^{3+}	ferric iron
FLVCR	feline leukemia virus, subgroup C, receptor
FPN1	ferroportin
G6Pc	glucose-6- phosphatase
GCL	glutamate-cysteine ligase
GPx	glutathione peroxidase
GR	glutathione reductase
GSH	reduced glutathione
GSSG	oxidized glutathione
GSTs	glutathione-S-transferases
GSX	total glutathione
H&E	standard hematoxylin and eosin staining
H^+	hydrogen
H_2O_2	hydrogen peroxide
HAMP	hepcidin
Hb	hemoglobin
HCl	hydrochloride
HCP1	heme carrier protein 1
HCT	hematocrit
HCV	hepatitis C virus
HH	hereditary hemochromatosis
HIC	hepatic iron content
HIFs	hypoxia inducing factors
HIV	human immunodeficiency virus
HJV	hemojuvelin
Hmox1	heme oxygenase-1 gene
$HO^{\bullet}$	hydroxyl radical
HO-1	heme oxygenase-1
Holo-Tf	holo-transferrin
Hprt	hypoxanthine phosphoribosyltransferase gene
HREs	hypoxia-response elements
HRG1	heme responsive gene 1
HSC	hepatic stellate cells
IDA	iron deficiency anemia
IFN-γ	interferon-γ

IL	interleukin
IRE	iron responsive element
IRP	iron regulatory protein
JH	juvenile hemochromatosis
K3EDTA	K3-ethylenediamine tetraacetic acid
KEAP1	kelch ECH associating protein 1
LDH	lactate dehydrogenase
M&M	materials and methods
MAF	small musculoaponeurotic fibrosarcoma
MAPK	mithogen-activated protein kinase
MCH	mean corpuscular hemoglobin
MCV	mean corpuscular volume
MDA	malondialdehyde
$MgCl_2$	magnesium chloride
MMPs	matrix metalloproteinases
mRNA	messenger ribonucleic acid
MZF1	myeloid zink finger 1
Na^+	sodium
NFE2L2/NRF2	nuclear factor-erythroid 2-related factor 2
NQO1	NAD(P)H:quinone oxireductase 1
NTBI	non-transferrin bound iron
O_2	oxygen
$O_2^{\bullet-}$	superoxide
PBS	phosphate buffered saline
PCA	perchloric acid
PCBP1	poly(rC)-binding protein
PCFT	proton coupled folate transporter
PCR	polymerase chain reaction
PEPCK-C	phosphoenolpyruvate carboxykinase
qPCR	real-time polymerase chain reaction
RBC	red blood cell
RNA	ribonucleic acid
ROS	reactive oxygen species
RT	room temperature
RT-PCR	reverse transcription polymerase chain reaction

SNP	single nucleotide polymorphism
SOD	superoxide dismutase
STAT3	signal transducer and activator of transcription 3
STEAP	six transmembrane epithelial antigen of the prostate
TBARS	thiobarbituric acid reactive substances
TBI	transferrin-bound iron
TBIS	total body iron stores
TCA	trichloroacetic acid
Tf	transferrin
TfR	transferrin receptor
TGF-β	transforming growth factor-β
TIBC	total iron-binding capacity
Timp1	tissue inhibitor of matrix metalloproteinase-1 gene
TIMPs	tissue inhibitors of metalloproteinases
TNFα	tumor necrosis factor alpha
Trx	thioredoxin
TUNEL	terminal deoxynucleotidyl transferase (TdT) dUTP Nick-End Labeling
Ub	ubiquitination
UTR	untranslated region
WT	wild-type
ZIP14	zinc transporter Zrt-Irt-like protein 14
α-SMA	α-smooth muscle actin

Introduction

1. Iron metabolism

Iron is essential for nearly all living organisms and plays an important role in several biochemical activities, such as oxygen sensing and transport, electron transfer, catalysis, energy production and DNA synthesis (Evstatiev and Gasche, 2012; Ganz, 2013; Papanikolaou and Pantopoulos, 2005). Iron is capable of accepting or donating electrons, switching between ferrous (Fe^{2+}) and ferric (Fe^{3+}) forms (Andrews, 1999; Evstatiev and Gasche, 2012; Papanikolaou and Pantopoulos, 2005). The redox potential of free iron can trigger the Fenton or Haber-Weiss reactions, which catalyze the production of toxic reactive oxygen species (ROS) (Evstatiev and Gasche, 2012; Lane et al., 2015; Papanikolaou and Pantopoulos, 2005). As ROS may damage DNA, proteins and lipid membranes (Andrews, 1999; Evstatiev and Gasche, 2012), iron is usually incorporated into proteins and prosthetic groups (Evstatiev and Gasche, 2012; Silva and Faustino, 2015). The intracellular iron content is thus tightly controlled through the regulation of iron import, storage and efflux (Evstatiev and Gasche, 2012; Lane et al., 2015; Yun and Vincelette, 2015).

1.1. Body iron distribution

The average adult human has 3-5 g of iron in the body, depending on gender and age (Evstatiev and Gasche, 2012; Ganz, 2013; Gkouvatsos et al., 2012). Over 2 g of iron are incorporated in the hemoglobin and the remaining iron is either stored in hepatocytes (~1000 mg) or circulates in a transit pool in reticuloendothelial macrophages (~600 mg). Iron can also be found in myoglobin (~300 mg), in iron-containing proteins (~8 mg) or circulating in the plasma bound to transferrin (~3 mg) (Andrews, 1999; Gkouvatsos et al., 2012; Papanikolaou and Pantopoulos, 2005) **(Figure 1)**.

1.2. Intestinal iron absorption

The regulation of iron absorption is a key element in iron homeostasis since there is no pathway for its excretion (Andrews, 1999; Gkouvatsos et al., 2012). Iron absorption (1-2 mg per day) takes place in the enterocytes of the duodenum and in the upper jejunum (Andrews, 1999; Evstatiev and Gasche, 2012). This serves to compensate for the daily loss of iron (1-2 mg per day) through sweating, desquamation of epithelial surfaces and bleeding, thus contributing modestly to the total iron demand in the body (Ganz, 2013; Gkouvatsos et al., 2012) **(Figure 1)**. However iron absorption can be enhanced, when

the body has higher needs of iron, or suppressed in cases of iron overload (Hentze et al., 2010).

Iron is essentially absorbed from food. There are two distinct forms of dietary iron that appear to be absorbed by separate mechanisms: heme iron and inorganic iron (non-heme iron) (Sharp, 2010; Wyllie and Kaufman, 1982). Heme, a protoporphyrin ring that binds iron (Dunn et al., 2007), is very abundant in meat products (Silva and Faustino, 2015) and is more bioavailable than the non-heme form (Gkouvatsos et al., 2012). Heme is released from hemoproteins in the stomach due to the low pH and to proteolytic enzymes (Silva and Faustino, 2015). Although the mechanism of heme uptake is not yet well characterized, it is known to occur via direct transport (Gkouvatsos et al., 2012) or via receptor-mediated endocytosis (Ganz, 2013; Silva and Faustino, 2015). A putative candidate for heme transporter in the enterocyte is heme carrier protein 1 (HCP1) (Shayeghi et al., 2005). HCP1, together with the proton coupled folate transporter (PCFT) (Silva and Faustino, 2015), is capable of internalizing heme. However, HCP1 affinity to heme is low (Laftah et al., 2009) and its nonredundant fuction is folate uptake in the duodenum (Ganz, 2013), revealing that HCP1 is not essential for duodenal heme uptake. Once inside the enterocyte, heme can migrate to the endoplasmatic reticulum (Dunn et al., 2007), where heme oxygenase-1 (HO-1) localized in the reticulum surface liberates ferrous iron, carbon monoxide and biliverdin from heme (Gkouvatsos et al., 2012; Silva and Faustino, 2015). Fe^{2+} can then follow the fate of inorganic iron. Heme can also be exported as an intact molecule via the putative heme exporter feline leukemia virus, subgroup C, receptor (FLVCR) (Khan and Quigley, 2011).

Non-heme iron, including iron-sulfur clusters, is present in the intestinal lumen in its insoluble oxidized Fe^{3+} form (Gkouvatsos et al., 2012). In order to be absorbed by the enterocyte, Fe^{3+} is reduced in the apical membrane by brush border reductases (Silva and Faustino, 2015). Duodenal cytochrome b (DCYTB) (McKie et al., 2001) was the first ferrireductase discovered and it uses ascorbate for the reduction reaction (Andrews and Schmidt, 2007). However, DCYTB proved not to be essential for the reduction of Fe^{3+} to Fe^{2+} (Gunshin et al., 2005). This suggests the existence of other ferrireductases, like six transmembrane epithelial antigen of the prostate 2 (STEAP2) (McKie et al., 2001; Ohgami et al., 2006). The reduced Fe^{2+} iron is transported across the apical membrane by the proton-coupled divalent metal transporter 1 (DMT1, SLC11A2, NRAMP2 or DCT1). DMT1 is a 12-transmembrane-segment protein that uses the proton gradient, generated by the intestinal Na^+/H^+ exchanger (Mackenzie et al., 2011), between the gut lumen and the enterocyte cytoplasma to perform the symport of Fe^{2+} coupled with H^+ (Gunshin et al., 1997), but it is not specific to iron (Andrews, 1999).

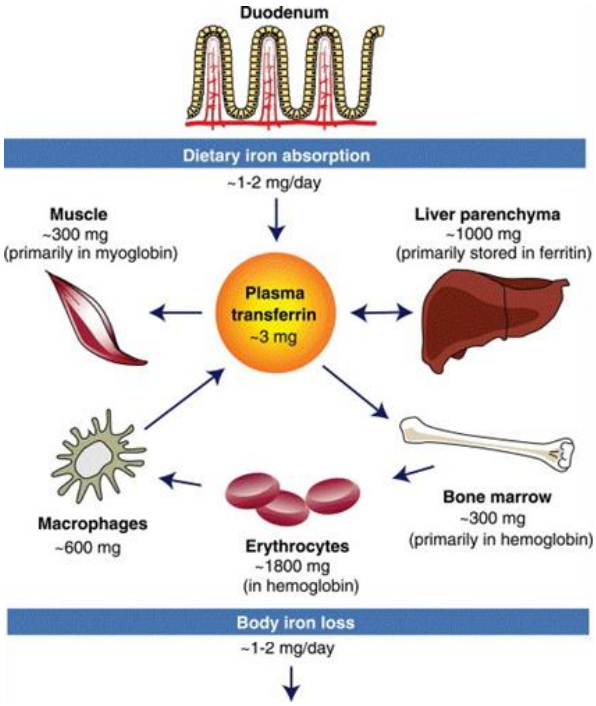

Figure 1. Iron distribution in the human body. Per day, 1-2 mg of iron enters and leaves the body. Dietary iron is absorbed by duodenal enterocytes and circulates bound to plasma transferrin. Most of the iron is incorporated into hemoglobin in erythroid precursors and mature red blood cells. The remaining iron is present in muscle fibers, in myoglobin, in parenchymal cells of the liver and in reticuloendothelial macrophages. Adapted from (Papanikolaou and Pantopoulos, 2005).

Inside enterocytes, the new acquired Fe^{2+} obtained from heme or non-heme iron has the same fate: it may be stored in ferritin, it can enter the hypothesized intracellular or "labile" iron pool (Dunn et al., 2007), it may be used for metabolic purposes (mainly by mitochondria) or it can be exported through the enterocyte basolateral membrane into the circulation (Papanikolaou and Pantopoulos, 2005) **(Figure 2)**.

1.3. Iron storage

In order to prevent cell damage through the production of ROS, the excess of iron in the cell is stored in an inert form – bound to ferritin. Cytoplasmic ferritin, a spherical nanocage protein with 24 units of ferritin heavy and light chains (Evstatiev and Gasche, 2012), is capable of storing large amounts of iron (Ganz, 2013). Ferrous iron is delivered by poly (rC)-binding protein (PCBP1) to ferritin and ferritin heavy chain oxidizes Fe^{2+} to Fe^{3+} (Ganz, 2013). Mitochondrial ferritin (Levi et al., 2001), another form of ferritin very similar to cytoplasmic ferritin, is also capable of storing iron, playing a protective role in conditions of iron overload (Richardson et al., 2010). Liver hepatocytes generally store 20-30% of the total body iron, mostly in the form of ferritin (Andrews and Schmidt, 2007). This renders the liver a crucial function in iron storage.

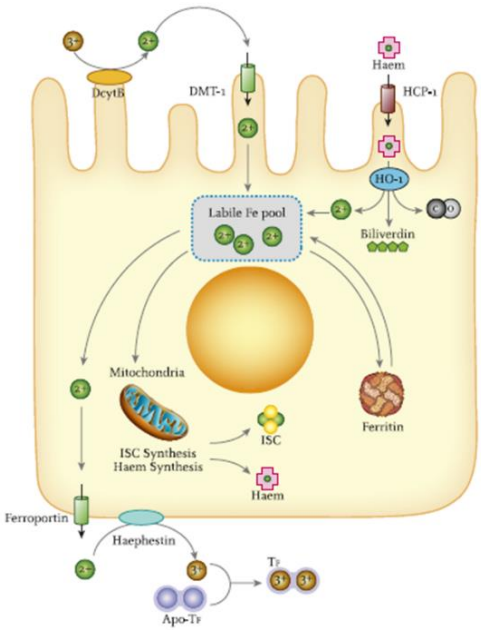

Figure 2. Heme and non-heme iron uptake, utilization and export by enterocytes. Heme iron enters the enterocyte via heme carrier protein 1 (HCP1) and Fe^{2+} is released after the breakup of heme by hemoxygenase (HO-1). Non-heme iron enters via divalent metal transporter 1 (DMT1), after a reduction step by duodenal cytochrome B (DCYTB). Ferrous iron can enter the labile iron pool, can be stored in ferritin, can be used by mitochondria or can be exported via ferroportin. Exported Fe^{2+} is oxidized by hephaestin and bound to transferrin (Tf). Adapted from (Evstatiev and Gasche, 2012).

Plasma ferritin, a soluble but iron-poor form of ferritin, contains mostly light chains and is derived primarily from macrophages (Cohen et al., 2010). Serum concentrations of ferritin correlate to body iron stores, and are thus considered an important clinical parameter. While it is still unknown how ferritin enters the circulation and what is its exact function, it is speculated that plasma ferritin acts like an iron scavenger, reducing oxidative stress (Evstatiev and Gasche, 2012).

1.4. Iron export

A crucial step for the entrance of iron in the body is the export of cytosolic iron into the circulation by ferroportin (FPN1 (Donovan et al., 2000), SLC40A1, IREG1 (McKie et al., 2000), MTP1 (Abboud and Haile, 2000)) (Gkouvatsos et al., 2012). Ferroportin, a 12-transmembrane domain protein, is the only known mammalian iron exporter (Ganz, 2013). It is expressed in the basolateral membranes of duodenal enterocytes, in the membranes of macrophages (Canonne-Hergaux et al., 2006) and in the sinusoidal surfaces of hepatocytes (Ramey et al., 2010). The export of iron requires ferroxidases, such as plasma ceruloplasmin, present in macrophages and hepatocytes membranes, (Healy and Tipton, 2007) and enterocyte membrane-bound hephaestin (Vulpe et al., 1999), that use oxygen to re-oxidize Fe^{2+} to Fe^{3+} (Ganz, 2013). Fe^{3+} can then be loaded

into the circulatory transferrin (Tf) to be delivered to cells or can circulate as non-transferrin bound iron (NTBI).

1.5. Iron transport and uptake

1.5.1. Transferrin-dependent mechanisms

Transferrin, a 75 to 80-kDa glycosylated protein, is an extracellular iron carrier (Ganz, 2013). Tf has two high-affinity binding sites for Fe^{3+} (Hentze et al., 2010) and circulates in the plasma in three states: apo-transferrin (apo-Tf), when no iron is bound; monoferric transferrin, bound to one Fe^{3+}; diferric transferrin, also known as holo-transferrin (holo-Tf), bound to two Fe^{3+} (Young and Bomford, 1984). Transferrin saturation is used as a clinical parameter: <16% indicates iron deficiency and >45% indicates iron overload; 30% is the normal saturation. When transferrin saturation exceeds 60%, NTBI starts to accumulate in the circulation, which can damage parenchymal cells (Hentze et al., 2010).

When bound to Tf, iron is nonreactive but very difficult to extract, so the entire iron-protein complex is internalized (Hentze et al., 2004). The cellular uptake of transferrin-bound iron (TBI) is mostly mediated by the transferrin receptor 1 (TfR1), at the cell membrane (Brown and Johnson, 1981). TfR1 is a transmembrane glycoprotein ubiquitously expressed (Hentze et al., 2004) and can bind one Tf molecule at each subunit (Aisen, 2004). The TBI/TfR1 complex undergoes endocytosis via clathrin-coated pits (Gkouvatsos et al., 2012). The entry of H^+ mediated by an ATP-dependent proton pump decreases the endosome pH, causing a conformational change in Tf and the release of Fe^{3+} (Gkouvatsos et al., 2012; Silva and Faustino, 2015). Apo-Tf remains bound to TfR1, while free Fe^{3+} is reduced by six transmembrane epithelial antigen of the prostate 3 (STEAP3) and exported to the cytoplasm by DMT1 (Silva and Faustino, 2015). Apo-Tf and TfR1 return to the cell surface (Hentze et al., 2004), in a process involving the trafficking protein SEC15L1 (Lim et al., 2005). Apo-Tf is then recycled to the bloodstream, where it can capture more iron (Gkouvatsos et al., 2012) **(Figure 3)**.

TBI/Tf uptake is also known to occur via TfR1-independent mechanisms. Transferrin receptor 2 (TfR2) (Kawabata et al., 1999), a protein homologous to TfR1, is believed to be one of them (Gkouvatsos et al., 2012). TfR2 is mainly expressed in hepatocytes and binds holo-Tf with 25-fold lower affinity than TfR1 (Robb et al., 2004). Mutations in TfR2 cause hereditary hemochromatosis (HH) (Camaschella et al., 2000; Fleming et al., 2002), a systemic iron overload disease, revealing that this protein is more important for the regulation of systemic iron homeostasis rather than for cellular iron uptake (Gkouvatsos et al., 2012).

Regardless of the existence of several pathways for the uptake of TBI, TfR1-mediated endocytosis is crucial for the organism, since it is indispensable for the delivery of iron to developing erythroid cells (Gkouvatsos et al., 2012).

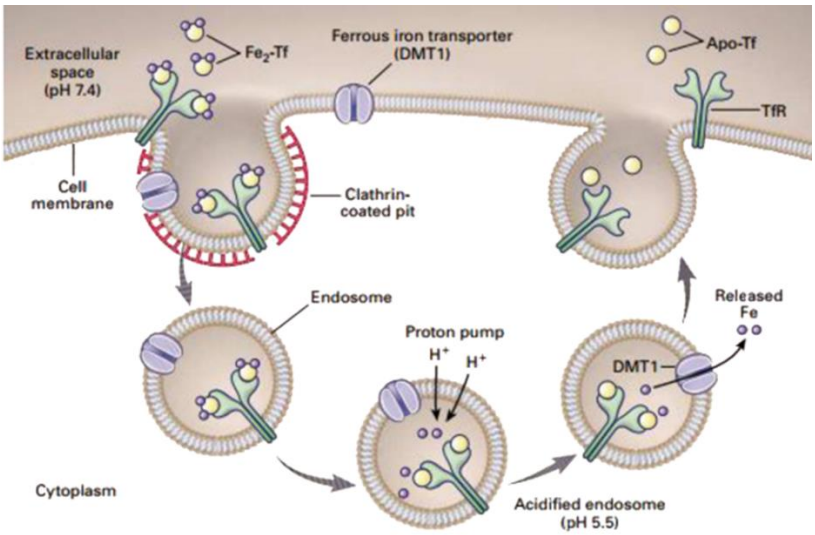

Figure 3. The Transferrin Cycle. Diferric transferrin (Fe_2-Tf) binds to transferrin receptors (TfR) on the cell surface. The Tf/TfR complex undergoes endocytosis via clathrin-coated pits, forming a specialized endosome. A proton pump decreases the pH within endosomes, what causes conformational changes in Tf and, consequently, the release of Fe^{3+}. The iron transporter DMT1 moves iron across the endosomal membrane, to enter the cytoplasm, after a reduction step by STEAP3. Apo-Tf and TfR are recycled back to the cell surface, and Apo-Tf is released from TfR to plasma for another uptake cycle. Adapted from (Andrews, 1999).

1.5.2. Transferrin-independent mechanisms

In iron overload conditions, such as HH, transferrin iron binding sites become supersaturated and circulating “free” iron increases (Hentze et al., 2004). NTBI is thought to circulate in the plasma bound to albumin or small organic acids, like citrate (Hider, 2002). The exact mechanism of NTBI uptake is still unclear, but it has been suggested that one or more cell surface ferrireductases are involved in the process (McKie et al., 2001). These enzymes reduce Fe^{3+} NTBI to Fe^{2+} NTBI, so it can be imported (Lane et al., 2015). DMT1 transporter seems to import NTBI (Lane et al., 2015), but the zinc transporter Zrt-Irt-like protein 14 (ZIP14) is the most probable NTBI transporter (Liuzzi et al., 2006).

1.6. Iron consumption: erythropoiesis

Two-thirds of the body iron is used by the erythroid bone marrow for erythropoiesis (Andrews and Schmidt, 2007). Erythroid precursors highly express transferrin receptors at the cell surface, promoting iron uptake via TfR-mediated endocytosis (Hentze et al., 2004). Once inside the cytoplasm, iron is driven to the mitochondrion via a cytosolic iron

chaperon, the PCBP1 (Shi et al., 2008), or directly from the endosome through a “kiss-and-run” mechanism (Silva and Faustino, 2015). Iron is then transported through the inner membrane by mitoferrins 1 and 2 (Paradkar et al., 2009; Shaw et al., 2006) for heme synthesis. Ferrous iron is incorporated into protoporphyrin IX by ferrochelatase (Evstatiev and Gasche, 2012). Most of the heme is used for hemoglobin production, but it can also be exported by FLVCR (Andrews and Schmidt, 2007).

1.7. Iron recycling: macrophages

Every day, a total of 25 mg of iron are needed for erythropoiesis. However, only 1-2 mg of iron enter the body through the enterocytes. Thus, macrophages play a crucial role in iron recycling (Hentze et al., 2004), providing nearly all of the available iron. Splenic and hepatic macrophages scavenge the senescent erythrocytes (Silva and Faustino, 2015). Once inside the phagolysosome, the action of hydrolytic enzymes and ROS releases hemoglobin or free heme from the erythrocyte to the vacuolar fluid (Silva and Faustino, 2015). HO-1, in the presence of O_2, cleaves heme to iron, carbon monoxide and biliverdin (Poss and Tonegawa, 1997).

Besides capturing TBI, macrophages are also capable of capturing free hemoglobin and free heme from the serum. Free hemoglobin is captured by haptoglobin (Kristiansen et al., 2001), a liver derived plasma protein. CD163 receptor recognizes this complex and promotes its endocytosis in the macrophage (Van Gorp et al., 2010). Free heme, in turn, is scavenged by hemopexin (Tolosano et al., 2010) and suffers endocytosis via the CD91 receptor (Hvidberg et al., 2005), which is not only present in the surface of macrophages but also in hepatocytes and other cell types (Gkouvatsos et al., 2012). There is a putative candidate for heme transport in macrophages, the heme responsive gene 1 (HRG1) (Rajagopal et al., 2008). HRG1, described in *Caenorhabditis elegans*, seems to be involved in the uptake of heme released by senescent erythrocytes (Ganz, 2013), in the phagolysosomes of macrophages (Delaby et al., 2012). Both free heme and free hemoglobin endocytosed by the macrophages are hydrolyzed and contribute to the iron pool (Caza and Kronstad, 2013) **(Figure 4)**.

1.8. Control of cellular iron homeostasis

Cellular iron homeostasis is regulated by a post-transcriptional mechanism that controls the synthesis of proteins involved in iron uptake, storage and release (Muckenthaler et al., 2008). This mechanism depends on two iron regulatory proteins (IRP): IRP1 and IRP 2, which post-transcriptionally control the expression of iron responsive element (IRE) containing mRNAs (Muckenthaler et al., 2008). IREs are located in the 5’ untranslated

region (UTR) of the mRNAs enconding TfR1, DMT1 and in the 3' UTR of ferritin and ferroportin mRNAs. In iron-depleted cells, IRPs either bind to 5' IRE, suppressing the translation of *FPN1* and ferritin mRNAs, or to 3' IRE, enhancing *TfR1* and *DMT1* mRNA stability and thus preventing its degradation. On the other hand, in iron-replete cells, IRP1 and IRP2 are inactivated. *TfR1* and *DMT1* mRNAs suffer degradation and *FPN1* and ferritin mRNAs undergo translation. This response promotes the detoxification of excess intracellular iron, by iron storage, and inhibits further iron uptake (Papanikolaou and Pantopoulos, 2005).

1.9. Control of systemic iron homeostasis

Systemic iron has to be tightly regulated, so cells have enough iron to suppress their needs but also avoid the toxicity associated with iron excess (Andrews and Schmidt, 2007). Hepcidin, a 25 amino acid peptide encoded by the *HAMP* gene, seems to regulate the major flows of iron and is in turn regulated by iron (Ganz, 2013). This hormone, which circulates in the blood plasma, is primarily produced and secreted by hepatocytes and is filtered by the kidneys (Park et al., 2001). Hepcidin post-transcriptionally controls the membrane concentration of ferroportin (Nemeth et al., 2004). When iron levels are high, hepcidin binds directly to ferroportin, leading to its internalization and degradation within lysosomes. As ferroportin is the only mammalian known iron exporter, this mechanism blocks the release of dietary, stored and recycled iron from the enterocytes, hepatocytes and macrophages, respectively (Nemeth et al., 2004).

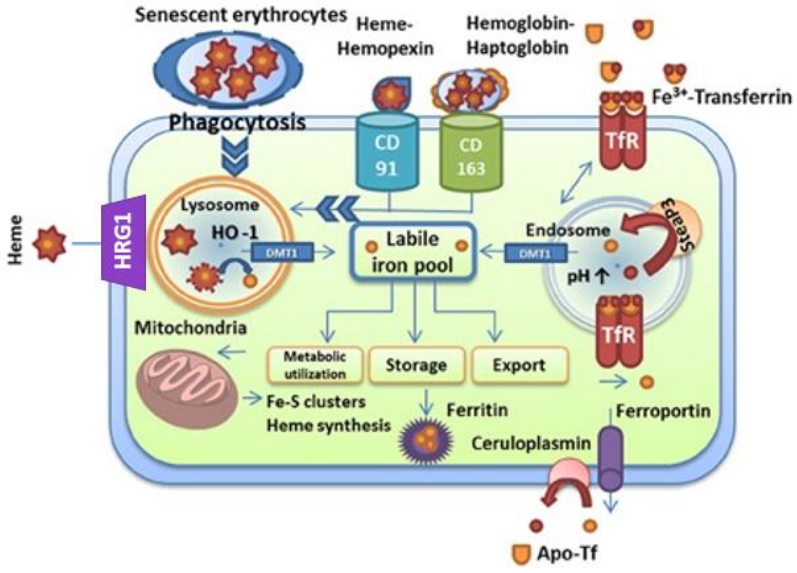

Figure 4. Iron recycling in macrophages. Senescent erythrocytes are scavenged by macrophages and HO-1 cleaves heme to iron. Hemopexin scavenges free heme and suffers endocytocis via the CD91 receptor. Haptoglobin captures free hemoglobin and is recognized by the CD163 receptor. HRG1 is a putative heme transporter. Adapted from (Caza and Kronstad, 2013).

1.9.1. Hepcidin regulation

Hepcidin is feedback-regulated by iron and this process involves intracellular and extracellular iron sensors. Iron sensors are coupled to transduction pathways that regulate hepcidin synthesis and secretion by hepatocytes (Ganz and Nemeth, 2012). Four of these iron sensors are proteins located at the cell surface: hemojuvelin (HJV), hemochromatosis-related membrane protein HFE, TfR1 and TfR2 (Silva and Faustino, 2015). Thus, hepcidin expression is inhibited in iron deficiency or when high amounts of iron are required for erythropoiesis (for example, in anemia or hypoxia) and is enhanced when iron stores are replenished or during inflammatory response, when erythropoiesis is restrained (Papanikolaou and Pantopoulos, 2005).

Hepcidin transcription in the liver is regulated by iron levels through two different pathways. The first one involves the hemochromatosis-related membrane protein HFE. This protein requires interaction with β2-microglobulin for normal presentation on the cell surface (Bacon, 1997), where it interacts with TfR1 and TfR2 and functions as a holo-Tf sensor (Ganz and Nemeth, 2012). The binding of HFE to TfR1 is competitively inhibited by holo-Tf. When transferrin-iron saturation increases, HFE is displaced from TfR1 and interacts with TfR2, which can bind both HFE and Fe_2-Tf simultaneously (Gao et al., 2009). The FeTf/HFE/TfR2 complex stimulates hepcidin expression through a mitogen-activated protein kinases (MAPK) and/or a bone morphogenetic protein (BMP) pathway signaling (Ganz and Nemeth, 2012). Conversely, when transferrin-iron saturation is low, HFE binds to TfR1 (Muckenthaler, 2014) and hepcidin expression is repressed. A second mechanism is the BMP signaling pathway, which is capable of integrating signals from the “Tf-Fe-sensing complex” and from hepatocytic iron stores (Hentze et al., 2010). HJV is a co-receptor of BMPs (in mice, BMP6) and binds to BMP type 1 and BMP type 2 receptors on the cell surface. The HJV-BMP6-BMP-receptor complex induces an intracellular BMP signaling cascade that activates the SMAD cascade. BMP6 activates, by phosphorylation, SMAD1, SMAD5 and SMAD8 proteins (Gkouvatsos et al., 2012). Activated p-SMAD1/5/8 interacts with SMAD4 and the whole complex translocates to the nucleus. In the nucleus, the complex binds to two BMP responsive elements (BMP-RE1 and BMP-RE2) at proximal and distal sites of hepcidin promoter, activating its transcription (Casanovas et al., 2009) **(Figure 5)**. It is suggested that BMP6 concentration can reflect the intracellular iron levels, since *BMP6* mRNA increases in the liver of mice subjected to iron loading (Kautz et al., 2008).

Hepcidin transcriptional regulation can also occur in inflammatory conditions. Interleukin-6 (IL-6), and possibly other inflammatory cytokines, induces the activation of the signal transducer and activator of transcription 3 (STAT3). STAT3 binds to a

regulatory element in the hepcidin promoter and enhances hepcidin transcription (Wrighting and Andrews, 2006). The increase of hepcidin causes hypoferremia, typical of the early stages of inflammation and infection, to limit the multiplication of iron-dependent extracellular microbes (Ganz and Nemeth, 2012). However, iron sequestration and hypoferremia may limit the iron available for erythropoiesis, leading to anemia of inflammation (anemia of chronic disease) (Ganz and Nemeth, 2012).

Erythropoietic precursors are the main iron consumers and the expansion of a precursor population suppresses hepcidin, allowing the mobilization of iron. The existence of an “erythroid regulator” that stimulates iron absorption in response to anemia and ineffective erythropoiesis has recently been demonstrated (Kautz et al., 2014). Erythropoietin (EPO), a glycoprotein hormone synthesized by the kidney, prevents the apoptosis of the erythropoietic precursors that have not begun the synthesis of hemoglobin (Silva and Faustino, 2015). EPO can directly suppress hepcidin expression, by attenuating the binding of the CCAAT/enhancer-binding protein alpha (C/EBPα) to the hepcidin promoter (Pinto et al., 2008). Hepcidin is also down-regulated by hypoxia. During hypoxia, erythropoiesis increases, in order to overcome the low levels of oxygen in the body. The hypoxia inducing factors (HIFs) are suggested to be involved in this process through a hypoxia-response elements (HREs)-mediated mechanism (Silva and Faustino, 2015).

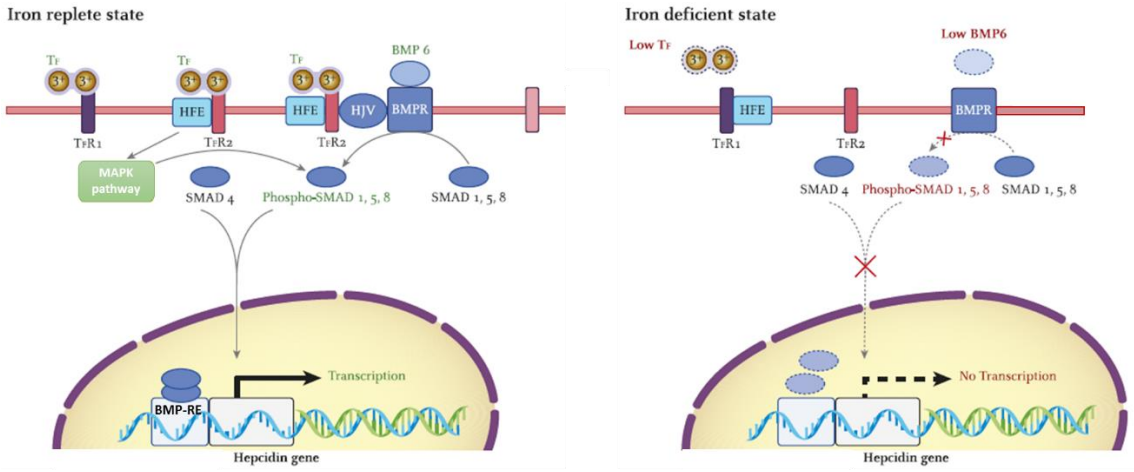

Figure 5. Regulation of hepcidin transcription. In iron deficient state, HFE binds to TfR1 and hepcidin isn’t expressed. In iron replete state, HFE is displaced from TfR1 and interacts with TfR2. This interaction stimulates hepcidin expression trough MAPK and/or BMP pathway. In iron replete cells, binding of BMP6 to the BMP receptor (BMPR) and to the coreceptor HJV also stimulates hepcidin expression. The HJV-BMP6-BMPR complex induces the phosphorylation of SMAD 1, 5 and 8. Phospho-SMAD 1, 5, 8 interacts with SMAD 4 and the whole complex translocates to the nucleus and binds to BMP-REs, activating hepcidin transcription. Adapted from (Evstatiev and Gasche, 2012).

2. Iron metabolism disorders

Although the body iron homeostasis is tightly controlled, several factors, either genetic or environmental, may lead to the development of iron overload or deficiency conditions. The iron overload disorders are classified as genetic or acquired. The genetic disorders are originated by mutations in iron metabolism genes, while the acquired ones correspond to secondary iron overload (Silva and Faustino, 2015).

2.1. Hereditary Hemochromatosis

Hereditary hemochromatosis (HH) is a group of primary genetic disorders of iron homeostasis. The primary cause of HH is often the insufficient production of hepcidin by hepatocytes, despite the high amounts of iron present in the body (Silva and Faustino, 2015). This leads to hyperabsorption of dietary iron, which is delivered to plasma resulting in increased Tf saturation and tissue iron accumulation (Pietrangelo, 2010). If phlebotomy, the most common treatment for HH, is not applied, iron can cause injury and organ dysfunction. The liver, in particular, accumulates large amounts of iron. Excess free iron is a potent deleterious hepatotoxic as well as a potential pro-fibrogenetic cofactor, since it is capable of generating ROS (Parola and Robino, 2001). In liver fibrosis, Kupffer cells (resident liver macrophages) give stimuli for the progression of the fibrogenetic process. Hepatic stellate cells (HSC) become “activated” and synthesize most of the extracellular matrix (ECM) proteins (Poli and Parola, 1997). The process is also accompanied by increased release of cytokines, such as IL-1 and IL-6 (Barbero-Becerra et al., 2015). The ECM components include collagen, mostly in the form of collagen-1, matrix metalloproteinases (MMPs) and tissue inhibitors of metalloproteinases (TIMPs) (Barbero-Becerra et al., 2015). TIMP1 is considered an important promoter of liver fibrosis (Fowell et al., 2011) and an inhibitor of activated HSC-apoptosis (Murphy et al., 2002). Fibrosis, the accumulation of extracellular matrix or scar tissue, represents a wound healing response to injury and ultimately can evolve to cirrhosis. Patients with cirrhosis, in turn, have increased risk of developing hepatocellular carcinoma. Other common clinical manifestations of HH are hypogonadism, cardiomyopathy, arthropathy and diabetes (Ganz and Nemeth, 2012; Pietrangelo, 2010).

According to the clinical outcomes and the genes affected in the disease, HH can be divided into *HFE*-related HH, juvenile hemochromatosis, *TfR2*-associated hemochromatosis and ferroportin-related HH. The molecular mechanism affected in the four types is the iron sensing-hepcidin axis (Silva and Faustino, 2015).

2.1.1. *HFE*-related HH

HFE-HH, also known as classic HH or HH-type I (Silva and Faustino, 2015), is the most common genetic disorder in populations of northern European ancestry, with a prevalence of 0.5% (Yun and Vincelette, 2015). This mildest form of HH is characterized by a gradual deposition of iron in organs with major clinical manifestation in males aged 40-50 years old and in post-menopausal women (Pietrangelo, 2010). Women are less frequently and less severely affected than men, probably because of menstruation (Pietrangelo, 2010), which allows the excretion of iron. *HFE*-HH is an autosomal recessive disease that is most frequently associated with the *HFE* C282Y mutation in homozigosity or, more rarely, in heterozigosity with the H63D gene mutation. (Yun and Vincelette, 2015). The H63D mutation results in the substitution of aspartic acid for histidine at amino acid 63 of the *HFE* gene. This mutation only causes HH if combined with the C282Y mutation (Ayonrinde et al., 2008). The C282Y mutation in *HFE*, a missense mutation, disrupts a disulfide bond that is essential for the β2-microglobulin binding. Thus, HFE is not carried to the cell surface and does not interact with TfR1, deregulating hepcidin expression (Pietrangelo, 2010). The majority of genetically affected individuals are identified because of laboratory abnormalities or family history rather than overt disease (Ganz and Nemeth, 2012), since only a small percentage of C282Y homozygotes develop HH symptoms (Pietrangelo, 2010; Wood et al., 2012). The incomplete penetrance of the disease suggests the existence of modifiers of clinical expression, which remain mostly unidentified. While alcohol abuse and male gender are known to favor clinical expression, genetic polymorphisms in genes associated with fibrogenesis, antioxidant activity and inflammation are also suspected to have a significant contribution (Bahram et al., 1999; Pietrangelo, 2010; Wood et al., 2012).

2.1.2. Non-HFE hereditary hemochromatosis

The remaining forms of HH are clinically more severe than *HFE*-HH. Juvenile Hemochromatosis (JH), also known as HH-type II, is an autosomal recessive disorder characterized by mutations in the *HJV* and *HAMP* genes (Ayonrinde et al., 2008; Roetto et al., 2003). JH presents an early onset of manifestations of iron overload, including cardiomyopathies and reproductive defects (Silva and Faustino, 2015), usually by the second and third decades of life (Ayonrinde et al., 2008).

TfR2-associated hemochromatosis (or HH-type III) is an autosomal recessive disorder that, as for *HFE*-HH, manifests from the third or fourth decade of life (Pietrangelo, 2010). However, HH-type III is characterized by mutations in the *TfR2* gene

and patients exhibit even greater variation in the severity of symptoms (Ayonrinde et al., 2008).

Ferroportin-related HH, also known as HH-type IV, is an autosomal dominant disease. It is associated with mutations in the *FPN* gene (Silva and Faustino, 2015) and the age of clinical onset is in the fourth to fifth decade of life (Pietrangelo, 2005). There are two forms of the disease: ferroportin loss of function and ferroportin gain of function. In the first case, mutants are unable to export iron from cells, which leads to cellular iron overload and low transferrin saturation. On the other hand, in the ferroportin gain of function form, cells are able to export iron but are insensible to down-regulation by hepcidin. This results in the constant absorption of iron by enterocytes and its constant release from cells, resulting in increased Tf saturation and parenchymal iron overload (Pietrangelo, 2010; Silva and Faustino, 2015).

3. Oxidative stress

As previously mentioned, oxidative stress can act as a modifier of the clinical expression of HH and it can cause cellular injury in organs that accumulate high amounts of iron, such as the liver. The oxidative metabolism is not equal throughout the liver, since the acinus, the basic functional unit of the liver, is divided in 3 zones. The hepatic lobule, the classical structural unit of the liver (Bioulac-Sage and Lebail B. Balabaud, 2007), has a shape of a hexagon, with the portal triads (hepatic artery, bile duct and portal vein) in the corners and a central vein in the central structure (LeCluyse et al., 2012). Parenchymal cells or hepatocytes radiate from the central vein to the perimeter of the lobule and define the acinus, which is demarcated into three discrete zones. Zone 1 is the periportal region, zone 2 is the midlobular region and zone 3 is the pericentral region (Rappaport, 1977) **(Figure 6)**. Oxygen tension is higher in zone 1, since blood enters the liver from the portal veins and hepatic arteries at the portal triads, flows through the sinusoidal microvasculature surrounded by the plates of parenchymal cells, and exits from the central vein (LeCluyse et al., 2012).

Iron, in the presence of aerobic respiration byproducts, like H_2O_2 and $O_2^{\bullet-}$, is capable of catalyzing the oxidation of biomolecules. This happens through the formation of the hydroxyl radical ($HO^{\bullet}$), by means of the Fenton and the Haber-Weiss reactions (Halliwell and Gutteridge, 1990; Stadtman, 1993):

$$H_2O_2 + Fe^{2+} \rightarrow Fe^{3+} + OH^- + HO^{\bullet} \text{ (Fenton reaction)}$$

$$O_2^{\bullet-} + Fe^{3+} \rightarrow Fe^{2+} + O_2$$

$$H_2O_2 + O_2^{\bullet-} \xrightarrow{Fe^{3+}} OH^- + HO^{\bullet} + O_2 \text{ (Haber-Weiss reaction)}$$

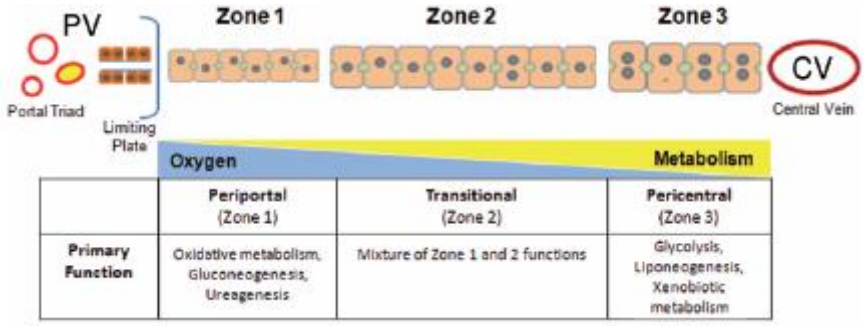

Figure 6. Structural and functional zonation of the liver. Adapted from (LeCluyse et al., 2012)

When the cellular concentration of ROS exceeds the capacity of the cell to eliminate them, oxidative damage occurs in DNA, RNA, proteins and lipids (Cabiscol et al., 2000; Tamarit et al., 1998). Free radicals attack directly polyunsaturated fatty acids in membranes and initiate lipid peroxidation, which decreases membrane fluidity and leads to the formation of more radicals and other lipid peroxidation byproducts, such as malondialdehyde (MDA) (Cabiscol et al., 2000). The modifications caused by ROS are deleterious to the cell, since they lead to a loss of function of membranes and proteins and block DNA replication or cause mutations (Cabiscol et al., 2000). Hence, organisms have developed a set of defense systems to mitigate the damaging effects of ROS (Tamarit et al., 1998).

3.1. Antioxidant defense

Chemically reactive oxygen has to be scavenged, in order to maintain an intracellular reducing environment (Cabiscol et al., 2000). Cellular antioxidant system can be divided into non-enzymatic and enzymatic. Non-enzymatic antioxidants include NADPH and NADH pools, β-carotene, ascorbic acid, α-tocopherol and glutathione (Cabiscol et al., 2000). As glutathione only contributes to the antioxidant defense in its reduced form (GSH), the enzyme glutathione reductase (GR) reduces the oxidized form (GSSG) using NADPH as a source of reducing power (Cabiscol et al., 2000). GR is constitutively active and inducible upon oxidative stress, so glutathione exists mostly in its reduced form (Zitka et al., 2012). The ratio of reduced to oxidized glutathione is a marker of cellular toxicity. Under normal conditions, GSH is present in mammalian cells in the concentration range of 1-10 mM. In a resting cell, the molar GSH:GSSG ratio exceeds 100:1, while in various models of oxidative stress, this ratio can decrease to values of 10:1 and even 1:1 (Chai et al., 1994). Several enzymes are capable of scavenging ROS, including: superoxide dismutase (SOD), catalase (CAT) and glutathione peroxidase (GPx). SOD, the first genuine ROS-metabolizing enzyme discovered (McCord and

Fridovich, 1969), dismutates superoxide ($O_2^{\bullet-}$) to hydrogen peroxyde (H_2O_2) (Nordberg and Arner, 2001):

$$2O_2^{\bullet-} + 2H^+ \rightarrow H_2O_2 + O_2$$

CAT, an heme-containing enzyme, catalyses the dismutation of H_2O_2 formed by SOD and other enzymes to water and molecular oxygen (Nordberg and Arner, 2001):

$$2\ H_2O_2 \rightarrow O_2 + 2H_2O$$

GPx is also capable of reducing H_2O_2, using glutathione as substrate, which liberates GSSG (Nordberg and Arner, 2001):

$$2GSH + H_2O_2 \rightarrow GSSG + 2H_2O$$

GR is then needed to complete the cycle, reducing GSSG to GSH.

Peroxiredoxins are enzymes capable of directly reducing peroxides, such as hydrogen peroxide and different alkylhydroperoxides, with the use of electrons provided by a physiological thiol like thioredoxin (Nordberg and Arner, 2001; Rhee et al., 2005). Thioredoxin reductase, homologous to GR, catalyzes the reduction of the redox-active disulfide in Trx (oxidized Trx) by NADPH (Zhong et al., 2000).

3.2. NRF2 pathway

Cells have programs to counteract the stress imposed by oxidants, as mentioned above. Under normal circumstances, enzymes involved in the antioxidant response are not expressed at their maximal capacity. However, in response to oxidative stress, the transcription of these enzymes is enhanced (Kensler et al., 2007). Nuclear factor-erythroid 2-related factor 2 (NFE2L2/NRF2) is the key transcription factor involved in this mechanism.

Many of the cytoprotective enzymes that take part in the antioxidant response are encoded by genes containing antioxidant response elements (ARE). The ARE is a cis-acting enhancer sequence located in the gene promoter region (Nguyen et al., 2003). NRF2 is a basic leucine zipper transcription factor that regulates transcriptional induction of ARE-containing genes in response to changes in the cellular redox status, such as during increased production of free radical species (Kensler et al., 2007; Lee et al., 2003). Under normal conditions, NRF2 is mainly localized in the cytoplasm through an interaction with Kelch ECH associating protein 1 (KEAP1) and the actin cytoskeleton (Kensler et al., 2007). Despite the fact that *NRF2* mRNA is constitutively expressed, KEAP1 targets NRF2 for polyubiquitination and degradation, resulting in a short protein half-life and, consequently, in the low basal expression of the cytoprotective enzymes and proteins in quiescent cells under normal physiological conditions (Kensler et al., 2007). During exposure to electrophiles or oxidative stress, KEAP1 becomes oxidized at

critical cysteine residues. As a result, NRF2 escapes KEAP1 control and translocates to the nucleus, where it dimerizes with small musculoaponeurotic fibrosarcoma (MAF) proteins and promotes the expression of ARE-containing genes (Kansanen et al., 2012; Suzuki et al., 2013). The binding to and regulation of NRF2 by KEAP1 have been explained by a “hinge and latch model” (Tong et al., 2006), as described in **Figure 7**.

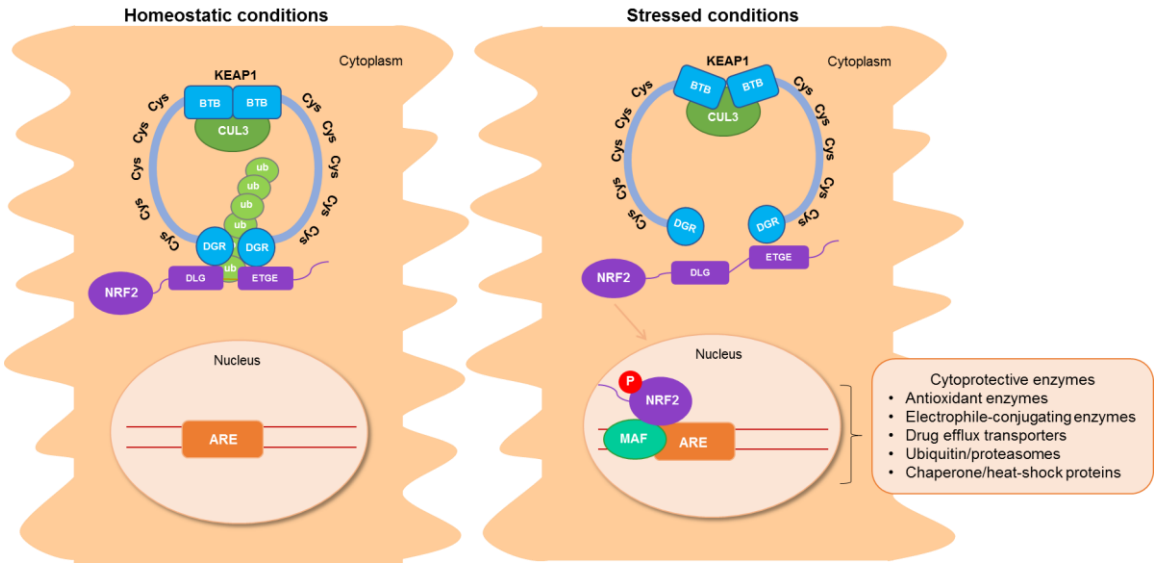

Figure 7. Activation of the KEAP1-NRF2-ARE pathway by oxidants/electrophiles. Under homeostatic conditions, NRF2 is mainly localized in the cytoplasm through an interaction with KEAP1 and the actin cytoskeleton. KEAP1 is a five-domain protein consisting of an N-terminal broad complex, Tramtrack and Bric-à-brac (BTB) domain, an intervening region with cysteine (Cys) residues, a C-terminal Kelch domain with double glycine repeats (DGR), and the C-terminal domain. KEAP1 homodimerizes at the BTB domain, which is also a binding site for Cullin 3 (Cul3). The KEAP1 homodimer binds to a single NRF2 molecule through the ETGE and DLG motifs of NRF2, each binding to a DGR domain in KEAP1. According to the proposed hinge and latch model (Tong et al., 2006), ETGE is a high-affinity motif (“hinge”) whereas DLG is a low-affinity one (“latch”). KEAP1 functions as an adaptor protein in the Cul3-based E3 ligase complex, which results in the polyubiquitination (Ub) of the lysine residues situated between the DLG and ETGE motifs, and subsequent proteasomic degradation of NRF2. Under stressed conditions, the modification of critical cysteine residues of KEAP1 destabilizes its binding to the DLG motif of NRF2, which blocks ubiquitination/proteasomal degradation and allows NRF2 to escape KEAP1 control and translocate into the nucleus. In the nucleus, NRF2 heterodimerizes with small MAF proteins and promotes the expression of ARE-containing genes involved in cell stress response, drug metabolism, detoxification, and transport. NRF2 may also be phosphorylated (P) by stress-activated kinases.

3.2.1. NRF2 target genes

Through the study of NRF2 target genes and pathways in mouse models, NRF2 was found to regulate the susceptibility to diseases. Besides, clustering of the NRF2-dependent upregulated genes in response to stress has revealed pathways involved in xenobiotic detoxification and antioxidant response (Kensler et al., 2007). Some of the genes upregulated by NRF2 are NAD(P)H:quinone oxireductase 1 (*NQO1*), heme oxygenase 1 (*HO-1*), glutamate-cysteine ligase (*GCL*) and glutathione-S-transferases (*GSTs*) (Klaassen and Reisman, 2010). These genes encode antioxidant and detoxifying

enzymes that are involved in ROS scavenging and in xenobiotics detoxification, in order to diminish cell damage. NRF2 also regulates the expression of transporters involved in the drug efflux (Klaassen and Reisman, 2010).

3.2.2. NRF2, a key protector against liver iron toxicity

NRF2 was recently shown to protect liver cells against iron toxicity *in vitro* and *in vivo*. Primary hepatocyte cultures from wild-type (WT) mice supplemented with ferric ammonium citrate (FAC, a source of inorganic iron that mimics NTBI found in the plasma of HH patients) showed increased levels of NRF2 in the nuclei, which was associated with the induction of cytoprotective genes (*Nqo1*, *Gclc* and *Gsta1*) in an NRF2-dependent manner. Moreover, FAC lead to a dose-dependent reduction in the activity of mitochondrial dehydrogenases in *Nrf2*$^{-/-}$ but not in WT hepatocytes. Authors suggested that *Nrf2*$^{-/-}$ cells are more susceptible to iron-induced oxidative stress than their WT counterparts, since iron increased 8-hydroxyguanine DNA glycosylase 1-sensitive sites (a marker of oxidatively damaged DNA) exclusively in *Nrf2*$^{-/-}$ hepatocytes. Likewise, an iron-rich diet caused a significant increase in the expression of cytoprotective genes in mouse liver in an NRF2-dependent manner. In this model of acute iron overload, *Nrf2*$^{-/-}$ mice displayed elevated activity of the serum transaminases alanine aminotransferase (ALT) and aspartate aminotransferase (AST) (enzymes released by injured hepatocytes), mitochondrial injury and oxidatively damaged DNA. The authors have also demonstrated that mito-TEMPOL, an antioxidant targeted to the mitochondria, abrogates the hepatotoxicity of dietary iron towards *Nrf2*$^{-/-}$ animals (Silva-Gomes et al., 2014).

3.2.3. *Nrf2* polymorfisms

The use of *Nrf2*$^{-/-}$ mouse in model systems has provided insights into the role of NRF2 in the pathogenesis of various human disorders. Furthermore, studies have revealed strong associations between *NRF2* sequence variations and disease risks. Most of the phenotype-associated variants are in the promoter region and presumed to be involved in *NRF2* gene regulation (Cho, 2013). For example, the single nucleotide polymorphisms (SNPs) Rs6721961 (C→A) and Rs35652124 (A→G) were found to reduce the transcription activity of NRF2 (Cho, 2013), decreasing NRF2-dependent gene transcription (Shimoyama et al., 2014). These SNPs are also known to be associated with Parkinson's disease and chronic obstructive pulmonary disease, among others (Cho, 2013).

4. Aims

The importance of NRF2 in the protection against hepatic iron toxicity in a model of acute iron overload (*Nrf2*$^{-/-}$ mouse fed an iron-rich diet) was recently demonstrated by the host laboratory (Silva-Gomes et al. 2014). This prompted us to study the effect of *Nrf2* suppression in a model of chronic iron overload that mimics human HH, the *Hfe*$^{-/-}$ mouse. The group has generated a double knock-out mouse for *Hfe* and *Nrf2* genes and investigated the potential occurrence of spontaneous liver injury in mice of 6-18 months of age, when comparing with wild-type and single knock-out animals. Previous results from the group revealed that, in the absence of NRF2, the mild hepatic iron overload observed in *Hfe*$^{-/-}$ mouse associated with increased necroinflammation, macrophage iron deposits and fibrosis along with ageing. This suggested that the pathology is age-dependent, which is compatible with the late onset of HH. The main aim of this work is to determine whether NRF2 acts as a modifier of the clinical expression of HH.

- By studying 24 months old *Hfe/Nrf2*$^{-/-}$ mice, we expect to determine if the lack of functional NRF2 signaling prompts the mouse model of HH to develop spontaneous fibrosis in aged individuals.
- We also expect to identify polymorphisms/genotypes in the human *NRF2* gene promoter that may influence disease penetrance in C282Y$^{+/+}$ patients.

This could increase current understanding of the role of NRF2 in the protection against hepatic iron toxicity, and help determine the risk of an HH patient developing iron overload-related liver disease.

Material and Methods

1. Animal study

1.1. Animals

Female wild-type (WT) (n=6), *Nrf2*$^{-/-}$ (Itoh et al., 1997) (n=8) and *Hfe*$^{-/-}$ mice (Bahram et al., 1999) (n=6) on a C57BL/6J background, and *Nrf2/Hfe*$^{-/-}$ mice generated by the group (n=7) were housed and bred at the 'Instituto de Biologia Molecular e Celular' animal facility until the age of 24 months. Mice were fed standard rodent chow (*Mucedola 4RF21*-GLP containing 480 mg/kg iron) *ad libitum* and were overnight fasted before sacrifice. Animals were anesthetized with isofluorane (B. Braun, Portugal) and blood was collected by retro-orbital bleeding. After performing cervical dislocation, mice were dissected for organ collection: tail, liver, spleen, pancreas and kidneys. Tissues were snap-frozen in liquid nitrogen and stored at -80 °C for subsequent RNA extraction and quantification of non-heme iron. Body, spleen and liver weight were determined.

The entire experiment was carried out in compliance with the recommendations of the European Convention for the Protection of Vertebrate Animals used for Experimental and Other Scientific Purposes (ETS 123) and 86/609/EEC Directive and Portuguese rules (DL 129/92). The animal experimental protocol was approved by 'Direção Geral de Alimentação Veterinária' and by the Institute's ethical committee. All researchers involved in animal processing attended a FELASA B course and the work was overseen by a researcher with FELASA C accreditation.

1.2. Hematological measurements

Blood was diluted 1:1 with 1,5% (v/v) K3-ethylenediamine tetraacetic acid (K3EDTA). Hemoglobin, red blood cell counts, hematocrit, mean corpuscular volume, mean corpuscular hemoglobin and the percentage of reticulocytes were assessed on a Coulter-S counter (Coulter Electronics, Fullerton, CA) , at a certified laboratory (Corelab, 'Centro Hospitalar do Porto', CHP, Portugal).

1.3. Serum analysis

Blood was allowed to sit for 30 min at room temperature (RT) and centrifuged at 10 000 ×g, for 10 min for serum collection. Alanine aminotransferase (ALT) activity, glucose, triglycerides and iron concentration, and the total iron-binding capacity (TIBC) were assessed on a Cobas C8000 analyzer (Roche Diagnostics, Mannheim, Germany) at the CHP Corelab. Transferrin saturation was calculated by dividing serum iron concentration

by TIBC. Serum insulin and erythropoietin (EPO) concentrations were measured using a mouse enzyme-linked immunosorbent assay (ELISA) kit (Mercodia, Sweden) and a commercially available rodent Quantikine Epo Immunoassay Kit (R&D Systems, USA), respectively. The lactate dehydrogenase activity in the serum was determined using a LDH colorimetric assay kit (Sigma-Aldrich, Germany) according to the manufacturer's protocol. The serum levels of a panel of cytokines/chemokines (GM-CSF, IFNγ, IL-1B, IL-6, IL-10, MCP-1 and TNFα) were determined with a multi-analyte detection system (Milliplex Map Kit – Mouse Cytokine/Chemokine Magnetic Bead Panel, Millipore, Germany), according to the manufacturer's instructions. Detection was performed with the xPonent software in the Luminex 200 (Luminex Corporation, USA), and data were analyzed through the MILLIPLEX Analyst software.

1.4. RNA extraction and cDNA synthesis

To isolate the total RNA from liver, spleen and kidneys, 1 mL of TRI Reagent® (Sigma-Aldrich, Germany) was added to 50-100 mg of tissue. Samples were homogenized and left at RT for 5 min. Samples were then centrifuged at 12 000 ×g for 10 min at 4°C and the cleared supernatant was transferred to a new tube. After an incubation of 5 min at RT, 200 µL of chloroform were added to the supernatant. The tubes were vigorously shaken by hand for 15 s, incubated at RT for 2-3 min and centrifuged at 12 000 ×g for 15 min at 4°C. The aqueous phase was transferred to a new tube and 500 µL of 100% (v/v) isopropanol were added. Tubes were homogenized by inversion and incubated at RT for 10 min. After a centrifugation at 12 000 ×g for 10 min at 4ºC, the supernatant was removed. The pellet was washed with 1 mL of 75% (v/v) ethanol and the tubes were vortexed and centrifuged at 7 500 ×g for 5 min at 4°C. The supernatant was removed and the pellet was air dried for 5-10 min. The RNA pellet was ressuspended in RNase-free water (Sigma-Aldrich, Germany) and incubated in a heat block at 55-60ºC for 10-15 min. RNA concentration was measured at 260 nm by a NanoDrop spectrophotometer (ThermoScientific, USA) and RNA integrity was assessed by capillary electrophoresis in Experion (Bio-Rad Laboratories, USA).

Extracted RNA was treated with DNase (*Turbo DNA-free™ kit*, Ambion, Life Technologies, USA), in order to remove contaminating genomic DNA. To a final quantity of 4 µg of RNA, 2.5 µL of 10× TURBO DNase Buffer and 1 µL of TURBO DNase were added. RNase free water was added up to a final volume of 25 µL. Samples were incubated at 37°C for 30 min and 2.5 µL of DNase Inactivation Reagent were added. After an incubation of 2 min at RT, samples were centrifuged at 10 000 ×g for 1.5 min and the RNA was transferred to a new tube.

First-strand cDNA was synthesized with the *ThermoScript RT-PCR system* (Invitrogen, Life Technologies, USA). 1 µL of Primer Oligo (dT) and 2 µL of dNTP mix were added to 9 µL of DNAse treated RNA. Samples were incubated at 65°C for 5 min and were posteriorly placed on ice. 4 µL of 5× cDNA Synthesis Buffer, 1 µL of dithiothreitol (DTT) 0,1 M, 1 µL of RNaseOUT, 1 µL of diethylpyrocarbonate (DEPC)-treated water and 1 µL of ThermoScript RT were added. Samples were incubated at 55°C for 60 min and then at 85°C for 5 min. 1 µL of RNase H was added and samples were incubated at 37°C for 20 min. Samples were diluted (1:2) with DEPC-treated water.

1.5. Real-time reverse-transcription (RT)-PCR

The relative transcription levels of selected genes in a target cDNA sample were determined by real-time polymerase chain reaction (qPCR) with the primers (STABvida, Portugal) listed in **Table 1**. PCR reactions were performed in duplicate and in a total volume of 20 µl. To each reaction, 10 µL of iQ SYBR Green Supermix (Bio-Rad Laboratories, USA), 0.08 µL of each primer from a stock solution at 50 µM, 8.84 µL of RNase free water and 1 µL of cDNA were added. PCR was performed in the iQ5 Real-Time PCR system (Bio-Rad) with the following amplification conditions: denaturation at 95°C for 4 min and 40 cycles of 94°C for 30 s, annealing at 59-61°C for 45 s, and extension at 72°C for 30 s. A standard curve, based on a serial dilution (1, 1:10 and 1:100) of a previously prepared liver cDNA pool, was performed for each gene. The quantity of each transcript was estimated against the respective standard curve and normalized against the quantity of the endogenous control gene hypoxanthine phosphoribosyltransferase (*Hprt*). The specificity of the PCR reaction and the absence of primer dimers were confirmed by melting curve analysis.

1.6. Quantification of non-heme iron

Non-heme iron in liver, spleen and kidney tissues stored at -80°C was measured by the bathophenanthroline method (Torrence and Bothwell, 1980). Tissue samples weighting approximately 100 mg were dried in a microwave oven (MDS 2000, CEM), in iron-free Teflon vessels (ACV-Advanced Composite Vessel; CEM, Mathews, NC). After determining dry tissue weights, samples were digested in 1 mL of acidic mixture [0.1 g/mL hydrochloric acid and 822 µL/mL trichloroacetic acid 37% (v/v)] for 20 h at 65°C. 1mL of chromogen reagent [5 volumes of deionized water, 5 volumes of saturated sodium acetate and 1 volume of 0.1% (w/v) bathophenanthroline sulfonate and 1% (v/v) thioglycolic acid] and 275 or 250 µL of deonised water were added to 25 (liver) or 50 µL (spleen and kidney) of the supernatant obtained in the digestion reaction. The standard

solution was prepared with 1 mL of chromogen reagent, 150 µL of deonised water and 150 µL of a stock iron standard solution [22.3 mg carbonyl iron powder, 1096 µL hydrochloric acid 36.5% (v/v) and deonised water to a final volume of 20 mL]. A colored product was obtained and the absorbance was measured spectrophotometrically at 535 nm with a µQuant equipment (BioTek, Germany).

Table 1. Sequences of the oligonucleotide primers used in qRT-PCR and the respective annealing temperatures.

Gene	Primer Forward (5' → 3')	Primer Reverse (5' → 3')	Ta (ºC)
Hprt[a]	AGATGGGAGGCCATCACATTGT	ATGTCCCCCGTTGACTGATCAT	59
Hamp[b]	CATGTTCCAGAGGCGAAGGAGG	GCAGCACATCCCACACTTTGATC	59
Acta2[c]	ACCCAGCACCATGAAGATCAAG	AGGTAGACAGCGAAGCCAGGA	59
Nqo1[c]	GTGCAGAAGCGAGCTGGAAATACTC	CGAATCTTGATGGAGGACTGGATGC	59
Col1a[c]	TCCTGGCAACAAAGGAGACAC	GGGCTCCTCGTTTTCCTTCT	59
Timp1[c]	CATCTGGCATCCTCTTGTTGCT	AAGGTGGTCTCGTTGATTTCTGG	59
Ccl2[c]	ATGATCCCAATGAGTAGGCTGGAG	GACCTCTCTCTTGAGCTTGGTGAC	59
Tnf-α[c]	CTGTAGCCCACGTCGTAGCA	CGGCAGAGAGGAGGTTGACT	59
Il-6[d]	CTGCAAGAGACTTCCATCCAG	AGTGGTATAGACAGGTCTGTTGG	60
Spic[c]	AAAGGGAGGAAGAGGCAGGAG	CCCAGAGTTCAGCGAGTGTTTC	59
G6pc[c]	CAATCTCCTCTGGGTGGCAGT	GCTGTTGCTGTAGTAGTCGGTGTCC	59
Pepck[c]	ATGCGACCCTTCTTCGGCTAC	GAACTTGCCATCTTTGTCCTTCC	59
Hmox1[c]	GAAGGGTCAGGTGTCCAGAGAAGG	CGCTCTATCTCCTCTTCCAGGGC	61
F4/80[e]	CTTTGGCTATGGGCTTCCAGTC	GCAAGGAGGACAGAGTTTATCGTG	59
Epo[c]	AATTCCTCCCAGCCACCAGAGA	AGACCCGGAAGAGCTTGCAGAA	59

a. (Silva-Gomes et al., 2014); **b.** (Ilyin et al., 2003); **c.** Designed with Primer 3 software (Rozen and Skaletsky, 2000); **d.** Kindly supplied by Tânia Cruz; **e.** (Wan et al., 2014); **Ta** = annealing temperature.

1.7. Histological analysis

Liver, spleen, pancreas, kidney and heart samples were fixed with 10% formalin for 24 h, dehydrated and embedded in paraffin. Three micrometer-thick sections of each organ were obtained and dried overnight at 37°C. Prior to each staining, sections were immersed twice in xylene for 10 min at room temperature, passed through descending concentrations of ethanol [100% (v/v), 96% (v/v), 70% (v/v) and 50% (v/v), each 5 min] and washed three times in distilled water for 5 min each. After the coloration, sections were dehydrated in ascending concentrations of ethanol and cleared in xylene for 10 min. Sections were covered with Entellan mounting medium (Merck, Germany) and a glass cover slip. Microscope slides were observed on a Light Microscope Olympus CX31

and photos were captured with a DP-25 Camera (Imaging Software Cell^B). All slides were examined by the same observer, in a blind manner (i.e. with no previous knowledge of the animals' genotypes).

1.7.1. Hematoxylin and eosin staining

Standard hematoxylin and eosin staining (H&E) was applied to all tissues to make a histopathological assessment of the preparations. Hydrated sections were immersed in Gill's Hematoxylin (Merck, Germany), rinsed in tap water and immersed in eosin (Merck, Germany) for 5 min each. Finally, sections were rinsed in tap water for 30 s. Liver sections were graded according to steatosis, inflammation and necrosis. Steatosis was graded as absent (<5%), light (5%–33%), moderate (>33%–66%), or severe (>66%) according to the amount of parenchyma affected. The assessment of steatosis grading was made at low magnification (4× and 10× objectives) and it considered only the portion of the liver section occupied by the hepatocytes (ignoring large bands of fibrosis, portal areas, vein profiles, etc.). The zonal distribution of steatosis was categorized into four patterns: zone 3 predominant, zone 1 predominant, pan-acinar or azonal (Chalasani et al., 2008). Lobular inflammation was divided into four categories, according to the number of visible foci at 10× objective: no foci, <4 foci, 4-8 foci, >8 per 100× field (Kleiner et al., 2005). Necrosis was graded as absent, spotty necrosis (one or a few necrotic hepatocytes), confluent necrosis and bridging necrosis.

1.7.2. Sirius red staining

Sirius red staining was applied to the liver sections, in order to evaluate the fibrotic area. Nuclei were stained with Mayer's hematoxylin (Sigma-Aldrich, Germany) for 8 min and sections were washed under running tap water for 5 min. Sections were then stained with a 0.1% (v/v) solution of Sirius red F3BA [Direct Red 80 (Sigma-Aldrich, Germany) in saturated aqueous solution of picric acid] for one hour at RT and rinsed two times in a 0.5% (v/v) HCl solution.

Fibrosis was graded as none (0), mild/moderate in zone 3, portal/periportal only (1), portal/periportal and perisinusoidal (2) bridging fibrosis (3) and cirrhosis (4) (Kleiner et al., 2005). The fibrotic area was then evaluated with a light microscope fitted with a polarisation filter, which renders the staining specific for type I collagen. Three random microscope fields of the liver, excluding regions of the capsule and the large portal tracts, were captured at 100× magnification and saved as .TIF files. Images were then analyzed using ImageJ software. Red Green Blue (RGB) stack type was selected and upper and

lower thresholds were defined to avoid pixel saturation. These remained unaltered during the measurement of the percentage of fibrotic area in a whole batch of images.

1.7.3. Perls' Prussian Blue staining

The presence of iron deposits in the different organs was assessed by Perls' Prussian Blue staining. Sections were stained with Perls solution [equal parts of 2% (w/v) potassium ferrocyanide and 2% (v/v) hydrochloric acid 37% (v/v)] for 30 min and washed in several changes of distilled water for 5 min. The sections were counterstained with Neutral Red [1 g Neutral Red (Sigma-Aldrich, Germany), 100 mL distilled water and 1 mL glacial acetic acid] for 1 min and rinsed in distilled water. Siderosis was graded according to the size of iron deposits, as well as their cellular and lobular location. Grading consisted in three scores: hepatocytic (ranging 0-36), sinusoidal (ranging 0-12) and portal (ranging 0-12). Hepatocytic iron was graded as 0 (absence of iron), 3 (faint staining), 6 (nonconfluent granules), 9 (confluent deposits) or 12 (large masses) according to granules size in each Rappaport area. Sinusoidal iron was graded as 0 (absence of iron), 1 (faint staining), 2 (small granules), 3 (large deposits) or 4 (clusters of overload cells) according to granules size in each Rappaport area. Portal iron was graded as 0 (absence of iron), 1 (deposits in < 1/3 of the portal tracts), 2 (deposits in 1/3 of the portal tracts), 3 (deposits in 2/3 of the portal tracts) or 4 (deposits in all portal tracts) according to the percentage of iron overloaded macrophages, biliary cells and vascular walls (Deugnier et al., 1993).

1.7.4. TUNEL assay

DNA fragmentation resulting from apoptotic cell death was determined by Terminal deoxynucleotidyl transferase (TdT) dUTP Nick-End Labeling (TUNEL) assay. Following dehydration, liver sections were washed in phosphate buffered saline (PBS) for 5 min. Sections were then incubated with proteinase K (20 µg/mL) in Tris-HCl 10mM for 20 min at 37ºC and for 10 min at RT and washed 2 times in PBS 1×. Microscope slides were incubated with the TUNEL reagents (50 µL Enzyme Solution and 450 µL Label solution) of the *In Situ Death Detection Kit, Fluorescein* (Roche Diagnostics, Germany) for 1 h at 37ºC. Sections were then washed 3 times in PBS 1×. Finally, sections were incubated with 0,2 µg/mL 4',6-diamidino-2-phenylindole (DAPI) in the dark for 15 min at RT. The microscope slides were mounted with Vectacshield (Vector Laboratories, USA) and sealed with nail polish. Ten random microscope fields of each liver were obtained with a 40× objective and the number of TUNEL-positive cells was counted. As a positive control, liver sections were treated with DNase.

1.8. Evaluation of oxidative stress

To evaluate oxidative stress parameters in the liver, a small portion of this organ was homogenized in a homogenizing solution [0.85 g KH_2PO_4 25 mM, 2.67 g $Na_2HPO_4.2H_2O$ 30 mM, 0.25 mL Triton X-100 0,1% (v/v) to a final volume of 250 mL, pH 7,0] in the proportion of 2 mL of solution per gram of fresh weight. Total protein was quantified with the *DC™ Protein Assay* (Bio-Rad, USA) as per the manufacturer's instructions and the homogenate was used for the following assays.

1.8.1. Thiobarbituric Acid Reactive Substances (TBARS) assay

100 µL of the homogenate were diluted with 200 µL of 10% (v/v) trichloroacetic acid (TCA). The dilution was vortexed and centrifuged at 6 000 rpm for 1 min at 4ºC. 200 µL of the diluted homogenate were incubated with 200 µL of 1% (w/v) thiobarbituric acid in a water bath at 95ºC for 40 min. After cooling down, the absorbance at 535 nm was measured in a spectrophotometer. The malondialdehyde (MDA) standard curve was calculated against previously determined values (Professor Maria João Martins, personal communication).

1.8.2. Quantification of the GSH/GSSG ratio

The homogenate obtained in **1.8.** was centrifuged at 13 000 rpm for 10 min at 4ºC. The supernatant was diluted with an equal part of 10% (v/v) perchloric acid (PCA) and centrifuged at 13 000 rpm for 2 min at 4ºC. 20 µL of the supernatant were utilized to quantify the total glutathione (GSX) and 200 µL to quantify the oxidized form (GSSG). The reduced form (GSH) was calculated as follows:

$$GSH = GSX - 2 \times GSSG$$

1.8.2.1. Quantification of the total gluthatione

20 µL of the supernatant obtained in **1.8.2.** were diluted 10 times with 5% (v/v) PCA in phosphate solution (10.2 g of $Na_2HPO_4.2H_2O$ 57.3 mM, 11.2 g of $NaH_2PO_4.H_2O$ 81.2 mM and 0.23 g dissodic EDTA 0.62 mM to a final volume of 1 L, pH 7,5). 200 µL of $KHCO_3$ 0.076 M were added and the tubes were vortexed and centrifuged at 13 000 rpm for 1 min at 4ºC. 100 µL of the supernatant were transferred into a 96-well plate in triplicate and 65 µL of the reagent solution (3.42 mg of NADPH 3.36 mM, 4.68 mg of DTNB 20 mM to a final volume of 3 mL in phosphate solution) were added. The plate was incubated for 15 min at 30ºC, protected from light. 40 µL of the glutathione reductase solution (10 units per mL of phosphate solution) were added and the absorbance at 405 nm was measured for 3 min. The trendline equation was defined.

1.8.2.2. Quantification of GSSG

200 µL of the supernatant obtained in **1.8.2.** were incubated with 10 µL of 2-vinylpyridine for 1 h at 4ºC with agitation. After adding 200 µL of 0.076 M $KHCO_3$, samples were vortexed and centrifuged at 13 000 rpm for 1 min at 4ºC. 100 µL of the supernatant were added into a 96-well plate and 65 µL of the reagent solution were added. The plate was incubated for 15 min at 30ºC, protected from light. 40 µL of the glutathione reductase solution were added and the absorbance at 405 nm was measured for 3 min. The trendline equation was defined.

1.9. Hydroxyproline Assay

Liver tissue (10 mg) was homogenized in 100 µL of distilled water. Protein quantification was performed with the *DC™ Protein Assay Kit* (Bio-Rad, USA). The quantity of hydroxyproline was determined with the Hydroxyproline Assay Kit (Sigma-Aldrich, Germany) following the manufacturer's instructions.

2. Human study

2.1. Patients

The human study was performed with stored DNA samples from Hereditary Hemochromatosis (HH) patients who had been referred to the CGPP laboratory Biobank for diagnosis. Samples were selected by the following criteria: 1) confirmed homozygosity for the *HFE* C282Y mutation; 2) a written informed consent from the patients allowing the use of their DNA samples for research purposes; 3) available stored DNA in good quality and sufficient quantity for the purpose of the study. From the 106 samples fulfilling these criteria, 67 were from patients referred from the HH clinics at the Hematology Service, Centro Hospitalar do Porto (CHP), and regularly followed up by Dr. Graça Porto, the clinician in charge at the HH clinic, and co-supervisor of this project. The availability of complete clinical information from this group of patients allowed us to use it for the clinical correlations study, after excluding putative confounding variables (see below in statistical analysis). The remaining 39 DNA samples were from patients referred for diagnosis by other external services and no complete clinical information was available, reason why they were not included in the clinical correlations study. Retrieved clinical data were anonymized and confidentiality was maintained during the whole analytical process according to Helsinki Declaration and Portuguese Law. The study received ethical approval by the CHP Ethics committee.

The general characteristics and the clinical manifestations of the 67 patients selected for the clinical correlation study are presented in **Table 2**.

Table 2. Patients' general characteristics and frequency of clinical manifestations.

	Males	Females	Total
n	42	25	67
Age	43 ± 12	46 ± 11.3	44 ± 12
Ferritin (ng/mL)	2201 ± 1795	902 ± 893	1716 ± 1641
TfSat (%)	82 ± 20	79 ± 16.2	80.5 ± 18.4
TBIS (g)	7.3 ± 4.8[a]	4.5 ± 3.4[b]	6.4 ± 4.5[c]
Mode of presentation (clinical diagnosis/family screening)	21/21	17/8	38/29
HCV+	1/42 (2.4%)	0/25	1/67 (1.5%)
Related individuals	5/42 (11.9%)	4/25 (16%)	9/67 (13.4%)
Frequency of clinical manifestation			
Skin pigmentation	8/42 (19%)	4/25 (16%)	12/67 (17.9%)
Diabetes	3/42 (7.1%)	0/25	3/67 (4.5%)
Hypoganadism	1/42 (2.4%)	0/25	1/67 (1.5%)
Arthropathy	5/42 (11.9%)	6/25 (24%)	11/67 (16.4%)
Chirrosis	9/42 (21.4%)	3/25 (12%)	12/67 (17.9%)

Mean ± standard deviation. TfSat (%): transferrin saturation. TBIS: total body iron stores. HCV+: Hepatitis C virus positive. [a]available in 31 only; [b]available in 14 only; [c]available in 45 only.

2.2. *NRF2* genotyping

Genotyping of known SNPs of the promoter region of the transcription factor NRF2 was performed by PCR amplification of a fragment of 284 bp using the forward primer 5'-GCG TGG TGG CTG CGC TTT-3' and the reverse primer 5'-CCG TGC CAC TGC CAA CTG C-3' (STABVida, Portugal). The PCR reaction consisted of 10 µL: 5 µL of master mix HotStarTaq Plus DNA Polymerase (*Type-it® Microsatellite PCR Kit*, Qiagen, Germany), 0.5 µL of primer forward 10 µM, 0.5 µL of primer reverse 10 µM and 1 µL of DNA in a concentration of 50 ng/µL. The amplification conditions were as follows: denaturation at 95°C for 5 min and 40 cycles of 95°C for 30 s, annealing at 63°C for 30 s, and extension at 72°C for 30 s with a final extension at 60ºC for 30 min.

The PCR fragment was genotyped at the CGPP laboratory by capillary electrophoresis (Sanger sequencing). The total sequencing reaction consisted of 8 µL: 2 µL of *BigDye® Terminator v1.1 Cycle Sequencing Kit* (Applied Biosystems, USA), 0.5 µL of 10 µM forward primer, 2.5 µL of purified PCR product and 3 µL of distilled water.

The amplification conditions were as follows: denaturation at 95°C for 5 min and 35 cycles of 96°C for 10 s, annealing at 50°C for 5 s, and extension at 60°C for 4 min. Samples were injected in the ABI 3130xl Genetic Analyzer (Applied Biosystems, USA) and the final product was precipitated in DyeEx 96 well plates (Qiagen, Germany). After sequencing the fragment, the Rs35652124, Rs670664, Rs150648896 and Rs6721961 SNPs in the *NRF2* promoter region were determined using the ProSeq3 software.

2.3. Datafile collection

For the purpose of statistical analysis, a datafile was created including, besides the genetic information obtained, the following patients' clinical information: gender and age at diagnosis, the systemic iron parameters serum ferritin, transferrin saturation; hematological parameters including the numbers of CD8+ T lymphocytes; the total body iron stores (TBIS) and/or hepatic iron concentration (HIC) assessed trough a liver biopsy or magnetic resonance imaging. The severity of the iron overload was graded according to the levels of TBIS (or HIC): >2 g (or >300µmol/g of HIC) corresponding to grade 1 (light overload), 2-4 g to grade 2 (moderate) and >4 g to grade 3 (severe). The presence or absence of the other clinical manifestations, such as skin pigmentation, diabetes, cirrhosis, hypogonadism and arthropathy was also registered.

3. Statistical analysis

3.1. Animal study

Results are presented as the mean and standard deviation. Unless stated otherwise, differences among multiple groups were compared by one-way analysis of variance (ANOVA) with Tukey's multiple comparison test using GraphPad Prism version 6.0 for Windows (GraphPad Software, California USA). The results were considered statistically significant when $p<0.05$.

3.2. Human study

Gene allele or genotype frequencies were estimated in unrelated individuals only (n = 97). For analyses of genotype/phenotype correlations we first selected the 67 patients regularly followed up at HH clinics at CHP and in whom complete clinical information was available. Further exclusion criteria included: viral infection, such as hepatitis and human immunodeficiency virus (HIV), auto-immune disease and alcoholic liver disease (n = 57). Given the small sample size, group analysis were restricted to some of the most frequent clinical manifestations of HH, namely cirrhosis, arthropathy, or symptomatic patients, who presented with clinical evidence of at least one of the following disease

manifestations: skin pigmentation, diabetes, hypogonadism, arthropathy, cirrhosis, and/or documented severe iron overload (serum ferritin > 2000 and TBIS > 5 g). For the purpose of analyzing the impact of particular genotypes on the clinical expression, namely on the frequency of liver cirrhosis, more strict clinical criteria were used. Given the low probability of clinical expression in asymptomatic, early diagnosed, females or young males (<30 years of age), these subjects were excluded from analysis. In addition, patients with severe iron overload but in whom a liver biopsy was not available (and thus the presence of cirrhosis could not be excluded) were also excluded (n = 36).

Quantitative results are presented as the mean and standard deviation. In order to fit into a normal distribution, serum ferritin values were logarithmic transformed. Differences between groups were compared by the Student´s t-test. The Chi-square test was applied to test the differences in allele and genotype frequencies. Data were analyzed using GraphPad Prism version 6.0 for Windows (GraphPad Software, California USA) and statistical significance accepted at $p \leq 0.05$.

Results

Animal study

1. Body, liver and spleen weights

The body weight of each animal was determined prior to sacrifice. *Nrf2/Hfe*$^{-/-}$ mice presented significantly decreased body weight compared to WT ($p<0.05$) and *Hfe*$^{-/-}$ ($p<0.0001$) mice **(Figure 8.A)**. Spleen and liver weights were also registered and their relative weights were calculated by dividing organ weight by body weight. No significant differences in relative liver and spleen weights were found **(Figure 8.B and 8.C)**.

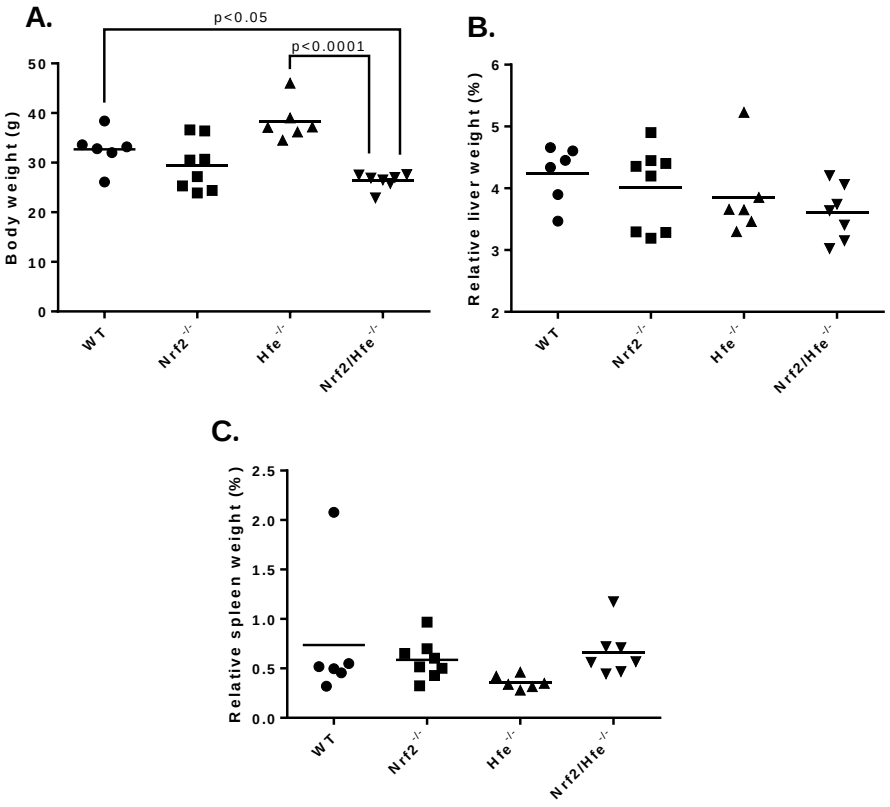

Figure 8. (A) Body weight and (B) percentage of relative liver and (C) spleen weights of WT, *Nrf2*$^{-/-}$, *Hfe*$^{-/-}$ and *Nrf2/Hfe*$^{-/-}$ mice.

2. Hematological parameters

The number of red blood cells (RBC) was significantly lower in *Nrf2/Hfe*$^{-/-}$ mice when compared to WT ($p<0.001$), *Nrf2*$^{-/-}$ ($p<0.01$) and *Hfe*$^{-/-}$ ($p<0.0001$) mice. Hemoglobin (Hb) was also significantly lower in *Nrf2/Hfe*$^{-/-}$ mice when compared to WT, *Nrf2*$^{-/-}$ ($p<0.05$) and *Hfe*$^{-/-}$ ($p<0.0001$) mice. *Nrf2/Hfe*$^{-/-}$ mice also presented a significantly decreased hematocrit (HCT) when compared to *Nrf2*$^{-/-}$ ($p<0.05$) and *Hfe*$^{-/-}$ ($p<0.0001$) mice **(Table 3)**. These data reveal that *Nrf2/Hfe*$^{-/-}$ mice were mildly anemic. This is in contrast with

Hfe$^{-/-}$ mice, which exhibited significantly higher levels of Hb and HCT when compared to their WT counterparts (p<0.05) **(Table 3)**.

In *Nrf2*$^{-/-}$ and *Nrf2/Hfe*$^{-/-}$ mice, the mean corpuscular volume (MCV) was significantly increased when compared to WT mice (p<0.05 and p<0.001, respectively. The mean corpuscular hemoglobin (MCH) was significantly increased in *Nrf2/Hfe*$^{-/-}$ mice when compared to WT (p<0.0001) and to *Nrf2*$^{-/-}$ (p<0.001) mice. *Hfe*$^{-/-}$ mice also showed a significantly higher MCH than WT (p<0.001) mice **(Table 3)**. Overall, the data suggest that the anemia of *Nrf2/Hfe*$^{-/-}$ mice is macrocytic and normochromic.

Reticulocytes are the earliest erythrocytes released into the bloodstream. Because they have a shorter life span (1 or 2 days) in the circulation compared to mature RBC (120 days), the reticulocyte parameters are reliable tools to evaluate the bone marrow erythroid activity (Velasco-Rodriguez et al., 2015). Results revealed a trend for increased percentage of reticulocytes in *Nrf2/Hfe*$^{-/-}$ mice **(Table 3)**. This indicates that the bone marrow was responding to the anemia, which suggests that the anemia of *Nrf2/Hfe*$^{-/-}$ mice is regenerative.

Table 3. Hematological parameters of WT, *Nrf2*$^{-/-}$, *Hfe*$^{-/-}$ and *Nrf2/Hfe*$^{-/-}$ mice.

	WT	***Nrf2*$^{-/-}$**	***Hfe*$^{-/-}$**	***Nrf2/Hfe*$^{-/-}$**
N	6	8	6	7
RBC (x10^6/µL)	8.9 ± 0.6	8.5 ± 0.7	9.3 ± 0.2	7.1 ± 0.8^{a,b,c}
Hb (g/dL)	13.3 ± 0.9	13.1 ± 0.9	15.1 ± 0.4^{d}	11.6 ± 1.3^{c,d,e}
HCT (%)	43.2 ± 3.1	44.6 ± 2.8	49.0 ± 2.1^{d}	39.3 ± 3.6^{c,e}
MCV (fL)	48.4 ± 1.6	52.8 ± 3.6^{d}	52.6 ± 1.2	56.0 ± 3.2^{a}
MCH (pg)	15.0 ± 0.5	15.5 ± 0.5	16.2 ± 0.1^{a}	16.4 ± 0.4^{f,g}
N	3	4	2	3
Reticulocytes (%)	3.7 ± 0.7	5.5 ± 1.9	4.6 ± 0.0	11.7 ± 8.9

Mean ± standard deviation. ^{a}p<0.001 vs. WT; ^{b}p<0.01 vs. *Nrf2*$^{-/-}$; ^{c}p<0.0001 vs. *Hfe*$^{-/-}$; ^{d}p<0.05 vs. WT; ^{e}p<0.05 vs. *Nrf2*$^{-/-}$; ^{f}p<0.0001 vs. WT; ^{g}p<0.001 vs. *Nrf2*$^{-/-}$.

3. Characterization of the anemia of *Nrf2/Hfe*$^{-/-}$ mice

To discover the possible cause of the anemia, several parameters were measured. Erythropoietin is a glycoprotein, produced by the kidney, essential for RBC production (Chateauvieux et al., 2011). We noted a trend for augmented transcript levels of *Epo* gene in the kidney and EPO levels in the serum of *Nrf2/Hfe*$^{-/-}$ mice **(Figure 9.A and 9.B)**.

On the other hand, serum lactate dehydrogenase (LDH) activity, a clinical marker of RBC hemolysis (Kato et al., 2006), was not altered in any of the four genotypes **(Figure 9.C)**.

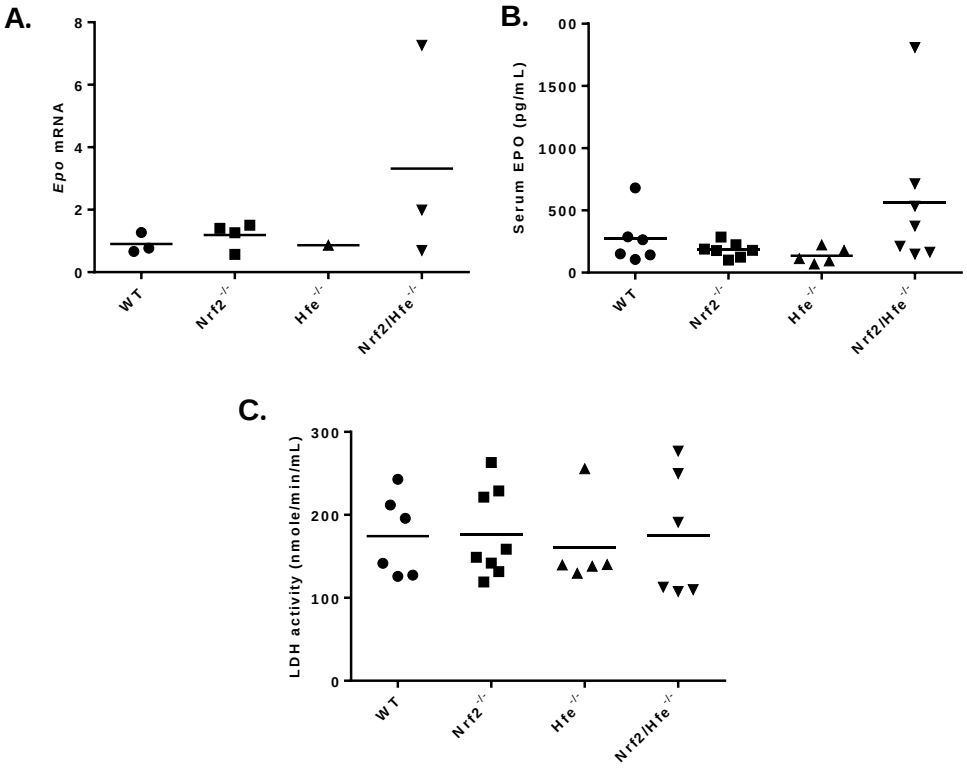

Figure 9. EPO levels and LDH activity in WT, *Nrf2*$^{-/-}$, *Hfe*$^{-/-}$ and *Nrf2/Hfe*$^{-/-}$ mice. (A) Transcript levels of *Epo* gene were measured in the kidney. (B) Levels of EPO and (C) LDH activity were measured in the serum.

In adult mice, erythropoiesis occurs in bone marrow and splenic red pulp (Sadahira and Mori, 1999). Macrophages have been postulated to function as nursing cells for the development and differentiation of erythroid cells (Bernard, 1991), so we decided to determine the transcription levels of *Spic* and *F4/80* genes in the spleen. Steady-state levels of *F4/80*, a cell-surface antigen expressed in tissue macrophages (Austyn and Gordon, 1981), were augmented in *Nrf2*$^{-/-}$ mice when compared to WT and *Nrf2/Hfe*$^{-/-}$ mice ($p<0.05$) **(Figure 10.A)**. *Spic*, which controls the development of red pulp macrophages, a splenic subset that removes senescent red blood cells (Gordon and Taylor, 2005), did not show statistically significant differences in its transcript levels in the spleen **(Figure 10.B)**. The transcript level of *Spic* was also assessed in the liver. Accordingly, no significant differences were detected **(Figure 10.C)**. Macrophages destroy aged or damaged red blood cells, but they need HO-1 to detoxify the heme released from the breakdown of the engulfed erythrocytes (Kovtunovych et al., 2010). Besides, *Hmox1* gene dosage has been implicated in the response of the hematopoietic system to stress (Fraser et al., 2011). We determined the transcript levels of *Hmox1*

gene in the liver and spleen and found no statistically significant difference **(Figure 10.D and 10.E)**.

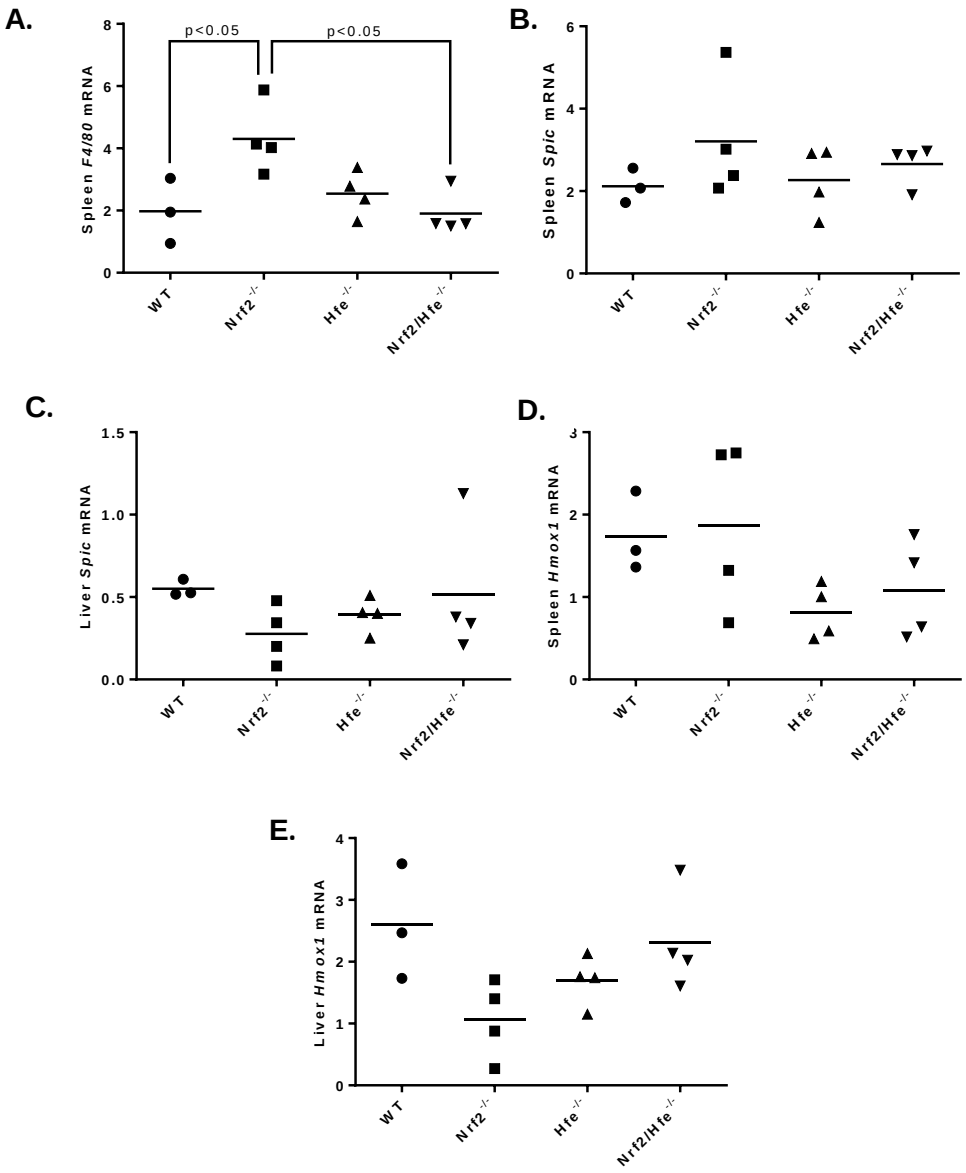

Figure 10. Expression of macrophages-associated genes in liver and spleen of WT, *Nrf2*$^{-/-}$, *Hfe*$^{-/-}$ and *Nrf2/Hfe*$^{-/-}$ mice. (A) Transcript levels of *F4/80* gene were measured in the spleen. (B) Transcript levels of *Spic* gene were measured in the spleen and (C) liver. (D) Transcript levels of *Hmox1* gene were measured in the spleen and (E) liver.

Since the mice employed in the present study were old (24 months of age), we considered important to investigate the possibility of an anemia of inflammation, which is why we evaluated a panel of proinflammatory cytokines/chemokines in the mouse serum. The levels of five cytokines (GM-CSF, IL-1b, IL-6, IL-10 and TNF-α) and one chemokine (MCP-1) exhibited no statistically significant difference between the four genotypes. However, IFN-γ was significantly augmented in *Nrf2*$^{-/-}$ mice in comparison to WT mice. **(Table 4)**.

Table 4. Levels of cytokines and chemokines in the serum of WT, *Nrf2*$^{-/-}$, *Hfe*$^{-/-}$ and *Nrf2/Hfe*$^{-/-}$ mice.

		WT	***Nrf2*$^{-/-}$**	***Hfe*$^{-/-}$**	***Nrf2/Hfe*$^{-/-}$**
Analyte (pg/mL)	**N**	6	8	5	7
	GM-CSF	0 ± 0	164.0 ± 213.2	142.9 ± 198.6	137.9 ± 263.3
	IFN-γ	0 ± 0	154.1 ± 252.4*	78.3 ± 108.1	69.19 ± 109.6
	IL-1b	6.0 ± 12.2	429.0 ± 802.0	10.7 ± 12.9	130.7 ± 343.0
	IL-6	23.4 ± 27.3	59.3 ± 68.9	15.2 ± 13.0	57.3 ± 55.4
	IL-10	0.4 ± 0.6	94.0 ± 164.7	6.6 ± 10.5	25.5 ± 52.4
	MCP-1	70.4 ± 46.0	396.5 ± 718.1	41.5 ± 38.9	200.5 ± 465.2
	TNFα	4.7 ± 3.5	44.3 ± 86.4	2.6 ± 2.6	25.1 ± 56.7

Mean ± standard deviation. *p=0.0359 vs. WT (non-parametric Kruskal-Wallis test with Dunn's multiple comparisons test)

4. Serum analysis

Serum analysis revealed that *Nrf2/Hfe*$^{-/-}$ mice were hypoglycemic, as they presented a significantly lower quantity of glucose in the serum at starvation compared to *Nrf2*$^{-/-}$ ($p<0.05$) and *Hfe*$^{-/-}$ ($p<0.01$) mice. The serum levels of triglycerides were not statistically different between the four genotypes **(Table 5)**.

Insulin, an anabolic pancreatic hormone, is secreted in response to increased blood glucose. This hormone signals the cells to increase glucose uptake, promotes glycogenesis in the liver and inhibits glucagon secretion from the pancreas, thus signaling the liver to stop producing glucose via glycogenolysis and gluconeogenesis (Aronoff et al., 2004). The serum levels of insulin were measured to determine if it could be a possible cause of the hypoglycemia observed in *Nrf2/Hfe*$^{-/-}$ mice, however there were no statistically significant differences between the four genotypes **(Table 5)**.

Table 5. Levels of glucose, triglycerides and insulin in the serum of WT, *Nrf2*$^{-/-}$, *Hfe*$^{-/-}$ and *Nrf2/Hfe*$^{-/-}$ mice.

	WT	***Nrf2*$^{-/-}$**	***Hfe*$^{-/-}$**	***Nrf2/Hfe*$^{-/-}$**
N	3	4	4	4
Glucose (mg/dL)	64.3 ± 8.3	75.8 ± 9.2	77.8 ± 16.9	42.8 ± 11.4^{a,b}
Triglycerides (mg/dL)	67.3 ± 6.5	65.5 ± 21.3	66.0 ± 18.9	76.0 ± 11.8
Insulin (µg/mL)	879.2 ± 633.8	560.6 ± 241.7	705.5 ± 217.7	539.3 ± 167.0

Mean ± standard deviation $^{a}p<0.05$ vs. *Nrf2*$^{-/-}$; $^{b}p<0.01$ vs. *Hfe*$^{-/-}$.

5. Expression of glucogenesis genes

The key gluconeogenic enzymes are phosphoenolpyruvate carboxykinase (PEPCK-C) and glucose-6- phosphatase (G6Pc) (Samuel et al., 2009). The transcript levels of *Pepck* and *G6pc* were assessed in the liver and no significant differences were found **(Figure 11.A and 11.B)**.

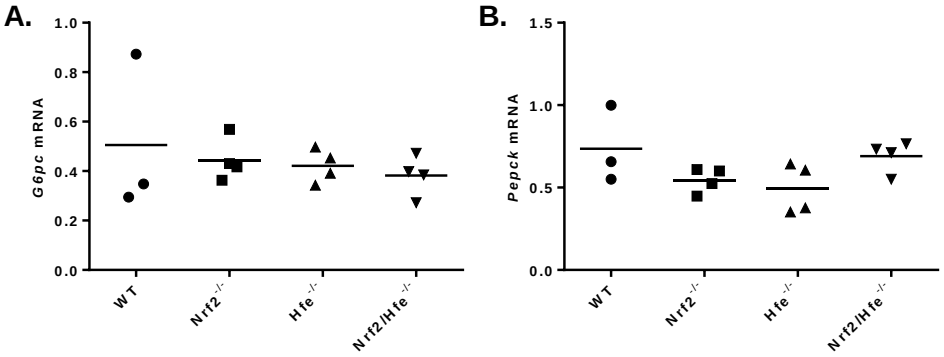

Figure 11. Expression of gluconeogenesis genes in the liver of WT, *Nrf2*$^{-/-}$, *Hfe*$^{-/-}$ and *Nrf2/Hfe*$^{-/-}$ mice. (A) Transcript levels of *G6pc* and (B) *Pepck* genes.

6. Iron metabolism

Hfe$^{-/-}$ mice provide an established model of systemic iron overload that mimics human HH (Bahram et al., 1999). *Nrf2*$^{-/-}$ mice are useful for studying oxidative stress responses, since the activation of ARE-containing genes by the transcription factor NRF2 is abrogated (Itoh et al., 1997). Hence, *Nrf2/Hfe*$^{-/-}$ mouse is a unique model for studying the effect of the oxidative stress generated by excessive iron. As expected, *Hfe*$^{-/-}$ mice presented significantly augmented serum iron compared to WT and *Nrf2*$^{-/-}$ mice ($p<0.0001$) **(Figure 12.A)**. Transferrin saturation was also significantly elevated when compared to WT, *Nrf2*$^{-/-}$ ($p<0.0001$) and *Nrf2/Hfe*$^{-/-}$ mice ($p<0.001$) **(Figure 12.B)**. It is worth noting that *Nrf2/Hfe*$^{-/-}$ mice did not present hyperferremia (augmented levels of serum iron), which would be expectable as the lack of the *Hfe* gene leads to systemic iron overload.

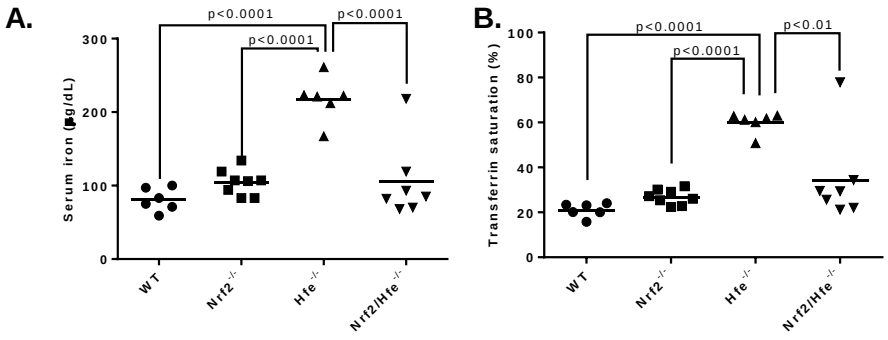

Figure 12. (A) Iron levels and (B) percentage of transferrin saturation in the serum of WT, *Nrf2*$^{-/-}$, *Hfe*$^{-/-}$ and *Nrf2/Hfe*$^{-/-}$ mice.

The transcript levels of hepcidin and the quantity of non-heme iron were assessed in the liver. *Hamp* mRNA levels in *Nrf2*$^{-/-}$, *Hfe*$^{-/-}$ and *Nrf2/Hfe*$^{-/-}$ mice were significantly decreased when compared to WT mice ($p<0.05$, $p<0.05$ and $p<0.001$, respectively) **(Figure 13.D)**, what was expectable for *Hfe*$^{-/-}$ and *Nrf2/Hfe*$^{-/-}$ mice since HFE is necessary for hepcidin transcription (Ganz and Nemeth, 2012). The quantity of non-heme iron in the liver was significantly increased in *Hfe*$^{-/-}$ and in *Nrf2/Hfe*$^{-/-}$ mice when compared to WT and *Nrf2*$^{-/-}$ mice ($p<0.001$) **(Figure 13.A)**. To evaluate whether the hepcidin expression was consistent with the hepatic iron stores, we divided the *Hamp* mRNA levels by the hepatic non-heme iron. This ratio was significantly decreased in *Hfe*$^{-/-}$ mice when compared to their WT counterparts ($p<0.001$) and in *Nrf2/Hfe*$^{-/-}$ mice when compared to WT ($p<0.001$) and *Nrf2*$^{-/-}$ ($p<0.05$) mice **(Figure 13.E)**.

The quantity of non-heme iron was also assessed in the spleen and kidneys. Spleen non-heme iron was not significantly different between the four genotypes **(Figure 13.B)**. We noted a trend for increased iron content in the kidney of *Nrf2* $^{-/-}$ and *Nrf2/Hfe*$^{-/-}$ mice, although this effect was not statistically significant **(Figure 13.C)**.

Perls' Prussian Blue staining was used to determine the presence of iron in the spleen, kidney, heart and pancreas. As illustrated in **Figure 14**, the spleen of the four genotypes presented high amounts of iron, which is expectable since splenic macrophages are responsible for scavenging the senescent erythrocytes. However, iron appeared to be present in higher quantities in the kidney, heart and pancreas of *Nrf2/Hfe*$^{-/-}$ mice when compared to WT, *Nrf2*$^{-/-}$ and *Hfe*$^{-/-}$ mice. It is worth noting that *Nrf2/Hfe*$^{-/-}$ pancreas accumulated iron in the exocrine pancreas (sparing the islets of Langherhans), siderophages and connective tissue. These data suggest that *Nrf2/Hfe*$^{-/-}$ mice accumulate more iron in the parenchyma of the different organs than the other genotypes.

Perls' Prussian Blue stained liver sections revealed the deposition of higher amounts of iron in *Hfe*$^{-/-}$ and *Nrf2/Hfe*$^{-/-}$ mice compared to WT and *Nrf2*$^{-/-}$ mice **(Figure 15)**. These liver sections were graded according to the distribution of iron in hepatocytes, sinusoids and portal veins. As expected, *Hfe*$^{-/-}$ and *Nrf2/Hfe*$^{-/-}$ livers presented significantly increased amounts of iron in hepatocytes when compared to WT ($p<0.0001$ and $p<0.05$, respectively) and to *Nrf2*$^{-/-}$ ($p<0.0001$ and $p<0.01$, respectively) livers. It is worth noting that *Hfe*$^{-/-}$ hepatocytes presented significantly augmented iron levels than *Nrf2/Hfe*$^{-/-}$ hepatocytes ($p<0.05$) **(Figure 16.A)**. *Nrf2/Hfe*$^{-/-}$ mice also presented significantly increased amounts of iron in the sinusoids when compared to WT ($p<0.0001$), *Nrf2*$^{-/-}$ ($p<0.0001$) and *Hfe*$^{-/-}$ ($p<0.001$) mice **(Figure 16.B)**. Although portal iron was not statistically different between mice of the four genotypes, *Hfe*$^{-/-}$ and *Nrf2/Hfe*$^{-/-}$ livers

presented higher amounts of iron in macrophages, biliary cells and vascular walls in comparison with WT and *Nrf2*$^{-/-}$ livers **(Figure 16.C)**. The total iron score, calculated as the sum of hepatic, sinusoidal and portal iron scores, was significantly augmented in *Hfe*$^{-/-}$ and *Nrf2/Hfe*$^{-/-}$ livers when compared to WT (p<0.001 and p<0.0001, respectively) and *Nrf2*$^{-/-}$ (p<0.0001) livers **(Figure 16.D)**.

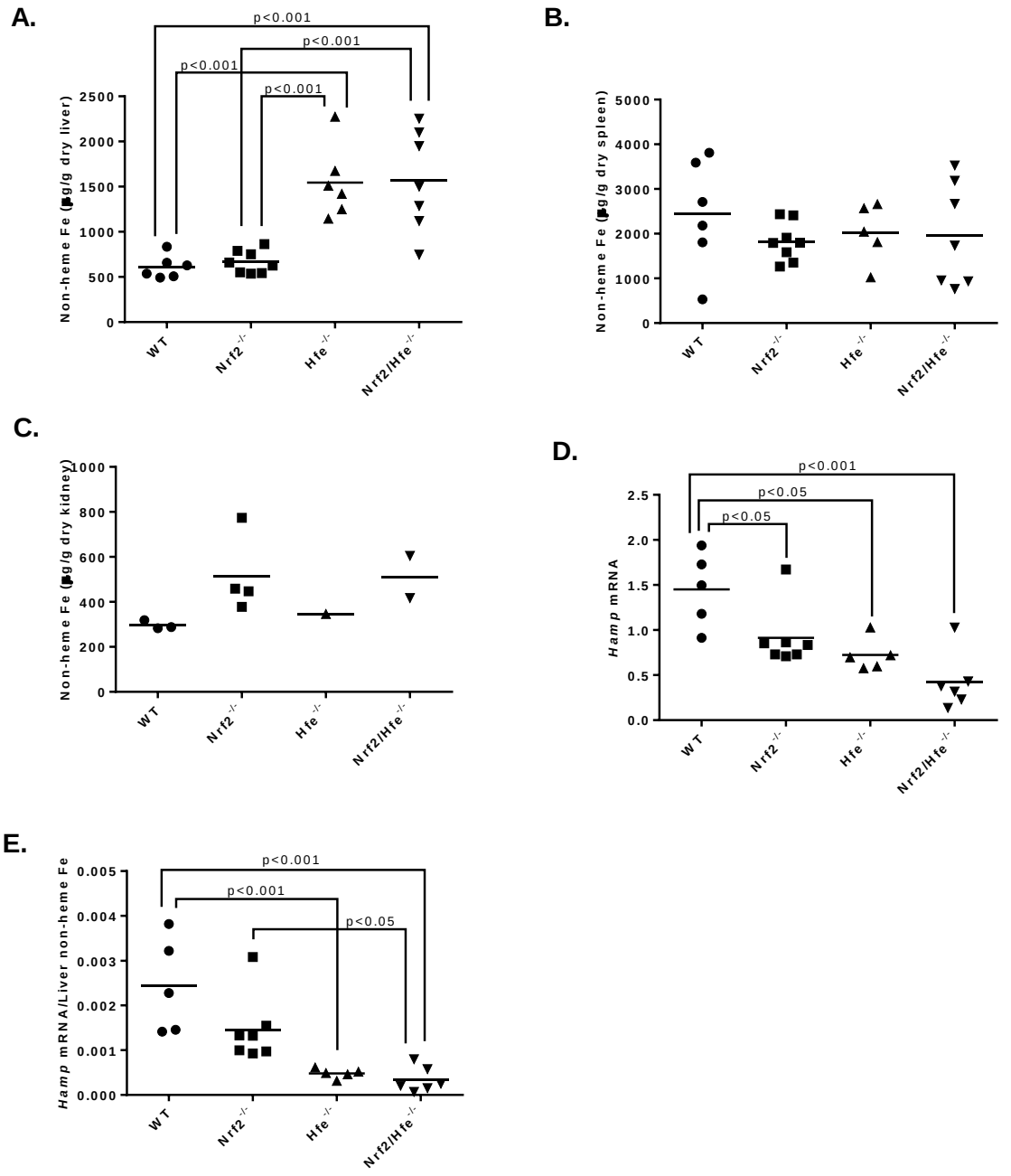

Figure 13. (A) Tissue non-heme iron content in the liver (B) spleen and (C) kidney of WT, *Nrf2*$^{-/-}$, *Hfe*$^{-/-}$ and *Nrf2/Hfe*$^{-/-}$ mice. (D) Transcript levels of *Hamp* gene and (E) *Hamp* mRNA/Liver non-heme iron ratio of WT, *Nrf2*$^{-/-}$, *Hfe*$^{-/-}$ and *Nrf2/Hfe*$^{-/-}$ livers.

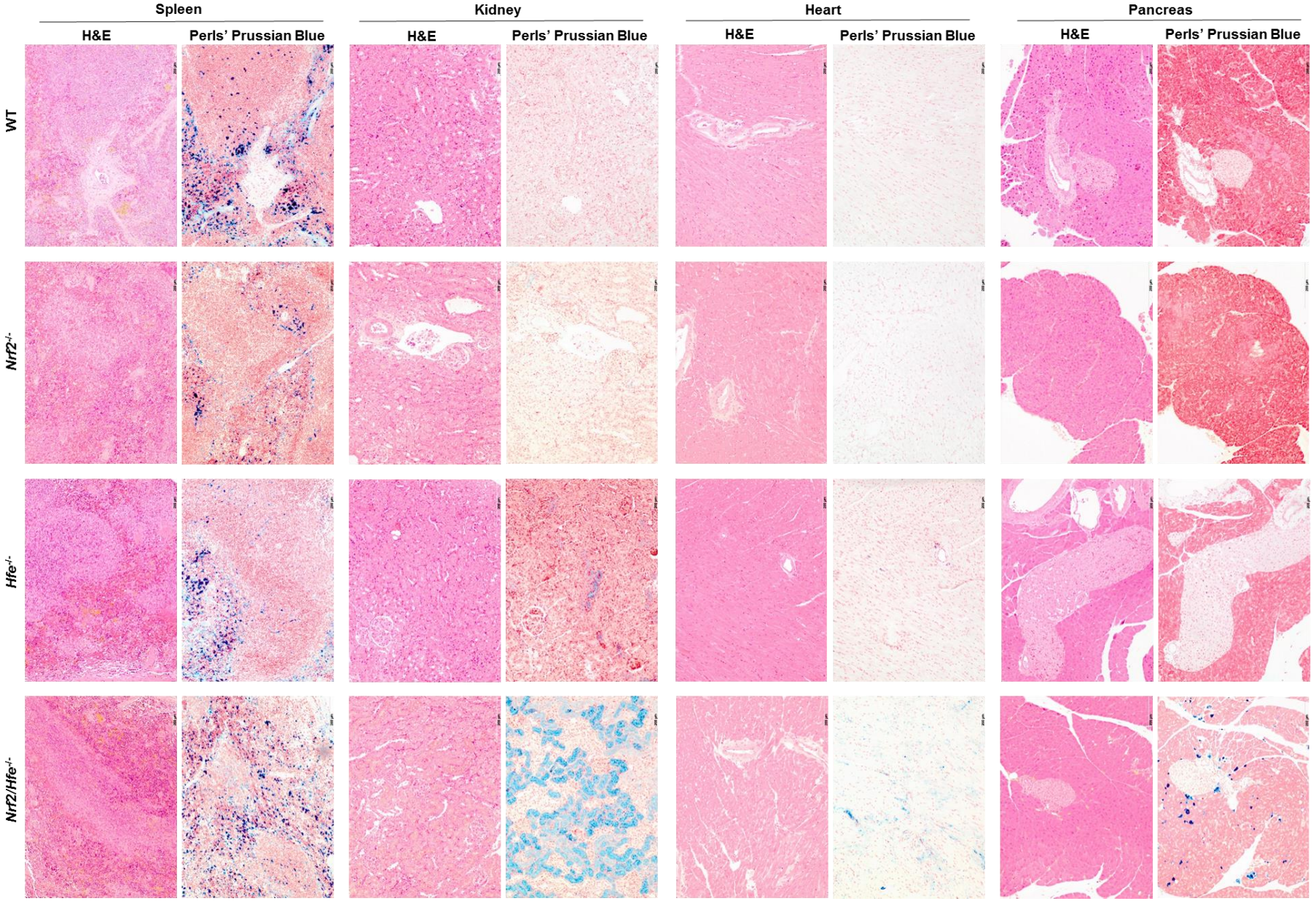

Figure 14. Representative images of H&E and Perls' Prussian Blue staining of spleen, kidney, heart and pancreas sections of WT, *Nrf2*$^{-/-}$, *Hfe*$^{-/-}$ and *Nrf2/Hfe*$^{-/-}$ *mice*. Original magnification 100×.

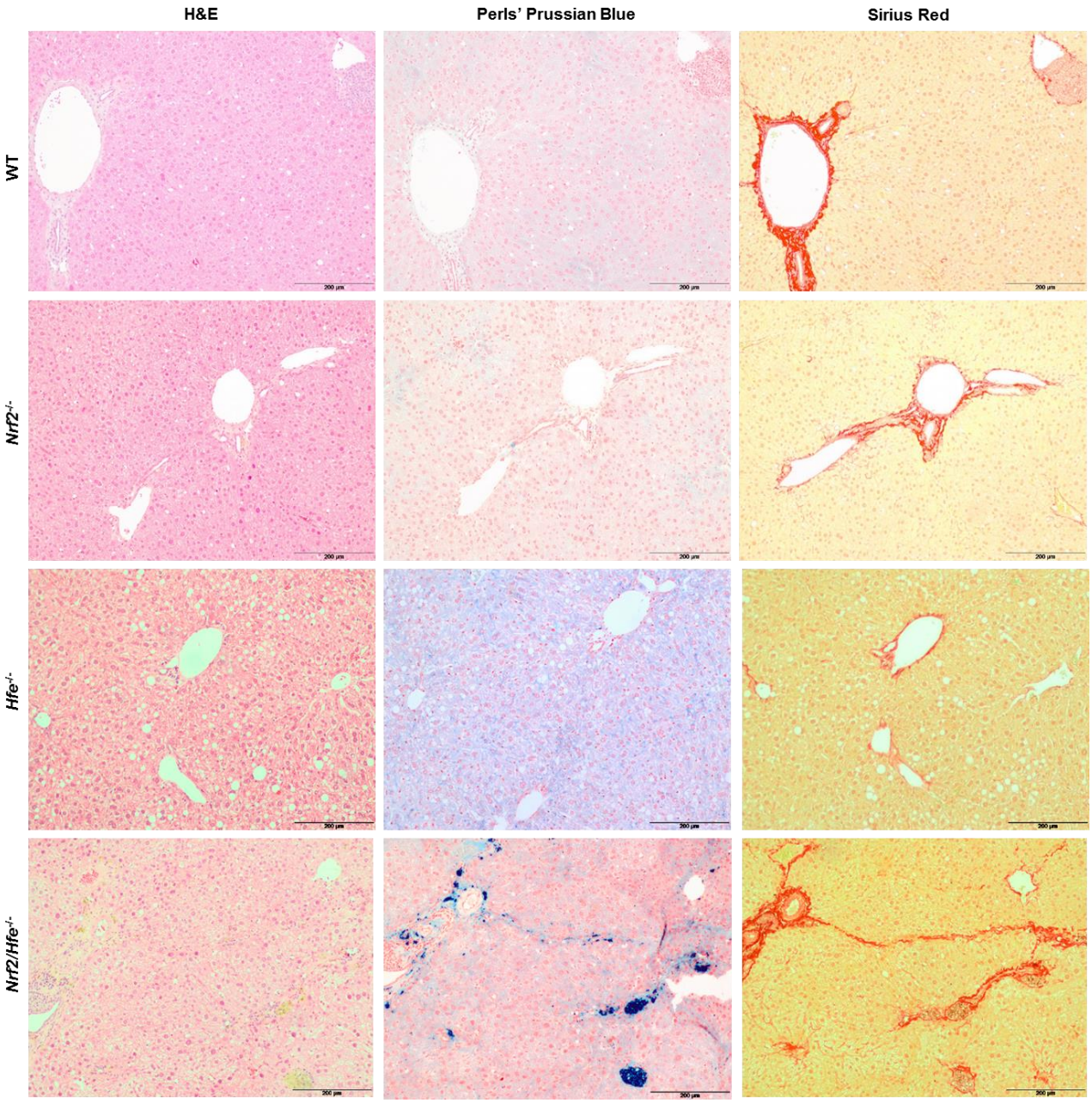

Figure 15. H&E, Perls' Prussian Blue and Sirius Red stained liver sections of WT, *Nrf2*$^{-/-}$, *Hfe*$^{-/-}$ and *Nrf2/Hfe*$^{-/-}$ mice. Bar = 200 µm.

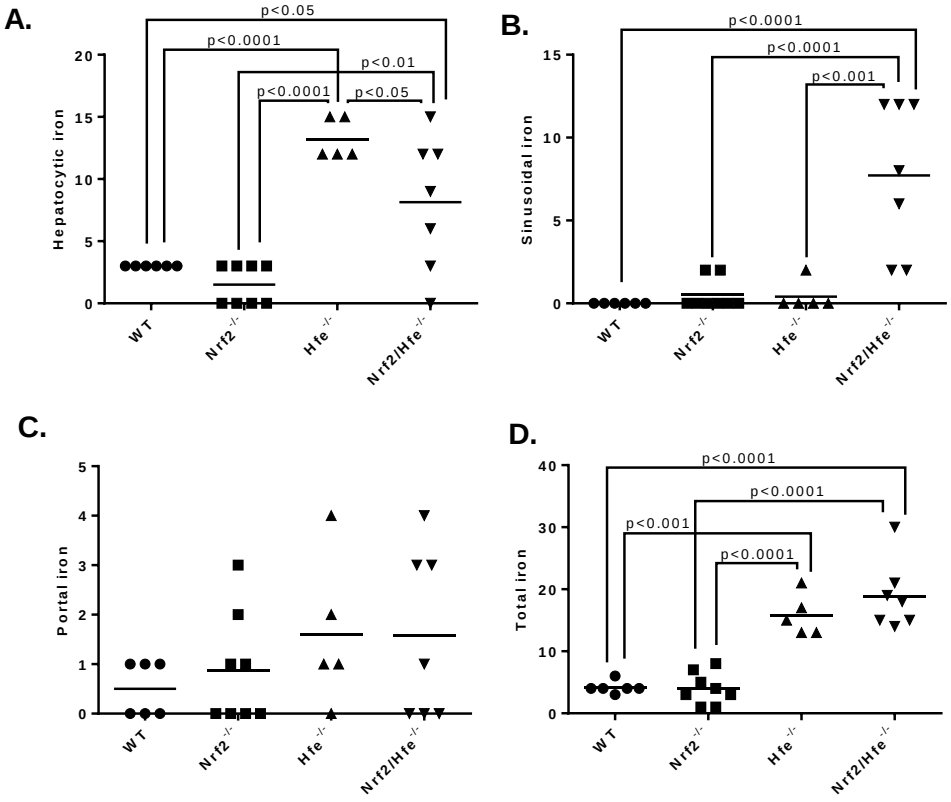

Figure 16. Histological grades of iron storage in WT, *Nrf2*$^{-/-}$, *Hfe*$^{-/-}$ and *Nrf2/Hfe*$^{-/-}$ livers. (A) Hepatocytic iron score: 0-36. (B) Sinusoidal iron score: 0-12. (C) Portal iron score: 0-12. (D) Total iron score: 0-60.

7. Oxidative stress

Iron is a potential biohazard since, under aerobic conditions, it can readily catalyze the generation of ROS (Papanikolaou and Pantopoulos, 2005), which, in turn, can damage DNA, proteins and lipid membranes (Andrews, 1999). As the cellular antioxidant defense is essential to protect from oxidative damage, we decided to measure the quantity of total (GSX), reduced (GSH) and oxidized (GSSG) glutathione in the liver. Even though the quantity of GSX, GSH and GSSG was not statistically different between the four genotypes, the GSH/GSSG ratio was significantly decreased in *Nrf2*$^{-/-}$ mice when compared to *Hfe*$^{-/-}$ ($p<0.05$). A low GSH/GSSG ratio, even if not statistically significant, was also observed in *Nrf2/Hfe*$^{-/-}$ mice **(Table 6)**.

Table 6. Levels of GSX, GSSG and GSH and GSH/GSSG ratio, in the serum of WT, *Nrf2*$^{-/-}$, *Hfe*$^{-/-}$ and *Nrf2/Hfe*$^{-/-}$ mice.

	WT	***Nrf2*$^{-/-}$**	***Hfe*$^{-/-}$**	***Nrf2/Hfe*$^{-/-}$**
N	6	8	5	7
GSX (nmol/mg protein)	405.1 ± 84.9	263.8 ± 39.2	410.7 ± 104.5	268.9 ± 78.8
GSSG (nmol/mg protein)	60.7 ± 2.6	52.7 ± 7.9	50.9 ± 7.2	50.6 ± 3.9
GSH (nmol/mg protein)	283.6 ± 80.3	158.4 ± 33.0	308.9 ± 90.9	167.7 ± 85.3
GSH/GSSG	4.6 ± 1.1	3.0 ± 0.7[a]	6.0 ± 1.0	3.4 ± 2.0

Mean ± standard deviation. [a]p<0.05 vs *Hfe*$^{-/-}$.

Lipid peroxidation is one of the consequences of the oxidative stress caused by high amounts of iron. A Thiobarbituric Acid Reactive Substances (TBARS) assay was performed as an indirect measurement of malondialdehyde (MDA), a byproduct of lipid peroxidation. We found no significant differences in the MDA concentration across the four experimental groups **(Figure 17.A)**.

NRF2 is a key transcription factor involved in the antioxidant defense (Kensler et al., 2007), so we decided to investigate the transcript levels of NAD(P)H:quinone oxireductase 1 (*Nqo1*), an antioxidant enzyme upregulated by NRF2 (Klaassen and Reisman, 2010), in the liver. As expected, *Nrf2*$^{-/-}$ and *Nrf2/Hfe*$^{-/-}$ livers showed significantly decreased levels of *Nqo1* transcript when compared to WT and *Hfe*$^{-/-}$ livers (p<0.0001) **(Figure 17.B)**.

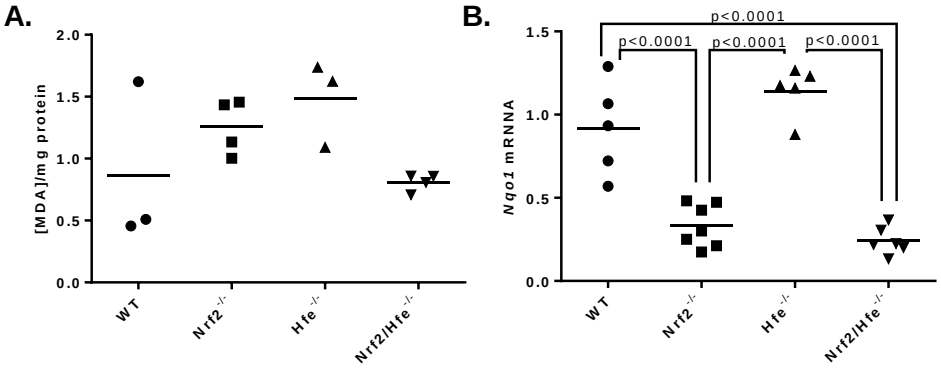

Figure 17. (A) MDA concentration and (B) *Nqo1* gene expression in the livers of WT, *Nrf2*$^{-/-}$, *Hfe*$^{-/-}$ and *Nrf2/Hfe*$^{-/-}$ mice.

8. Liver fibrosis

Liver fibrosis is one of the major consequences of the excessive iron accumulation in HH patients and is characterized by excessive deposition of extracellular matrix (ECM) (Bataller and Brenner, 2005). Transforming growth factor (TGF)-β, the most prominent profibrotic cytokine that contributes to the development of hepatic fibrosis, signals the transcription of fibrogenic genes, such as collagen and fibronectin. In fibrotic liver, augmented (TGF)-β signaling stimulates transdifferentiation of hepatic stellate cells (HSCs) to α-smooth muscle actin (α-SMA)-positive myofibroblasts, the main producers of excessive ECM proteins. TGF-β is also capable of suppressing the activity of ECM degrading proteases, such as matrix metalloproteinases, via upregulation of their inhibitors, including tissue inhibitor of matrix metalloproteinase (TIMP)-1, leading to decreased ECM degradation (Oh et al., 2012). We evaluated the expression of genes involved in liver fibrosis, including alpha-smooth muscle actin (*Acta2*), type I collagen (*Col1a1*) and *Timp1* genes. Levels of *Acta2* and *Timp1* genes were not statistically different in the livers of mice of the four genotypes **(Figure 18.A and 18.C)**. However, the transcript levels of *Col1a1* were significantly augmented in *Nrf2/Hfe*$^{-/-}$ mice when compared to *Nrf2*$^{-/-}$ mice ($p<0.05$) **(Figure 18.B)**. 4-Hydroxyproline is a major component of collagen, comprising around 13.5% of its amino acid composition (Neuman and Logan, 1950), which is why we also determined the quantity of hydroxyproline in the liver. The quantity of hydroxyproline tended to augment in *Nrf2/Hfe*$^{-/-}$ mice in comparison to WT, *Nrf2*$^{-/-}$ and *Hfe*$^{-/-}$ mice **(Figure 18.D)**. The hepatic fibrotic area was evaluated through a Sirius Red Staining. After analyzing three random microscope fields of the liver under polarized light, obtained at 100× magnification, we observed that the percentage of fibrotic area was significantly increased in *Nrf2/Hfe*$^{-/-}$ mice compared to WT ($p<0.05$), *Nrf2*$^{-/-}$ and *Hfe*$^{-/-}$ mice ($p<0.01$) **(Figure 18.E)**.

Sirius Red stained liver sections were also graded according to the level of fibrosis. As illustrated in **Figure 15**, *Nrf2/Hfe*$^{-/-}$ mice presented a more exuberant phenotype of fibrosis (bridging fibrosis) than WT, *Nrf2*$^{-/-}$ and *Hfe*$^{-/-}$ mice. Fibrosis degree was significantly augmented in *Nrf2/Hfe*$^{-/-}$ livers in comparison to WT ($p<0.01$), *Nrf2*$^{-/-}$ ($p<0.05$) and *Hfe*$^{-/-}$ ($p<0.001$) livers **(Figure 19)**.

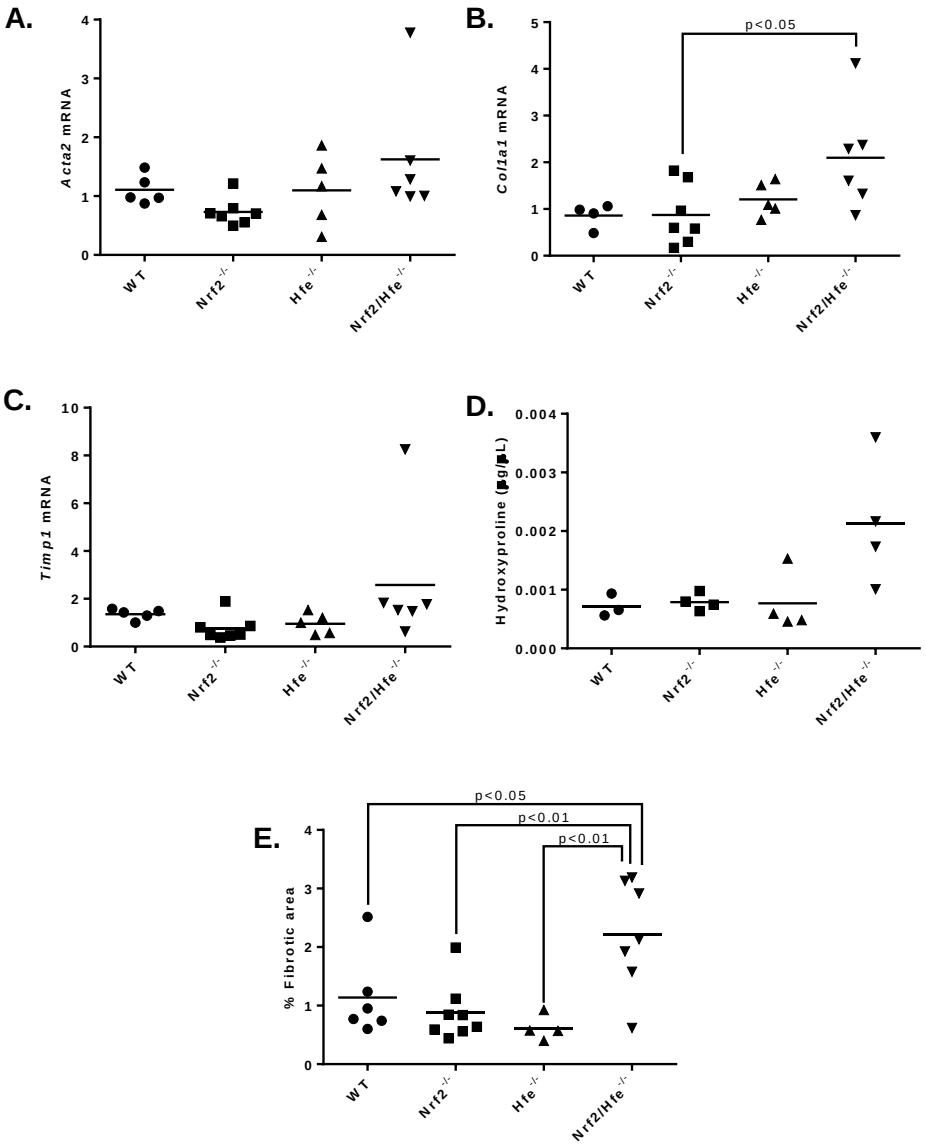

Figure 18. Hepatic fibrosis and expression of fibrogenic genes in the livers of WT, *Nrf2*$^{-/-}$, *Hfe*$^{-/-}$ and *Nrf2/Hfe*$^{-/-}$ mice. (A) Transcript levels of *Acta2* (B) *Col1a1* and (C) *Timp1* genes in the liver. (D) Hepatic quantity of hydroxyproline and (E) percentage of hepatic fibrotic area.

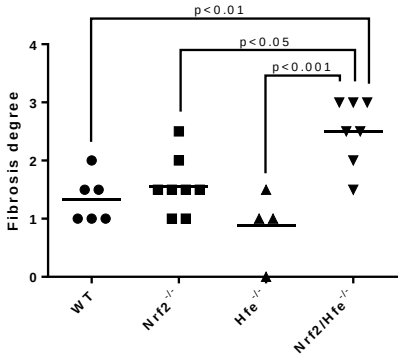

Figure 19. Fibrosis degree of WT, *Nrf2*$^{-/-}$, *Hfe*$^{-/-}$ and *Nrf2/Hfe*$^{-/-}$ livers. Fibrosis degree: 0. none. 1. mild/moderate in zone 3, portal/periportal only. 2. portal/periportal and perisinusoidal 3. bridging fibrosis. 4. cirrhosis.

9. Hepatic inflammation and steatosis

During local liver injury, resident Kupffer cells initiate an immune response, releasing a variety of chemical messengers such as cytokines, like tumour necrosis factor alpha (TNFα) and interleukin (IL)-6, and chemokines, such as CCL-2, that initiate the acute-phase response and inflammation (Liaskou et al., 2012). Besides, it is known that NRF2 is involved in the inhibition of inflammation (Kensler et al., 2007). To evaluate liver inflammation, the transcript levels of *Tnf-α*, *Il-6* and *Ccl-2* genes were assessed in the liver. No significant differences in the transcript levels of *Tnf-α* and *Ccl2* genes were found and (**Figure 20.A and 20.B)**, contrary to expected, *Nrf2*$^{-/-}$ and *Nrf2/Hfe*$^{-/-}$ livers showed decreased levels of *Il-6* in comparison to WT livers ($p<0.05$) **(Figure 20.C)**.

H&E staining was applied to assess hepatic inflammation and steatosis. H&E stained liver sections are presented in **Figure 15**. No significant differences were found in the lobular inflammation degree of the four genotypes **(Figure 21.A)**. These data suggest that the low levels of inflammation found in the liver may be due to the advanced age of the model. Steatosis degree was significantly augmented in *Hfe*$^{-/-}$ livers compared to WT, *Nrf2*$^{-/-}$ and *Hfe/Nrf2*$^{-/-}$ livers ($p<0.0001$) **(Figure 21.B)**, fact that was previously reported by other authors (Tan et al., 2011). Steatosis was localized in the liver Rappaport zone one (periportal).

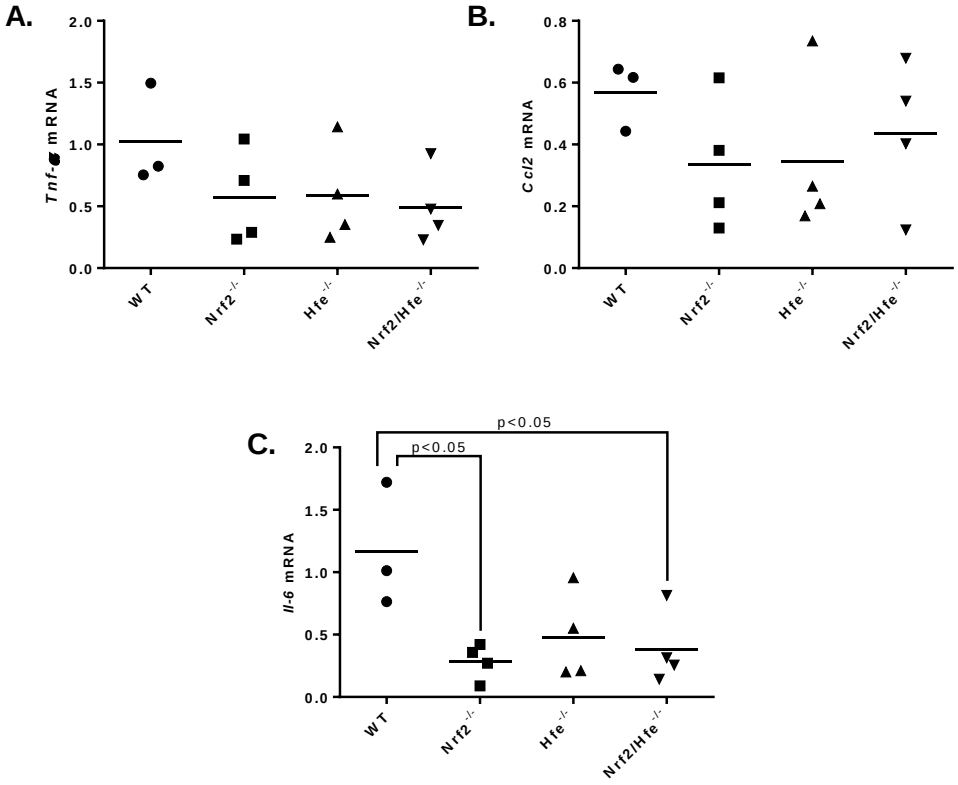

Figure 20. Expression of proinflammatory genes in the liver of WT, *Nrf2*$^{-/-}$, *Hfe*$^{-/-}$ and *Nrf2/Hfe*$^{-/-}$ mice. (A) Transcript levels of *Tnf-α* (B) *Ccl2* and (C) *Il-6* genes.

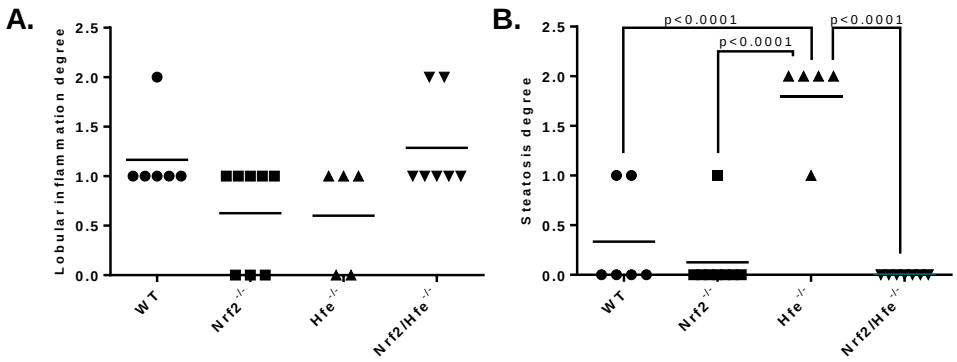

Figure 21. H&E grading of lobular inflammation and steatosis in WT, *Nrf2*$^{-/-}$, *Hfe*$^{-/-}$ and *Nrf2/Hfe*$^{-/-}$ liver sections. (A) Lobular inflammation degree: 0. no foci; 1. <4 foci per 100× field; 2. 4-8 foci per 100× field; 3. >8 per 100× field. (B) Steatosis degree: 0. absent (<5% of parenchyma); 1. light (5-33% of parenchyma); 2. moderate (33-66% of parenchyma); 3. severe (>66% of parenchyma).

10. Liver damage

Alanine aminotransferase (ALT) activity, a serum marker for liver damage, was assessed. We found no statistical differences between the four genotypes **(Figure 22.A)**. Hepatic cell death was assessed through a Terminal deoxynucleotidyl transferase (TdT) dUTP Nick-End Labeling (TUNEL) assay, which detects DNA fragmentation. The number of TUNEL-positive cells was significantly increased in *Nrf2/Hfe*$^{-/-}$ mice when compared to WT mice ($p<0.05$) **(Figure 22.B)**. Representative images of each group and positive and negative controls for the TUNEL assay are presented in **Figure 23**.

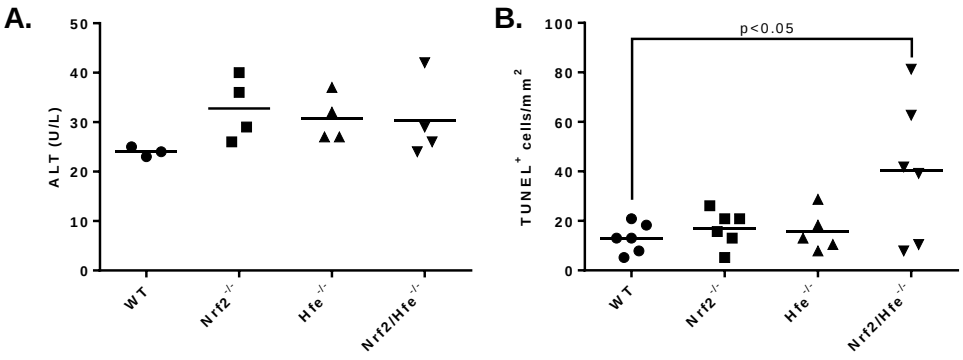

Figure 22. Levels of (A) serum ALT and (B) TUNEL-positive cells in the liver of WT, *Nrf2*$^{-/-}$, *Hfe*$^{-/-}$ and *Nrf2/Hfe*$^{-/-}$ mice.

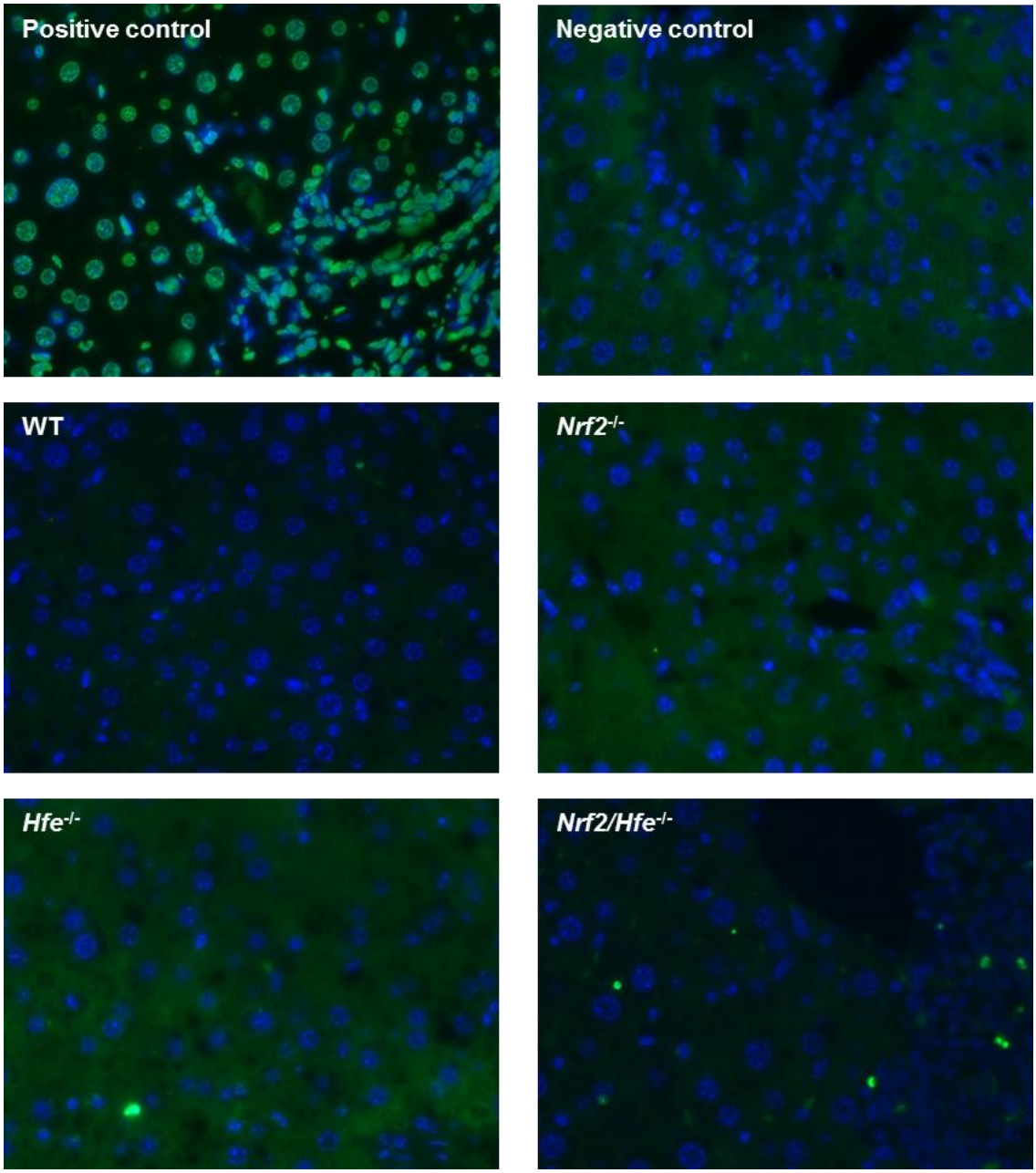

Figure 23. TUNEL assay. Positive and negative controls and representative liver sections of WT, *Nrf2*$^{-/-}$, *Hfe*$^{-/-}$ and *Nrf2/Hfe*$^{-/-}$ mice. Original magnification: 400×.

The degree of liver necrosis was assessed in the H&E stained liver sections. Of note, confluent necrosis was observed in 6 out of the 7 *Nrf2/Hfe*$^{-/-}$ individuals, which thus exhibited significantly more hepatocellular necrosis than WT, *Nrf2*$^{-/-}$ and *Hfe*$^{-/-}$ mice ($p<0.0001$) **(Figure 24.C)**.

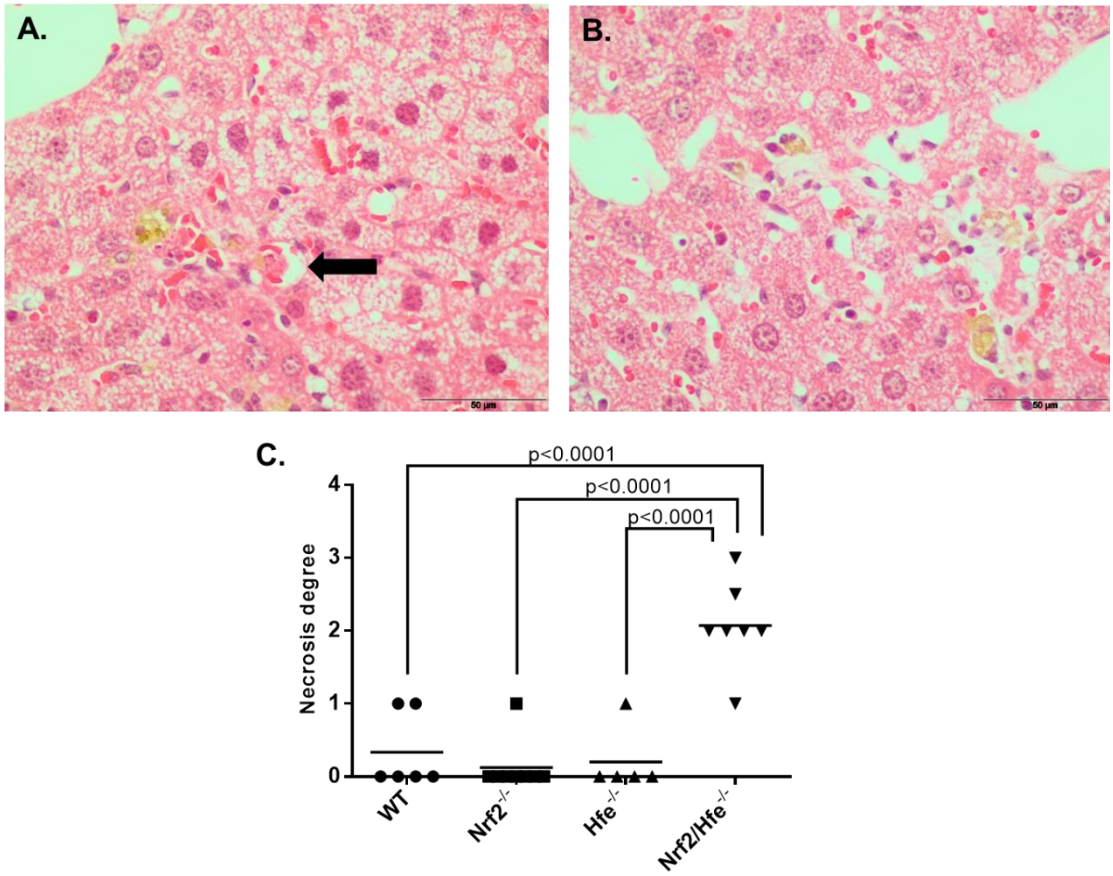

Figure 24. Representative H&E stained liver sections of *Nrf2/Hfe*$^{-/-}$ mice showing (A) spotty necrosis and (B) confluent necrosis. (C) H&E grading of necrosis in WT, *Nrf2*$^{-/-}$, *Hfe*$^{-/-}$ and *Nrf2/Hfe*$^{-/-}$ liver sections. 0. absent. 1. spotty necrosis (one or a few necrotic hepatocytes). 2. confluent necrosis. 3. bridging necrosis.

Human study

In order to properly perform the SNP genotyping of Rs35652124, Rs670664, Rs150648896 and Rs6721961 of the *NRF2* promoter region, the first approach was to optimize the PCR protocol to avoid the appearance of non-specific bands in the electrophoresis gel. Different enzymes (Taq DNA Polimerase from ThermoFisher Scientific, Lithuania; *Type-it® Microsatellite PCR Kit* from Qiagen, Germany), annealing temperatures (61-63 ºC), annealing and extension time (1 min and 30 s) and concentrations of $MgCl_2$ (1.5 and 2mM) and template DNA (10, 50 and 100 ng/µL) were tested. A single PCR product was consistently obtained when using the *Type-it® Microsatellite PCR Kit*, increasing the annealing temperature to 63ºC, decreasing the annealing and extension time for 30 s and setting the template DNA at 50 ng/µL. Representative agarose gel from the original protocol and from the optimized one are presented in **Figure 25**.

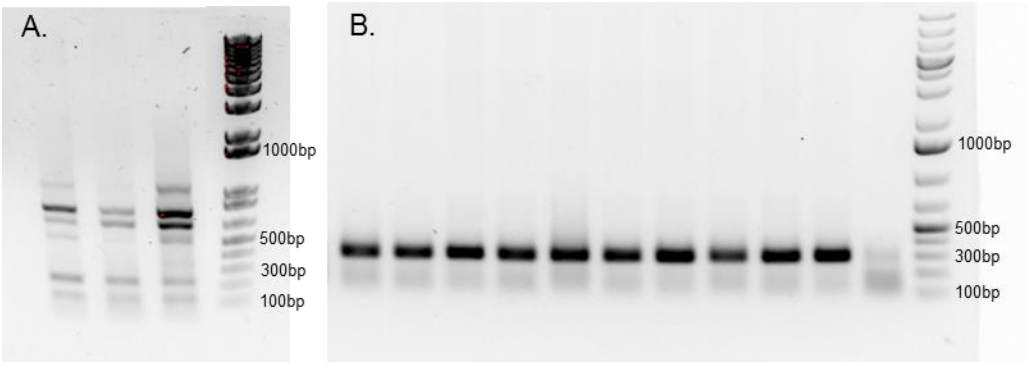

Figure 25. PCR amplification of a 284 bp fragment of the *NRF2* promoter region. PCR products were separated by gel electrophoresis and visualized under UV after ethidium bromide staining. Representative images of the PCR products obtained (A) prior to and (B) after optimization are depicted.

The PCR fragment was genotyped and the SNPs were determined with ProSeq3 software. An example of an electropherogram is presented in **Figure 26**. Allele frequencies of Rs35652124 (T > C), Rs670664 (C > T), Rs150648896 (C > T) and Rs6721961 (G > T) SNPs were calculated in unrelated patients, as described in Materials and Methods (M&M). Frequencies of the actual sample and reference frequencies from Ensembl are presented in **Table 7**. We concluded that there were no significant differences between the frequencies of the actual sample and the frequencies reported in Ensembl for the European population.

As a first approach to address the genotype/phenotype correlations, we estimated the allele frequencies of the different SNPs in groups of patients divided according to the

expression of specific clinical manifestations of disease, as described in M&M. The respective allele frequencies are presented in **Table 8**.

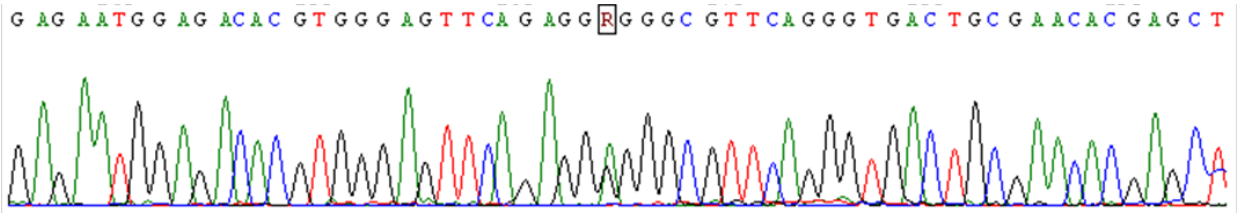

Figure 26. Representative elecropherogram. The R inside a square represents a heterozygote individual for Rs35652124 SNP.

Table 7. Actual sample and reference allele frequencies.

	Actual sample				Reference			
	Rs35652124	**Rs6706649**	**Rs150648896**	**Rs6721961**	**Rs35652124**	**Rs6706649**	**Rs150648896**	**Rs6721961**
freq (T)	0.680 (132)	0.103 (20)	0.000 (0)	0.098 (19)	0.694 (698)	0.111 (112)	0.000 (0)	0.125 (126)
freq (C)	0.320 (62)	0.897 (174)	1.000 (194)		0.306 (308)	0.889 (894)	1.000 (1006)	
freq (G)				0.902 (175)				0.875 (880)

Frequency (number of alleles). The reference frequencies were obtained in Ensembl for the European population.

Table 8. Allele frequencies in patients stratified according to the clinical manifestations of disease.

		Presence of Cirrhosis		**Presence of Arthropathy**		**Clinical Presentation**	
		+	–	+	–	**Symptomatic**	**Assymptomatic**
	n	**11**	**46**	**11**	**46**	**24**	**33**
Rs35652124	**freq (T)**	0.818 (18)	0.641 (59)	0.682 (15)	0.674 (62)	0.750 (36)	0.621 (41)
	freq (C)	0.182 (4)	0.359 (33)	0.318 (7)	0.326 (30)	0.250 (12)	0.379 (25)
Rs6706649	**freq (T)**	0.182 (4)	0.141 (13)	0.091 (2)	0.163 (15)	0.146 (7)	0.152 (10)
	freq (C)	0.818 (18)	0.859 (79)	0.909 (20)	0.837 (77)	0.854 (41)	0.848 (56)
Rs150648896	**freq (T)**	0.000 (0)	0.000 (0)	0.000 (0)	0.000 (0)	0.000 (0)	0.000 (0)
	freq (C)	1.000 (22)	1.000 (92)	1.000 (22)	1.000 (92)	1.000 (48)	1.000 (66)
Rs6721961	**freq (T)**	0.045 (1)	0.065 (6)	0.136 (3)	0.043 (4)	0.104 (5)	0.030 (2)
	freq (G)	0.955 (21)	0.935 (86)	0.864 (19)	0.957 (88)	0.896 (43)	0.907 (64)

Although, in general, no statistically significant differences were found among groups, it is worth noting that the frequency of the allele T in Rs35652124 SNP was higher in patients with cirrhosis (presence of cirrhosis +) and in symptomatic patients than in patients without cirrhosis (presence of cirrhosis –) or asymptomatic patients **(Table 8)**.

The frequency of each genotype was next calculated in all unrelated patients **(Table 9)**. The T/C-C-C-G genotype was the most frequent, while the T-T/C-C-T/G was the rarest one.

Table 9. Frequencies of the several genotypes in 97 patients.

Genotype	n	freq
T/C-C-C-G	28	0,289
T-C-C-G	22	0,227
T-C-C-T/G	13	0,134
C-C-C-G	12	0,124
T-T/C-C-G	8	0,082
T/C-C-C-T/G	5	0,052
T/C-T/C-C-G	5	0,052
T-T-C-G	3	0,031
T-T/C-C-T/G	1	0,010

Genotype: Rs35652124-Rs670664-Rs150648896-Rs6721961.

As for allele frequencies, genotype frequencies were also calculated in relation to the clinical phenotype, i.e., for groups of patients with cirrhosis, arthropathy or any manifestations **(Table 10)**. Although not statistically significant, the total number genotypes homozygous for allele T in Rs35652124 SNP (Total TT) was higher in patients with cirrhosis, arthropathy and symptomatic patients than in patients without these features. Accordingly, the total number of genotypes with allele C in homozygosity or heterozygosity in Rs35652124 SNP (Total with C) was increased in patients without cirrhosis, arthropathy or asymptomatic.

Since the previous results suggested that the allele C in Rs35652124 SNP may have a protective effect in HH patients, we further analyzed data comparing genotypes homozygous for allele T (Total TT) and genotypes homozygous/heterozygous for allele C (Total with C) in Rs35652124 SNP. For that purpose, we compared the two genotype groups (Total TT and Total with C) for the following variables: age, iron parameters, total lymphocytes and lymphocyte subsets (CD4+ and CD8+) and the clinical manifestations of the disease. As described in M&M, for all the clinical variables analyzed, asymptomatic, early diagnosed females and young males (<30 years of age) were excluded. For the specific purpose of estimating the frequency of cirrhosis, the cases where we had no confirmatory liver biopsy available were also excluded. The results are summarized in **Table 11**.

Table 10. Genotype frequencies in patients with or without cirrhosis, arthropathy and symptoms.

	Presence of Cirrhosis				Presence of Arthropathy				Clinical Presentation			
	+		-		+		-		Symptomatic		Assymptomatic	
	n	**freq**	**n**	**freq**	**n**	**freq**	**n**	**freq**	**n**	**freq**	**n**	**freq**
T-C-C-G	3	0,273	8	0,174	3	0,273	8	0,174	5	0,208	6	0,182
T-C-C-T/G	1	0,091	4	0,087	2	0,182	3	0,065	4	0,167	1	0,030
T-T/C-C-G	3	0,273	5	0,109	0	0,000	8	0,174	4	0,167	4	0,121
T-T-C-G	0	0,000	3	0,065	1	0,091	2	0,043	1	0,042	2	0,061
T-T/C-C-T/G	0	0,000	1	0,022	0	0,000	1	0,022	0	0,000	1	0,030
Total TT	**7**	**0,636**	**21**	**0,457**	**6**	**0,545**	**22**	**0,478**	**14**	**0,583**	**14**	**0,424**
T/C-C-C-G	3	0,273	15	0,326	2	0,182	16	0,348	6	0,250	12	0,364
T/C-C-C-T/G	0	0,000	1	0,022	1	0,091	0	0,000	1	0,042	0	0,000
T/C-T/C-C-G	1	0,091	1	0,022	0	0,000	2	0,043	1	0,042	1	0,030
C-C-C-G	0	0,000	8	0,174	2	0,182	6	0,130	2	0,083	6	0,182
Total with C	**4**	**0,364**	**25**	**0,543**	**5**	**0,455**	**24**	**0,522**	**10**	**0,417**	**19**	**0,576**

Genotype: Rs35652124-Rs670664-Rs150648896-Rs6721961. Total TT: genotypes homozygous for allele T in rs35652124. Total with C: genotypes with allele C in homozygosity or heterozygosity in Rs35652124 SNP**.**

Table 11. Clinical characterization of the genotypes groups.

	Total TT	Total with C	Significant level
n	20	16	
Age	48 ± 12	46 ± 8	
Ferritin (ng/mL)	2378 ± 1928	1550 ± 976	
TfSat (%)	80 ± 20	86 ± 19	
TBIS (g)	9.6 ± 5.2	4.8 ± 2.6	p=0,01
Lymphocytes	1.70 ± 0.68	2.18 ± 0.66	
CD4+	0.76 ± 0.33	0.97 ± 0.29	
CD8+	0.40 ± 0.28	0.47 ± 0.19	
Frequency of the clinical manifestations			
Skin pigmentation	5/16 (31.3%)	2/13 (15.4%)	
Diabetes	2/16 (12.5%)	1/13 (7.7%)	
Hypogonadysm	1/16 (6.3%)	0/13 (0%)	
Arthropathy	3/16 (18.8%)	1/16 (6.3%)	
Cirrhosis	7/16 (43.8%)	0/13 (0%)	p = 0.05
Any clinical manifestations	8/16 (50.0%)	2/13 (15.4%)	

Mean ± standard deviation. Total TT: genotypes homozygous for allele T in rs35652124. Total with C: genotypes with allele C in homozygosity or heterozygosity in Rs35652124 SNP. TfSat (%): transferrin saturation. TBIS: total body iron stores. [a]p = 0.01 vs genotypes with allele C in homozygosity or heterozygosity in Rs35652124 SNP.

No significant differences were found between the two groups in terms of age, biochemical and hematological parameters. However, TBIS was significantly increased in genotypes homozygous for allele T in Rs35652124 SNP (Total TT) when compared to genotypes homozygous/heterozygous for allele C in Rs35652124 SNP (Total with C) ($p = 0.01$) **(Table 11).** Cirrhosis was significantly increased in genotypes homozygous for allele T in Rs35652124 SNP (Total TT) when compared to genotypes homozygous/heterozygous for allele C in Rs35652124 SNP (Total with C) ($p = 0.5$). Although not statistically significant, symptomatic patients had more commonly genotypes homozygous for allele T in Rs35652124 SNP (Total TT) ($p = 0.10$).

Discussion

Animal study

1. *Hfe* and *Nrf2* genes in erythropoiesis

Hfe$^{-/-}$ mice exhibited significantly higher levels of Hb and HCT when compared to WT mice. These data are in agreement with several reports that showed erythropoietic alterations in HH patients, including increased Hb levels, reticulocyte counts, HCT, MCV, MCH, and MCH concentration (Barton et al., 2000; Feeney et al., 2005; McLaren et al., 2007). A study by Ramos et al., 2011 demonstrated that the *Hfe* gene influences erythropoiesis by limiting hepcidin expression under conditions of simultaneous iron overload and stress erythropoiesis, and by impairing transferrin-bound iron uptake by erythroid cells. This dual role for *Hfe* avoids the toxicity associated with iron overload under conditions of high iron availability and limits erythroid iron intake under conditions of iron deficiency (Ramos et al., 2011).

In contrast with *Hfe*$^{-/-}$ mice, *Nrf2/Hfe*$^{-/-}$ mice presented low values of RBC, Hb and HCT, which indicates that they were mildly anemic. Their MCV and MCH values were increased, indicating that the anemia was macrocytic and normochromic. Macrocytic anemia is characterized by the presence of abnormally large RBCs in the peripheral blood and can be divided into two categories, megaloblastic and nonmegaloblastic, based on the examination of the bone marrow. The etiologies associated with macrocytic anemia include nutritional deficiencies (e.g., vitamin B12 and folate), drugs, primary bone marrow disorders (e.g., myelodysplasia and leukemia) and other chronic illnesses (e.g. alcoholism and hypothyroidism). Megaloblastic anemia is highly suspicious of a vitamin B12 or folate deficiency and is characterized by large and oval shaped erythroblasts that contain a characteristic immature, lacy nucleus (Aslinia et al., 2006). *Nrf2/Hfe*$^{-/-}$ mice had the lowest body weight, so we suspected that the anemia could be due to low intestinal absorption of nutrients, namely vitamin B12 and folate. This hypothesis was excluded since megaloblasts were not observed in bone marrow smears (Tiago Duarte, personal communication). The percentage of reticulocytes was increased in *Nrf2/Hfe*$^{-/-}$ mice, indicative of a regenerative anemia. With regenerative anemia, the bone marrow responds appropriately to the decreased red cell mass by increasing RBC production and releasing reticulocytes. Typically, regenerative anemia is caused by hemorrhage or hemolysis (Kahn, 2010). Serum LDH activity was not altered in *Nrf2/Hfe*$^{-/-}$ mice, which indicates that the anemia did not result from RBC hemolysis.

Erythroid colony-forming units adhere to a resident macrophage and differentiate to erythroblasts in the presence of EPO, resulting in the formation of an erythroblastic island. So, resident macrophages play a supportive role in erythropoiesis, probably by preventing apoptosis of the erythroid precursors (Sadahira and Mori, 1999), and EPO stimulates the erythroid progenitors in the bone marrow to proliferate (Beguin et al., 1993). Transcript levels of *Epo* gene in the kidney and EPO levels in the serum were slightly augmented, even if not statistically significant, in *Nrf2/Hfe*$^{-/-}$ mice. This indicates that the kidney was responding to the low levels of RBC and that erythropoiesis was not compromised due to lack of EPO. *Spic* transcript levels were not altered in the liver and spleen of *Nrf2/Hfe*$^{-/-}$ mice and *F4/80* transcript levels were also not altered in the spleen of *Nrf2/Hfe*$^{-/-}$ mice. These data indicate that the anemia was not caused by lack of macrophages to nurse the development and differentiation of erythroid cells. HO-1 is responsible for the disposal of the potentially toxic heme (Fraser et al., 2011). HO-1 deficiency in humans appears to be an extremely rare condition with only two live births reported. Both patients presented severe anemia (Kartikasari et al., 2009; Yachie et al., 1999). *Nrf2/Hfe*$^{-/-}$ mice did not present significant alterations in the levels of *Hmox1* in the liver and spleen, which indicates that the anemia did not result from lack of HO-1.

The pro-inflammatory state of aging may result in anemia (Roy, 2010). Since mice employed in the study were 24 months of age, anemia of inflammation (AI) could be a possible cause of the low RBC count in *Nrf2/Hfe*$^{-/-}$ mice. AI is typically normochromic and normocytic and is characterized by low serum iron and reticulocyte count, decreased transferrin saturation and bone marrow sideroblasts and increased reticuloendothelial iron and hepcidin levels (Cartwright, 1966). In certain cases, EPO production is not sufficiently increased relative to the severity of the anemia and erythrocyte life span is decreased (Roy, 2010). These features of AI suggest that the immune response promotes iron sequestration, but also inhibits the production and survival of erythrocytes (Weiss and Goodnough, 2005). Cytokines, such as IL-6, TNFα and IL-1, are linked to AI. IL-6 correlates with hemoglobin concentration and TNFα and IL-1 have been implicated in the inhibition of multiple stages of erythroid development (Weiss and Goodnough, 2005). The hypothesis that *Nrf2/Hfe*$^{-/-}$ mice could have AI was excluded. Even though they presented low levels of serum iron and decreased transferrin saturation when compared to *Hfe*$^{-/-}$ mice (they should have presented higher values due to the lack of HFE), reticulocyte count was not decreased, *Hamp* transcript levels in the liver were not increased and the levels of GM-CSF, IFN-γ, IL-1b, IL-6, IL-10, MCP-1 and TNFα were not significantly increased. These data lead us to discard the AI.

Iron deficiency anemia (IDA) is characterized by microcytosis and hypochromasia with inadequate regeneration, and low serum iron, iron saturation and ferritin (Naigamwalla et al., 2012). As *Nrf2/Hfe*$^{-/-}$ mice had low body weight and low serum iron levels, the decreased iron intestinal absorption could be the source of the anemia. However IDA was also excluded since the anemia was macrocytic, normochromic and regenerative. The fact that the *Nrf2/Hfe*$^{-/-}$ mice anemia is regenerative is by itself an exclusion factor for IDA, since there must exist available iron for the development of reticulocytes.

Further investigation needs to be done to determine the origin of the anemia of *Nrf2/Hfe*$^{-/-}$ mice. NRF2 has been proven to play a critical role in the survival of RBCs, by regulating intracellular ROS levels when selenoproteins, enzymes with antioxidant properties, are depleted (Kawatani et al., 2011). So, we can only speculate that the lack of both *Nrf2* and *Hfe* genes prompt the mice to the development of anemia, since *Hfe* is essential to balance the iron uptake by RBC and *Nrf2* is needed to increase RBC survival in the presence of ROS.

2. *Hfe* and *Nrf2* genes in gluconeogenesis

It has been demonstrated that the targeted inactivation of the *Hfe* gene in mice results in decreased insulin secretory capacity (Cooksey et al., 2004). Iron overload is common in type 2 diabetes (Fernandez-Real et al., 2002; Ford and Cogswell, 1999; Forouhi et al., 2007) and the most commonly studied model for iron associated diabetes is HH (Huang et al., 2011). Conversely, iron depletion seems to be protective against the development of diabetes (Huang et al., 2011). In contrast to previous descriptions of diabetes in *Hfe*$^{-/-}$ mice in the literature, in our study *Hfe*$^{-/-}$ mice were not diabetic and *Nrf2/Hfe*$^{-/-}$ mice were hypoglycemic, as they presented significantly decreased serum glucose at starvation. Moreover, *Hfe*$^{-/-}$ and *Nrf2/Hfe*$^{-/-}$ mice presented normal values of insulin when compared to WT mice. As insulin is responsible for the reduction of plasma glucose levels, and no significant differences were found in mice of the four genotypes, we can conclude that insulin levels were not the cause of the hypoglycemia of *Nrf2/Hfe*$^{-/-}$ mice. To further investigate the hypoglycemia in *Nrf2/Hfe*$^{-/-}$ mice, we aimed to determine if a defect in gluconeogenesis was the origin of the low levels of glucose. Gluconeogenesis is *de novo* synthesis of glucose from noncarbohydrate precursors, such as lactate, pyruvate, glycerol and alanine. The rate of gluconeogenesis is controlled principally by the activities of PEPCK, fructose-1,6-bisphosphatase and glucose-6-phosphatase (Yoon et al., 2001). No significant differences were detected in *G6pc* and *Pepck* transcript levels in *Nrf2/Hfe*$^{-/-}$ liver. Hence, we have no evidence that the hypoglycemia of *Nrf2/Hfe*$^{-/-}$ mice

was due to compromised gluconeogenesis. It is thus possible that the hypoglycemia at starvation is simply the result of the worse body condition of *Nrf2/Hfe*$^{-/-}$ mice, which is illustrated by the decreased body weight when compared to all the other genotypes. Further investigation should be done to clarify the origin of the low levels of glucose in *Nrf2/Hfe*$^{-/-}$ mice.

3. *Hfe* and *Nrf2* genes in iron metabolism

The *Hfe*$^{-/-}$ mouse is a model of systemic iron overload and mimics human HH (Bahram et al., 1999). As expected, *Hfe*$^{-/-}$ mice presented significantly augmented serum iron and transferrin saturation when compared to other genotypes. However, *Nrf2/Hfe*$^{-/-}$ mice did not present augmented levels of these parameters as would be expectable since the lack of *Hfe* gene deregulates hepcidin expression and leads to systemic iron overload. The surprisingly low levels of serum iron in *Nrf2/Hfe*$^{-/-}$ mice were not observed in younger animals (Tiago Duarte, personal communication) and may be a consequence of the anemia. The increased bone marrow iron demand (for erythrocyte production) may have contributed to these low levels. Likewise, since there are less erythrocytes being recycled by macrophages, consequently, less iron is expected to be released into the bloodstream. The lack of *Nrf2* gene seems to have no influence on serum iron and transferrin saturation, as the values of *Nrf2*$^{-/-}$ mice were identical to the ones of WT mice.

Nrf2$^{-/-}$*, Hfe*$^{-/-}$ and *Nrf2/Hfe*$^{-/-}$ livers presented significantly decreased *Hamp* mRNA levels in comparison with WT livers. Low levels of *Hamp* transcript in *Hfe*$^{-/-}$ and *Nrf2/Hfe*$^{-/-}$ livers were expected, since it was previously reported that the hepatic expression of hepcidin is inappropriately low in the *Hfe*$^{-/-}$ mouse (Ahmad et al., 2002). However, lower levels were not expected for *Nrf2*$^{-/-}$ mice. Further investigation needs to be done to determine if the *Nrf2* gene is involved in the regulation of *Hamp* transcription. The amount of non-heme iron in the liver was significantly augmented in *Hfe*$^{-/-}$ and *Nrf2/Hfe*$^{-/-}$ mice when compared to *Nrf2*$^{-/-}$ and WT mice. The increased hepatic non-heme iron, a feature of *Hfe*$^{-/-}$ model (Bahram et al., 1999), was likely due to the decreased hepcidin expression, which allows increased intestinal iron uptake and its delivery to plasma, resulting in increased Tf saturation and tissue iron accumulation. The *Hamp* mRNA/Liver non-heme Fe ratio is a measure of whether the hepcidin expression is adequate to the hepatic iron stores. The ratio was significantly decreased in *Hfe*$^{-/-}$ and *Nrf2/Hfe*$^{-/-}$ mice when compared to WT mice. These data indicate that the hepcidin expression is insufficient to face the hepatic iron content of *Hfe*$^{-/-}$ and *Nrf2/Hfe*$^{-/-}$ mice, which is in agreement with the lack of *Hfe* gene. It also indicates that, despite *Nrf2*$^{-/-}$ mice presenting low levels of *Hamp* mRNA, the hepcidin expression is in agreement with the hepatic iron

content. A previous study by Ahmad et al., 2002 have already reported that the normal relationship between iron stores and liver hepcidin expression is altered with the loss of *Hfe* gene (Ahmad et al., 2002). The spleen and kidney non-heme iron contents were not significantly different between the mice of the four genotypes, indicating that the non-heme iron content of these organs is not influenced by the genotype.

Perls' Prussian Blue staining revealed that the spleen of the mice of the four genotypes accumulated high amounts of iron, whereas iron deposition was only detected in the kidney, heart and pancreas of *Nrf2/Hfe*$^{-/-}$ mice. The spleen is an organ known to accumulate large amounts of iron, as spleen macrophages are the main responsible for erythrophagocitosis (Knutson and Wessling-Resnick, 2003). Our findings are surprising, since *Nrf2/Hfe*$^{-/-}$ mice are mildly anemic, but also presented large amounts of iron in Perls' Prussian Blue staining. *Nrf2/Hfe*$^{-/-}$ mice seem to accumulate higher amounts of iron in the parenchyma of the several organs than the other genotypes, in spite of the anemia.

Liver sections stained with Perls' Prussian Blue revealed higher amounts of iron deposits (hemosiderin) in *Hfe*$^{-/-}$ and *Nrf2/Hfe*$^{-/-}$ mice than in *Nrf2*$^{-/-}$ and WT mice. Hepatocytic iron was significantly increased in *Hfe*$^{-/-}$ and *Nrf2/Hfe*$^{-/-}$ mice when compared to WT and *Nrf2*$^{-/-}$, but the amount of iron in the hepatocytes of *Hfe*$^{-/-}$ mice was significantly higher than the one in *Nrf2/Hfe*$^{-/-}$. Hepatocytes are an important site of iron storage in the form of ferritin, so it was already expected that *Hfe*$^{-/-}$ and *Nrf2/Hfe*$^{-/-}$ hepatocytes presented high amounts of iron, since the lack of HFE leads to increased iron uptake. What was an interesting finding was the fact that the *Hfe*$^{-/-}$ hepatocytes presented higher levels of iron than *Nrf2/Hfe*$^{-/-}$ hepatocytes. These finding can be related to the anemia of the *Nrf2/Hfe*$^{-/-}$ mice, since there was less iron in circulation and, consequently, less iron to be stored in ferritin. On the other hand, sinusoidal iron was only augmented in *Nrf2/Hfe*$^{-/-}$ mice. Sinusoidal iron corresponds to deposits of iron in Kupffer cells and endothelial cells inside the liver sinusoids. A characteristic feature of mouse models of HH is the iron-deficient phenotype of their macrophages, enterocytes and adipocytes in spite of systemic iron overload (Fleming and Ponka, 2012). The presence of iron in *Nrf2/Hfe*$^{-/-}$ sinusoids was unexpected, not only because of the iron-depletion phenotype expected, but also because of the anemia. We can hypothesize that the lack of *Nrf2* somehow modulates iron metabolism in *Hfe*$^{-/-}$ mice, by shifting iron deposition from the liver parenchyma to the sinusoidal cells. Possible explanations for this shift are the phagocytosis of dead hepatocytes or increased erythrophagocytosis by sinusoidal cells.

4. *Hfe* and *Nrf2* genes and oxidative stress

The liver is capable of accumulating high amounts of iron. The excess free iron leads to liver damage due to ROS formation. NRF2 upregulates many cytoprotective enzymes that take part in the antioxidant response and plays an important role in the hepatic aging process. It has been demonstrated that age-related decrease in resistance to oxidative stress results from the lower expression of antioxidant enzymes, including GPx, GR, CAT, and NQO1 (Shih and Yen, 2007). Furthermore, with age, there is a substantial reduction in glutathione (GSH) levels and in the expression and activity of glutamate cysteine ligase, the rate controlling enzyme in GSH synthesis (Suh et al., 2004). These events are accompanied by lower levels of NRF2 protein and a reduction in NRF2/ARE binding, as well as increased markers of protein and lipid oxidation (Shih and Yen, 2007; Suh et al., 2004). The reason why aging organisms gradually lose the ability to activate NRF2 is currently not understood (Hayes and Dinkova-Kostova, 2014), but a decline in NRF2 signaling is presumed to contribute to the age-related hepatic oxidative stress. Transcript levels of *Nqo1* showed a significant decrease in *Nrf2* $^{-/-}$ and *Nrf2/Hfe* $^{-/-}$ livers when compared to WT and *Hfe* $^{-/-}$ livers. This result was expected since the antioxidant enzyme NQO1 is upregulated by NRF2. GSX, GSH and GSSG did not show significant differences between the livers of the four genotypes. However, the GSH/GSSG ratio was significantly decreased in *Nrf2* $^{-/-}$ livers when compared to *Hfe* $^{-/-}$ livers. This ratio represents the balance between the reduced form of glutathione (GSH) and the oxidized one (GSSG). A predominance of the oxidized form is suggestive of oxidative stress. GSH/GSSG ratio was expected to be low in the absence of *Nrf2* gene, so it is surprising that *Nrf2/Hfe* $^{-/-}$ livers did not present an even lower ratio. MDA concentration, a marker of lipid peroxidation, did not show significant differences between the livers of the four genotypes. The lack of differences in MDA concentration may be possibly due to the late age of the model, since, as mentioned before, the markers of lipid peroxidation tend to augment with age.

5. *Hfe* and *Nrf2* genes in liver fibrosis

One of the main consequences of HH is liver fibrosis, the accumulation of extracellular matrix or scar tissue in the liver. Even if not statistically significant, the levels of *Acta2* transcript were slightly augmented in *Nrf2/Hfe* $^{-/-}$ mice. This indicates that HSCs are being transdifferentiated to α-SMA-positive myofibroblasts, the main producers of ECM. *Col1a1* gene, one of the genes involved in liver fibrosis, and the percentage of liver fibrotic area were significantly augmented in *Nrf2/Hfe* $^{-/-}$ mice compared to *Nrf2* $^{-/-}$ mice and to WT, *Nrf2* $^{-/-}$ and *Hfe* $^{-/-}$ mice, respectively. Hydroxiproline, the major component of

collagen, and TIMP-1, an inhibitor of matrix metalloproteinases (responsible for ECM degradation), were also slightly augmented in *Nrf2/Hfe*$^{-/-}$ mice. The degree of fibrosis was further assessed in liver sections stained with Sirius Red. Fibrosis was more exuberant in *Nrf2/Hfe*$^{-/-}$ mice. While in WT, *Nrf2* $^{-/-}$ and *Hfe*$^{-/-}$ livers fibrosis was mild/moderate and localized in zone 3 or in portal/periportal areas, *Nrf2/Hfe*$^{-/-}$ livers presented bridging fibrosis, with collagen fibers linking portal and central veins. These data are compatible with augmented production of ECM and decreased ECM degradation in *Nrf2/Hfe*$^{-/-}$ mice. It is worth noting that the amount of non-heme Fe present in the liver of *Hfe*$^{-/-}$ and *Nrf2/Hfe*$^{-/-}$ mice was very similar, but the former are protected from fibrosis. Our findings thus indicate that *Nrf2* gene is important in the progression of HH.

6. *Hfe* and *Nrf2* genes in liver inflammation and steatosis

Increased iron stores are correlated with markers of chronic inflammation and the adaptation to iron deficiency confers resistance to infection and improves the inflammatory condition. Hepcidin is upregulated by inflammatory stress response pathways and triggers systemic iron withdrawal and sequestration due to ferroportin down-regulation (Wessling-Resnick, 2010). Despite the large contribution of hepcidin, other stress response pathways also participate in the inflammatory response, including cytokine-mediated effects elicited by tumor necrosis factor-α (TNF-α) and interferon-γ (IFN-γ) (Weiss, 2009). During inflammation, several cytokines, like IL-6, and chemokines, such as CCL-2, are released (Liaskou et al., 2012). Although no significant differences were detected in the levels of *Tnf-α* and *Ccl2* genes in the livers of the mice of the four genotypes, significantly decreased levels of *Il-6* transcript were detected in *Nrf2*$^{-/-}$ and *Nrf2/Hfe*$^{-/-}$ livers when compared to WT and *Hfe*$^{-/-}$ livers. These results were not expected, since NRF2 is reported to have an anti-inflammatory role (Kensler et al., 2007). We expected to see higher levels of markers of inflammation in *Nrf2*$^{-/-}$ and *Nrf2/Hfe*$^{-/-}$ livers, since the antioxidant defense is compromised due to the lack of NRF2. Nevertheless, despite of the low transcript levels of cytokines and chemokines in the liver of *Nrf2*$^{-/-}$ and *Nrf2/Hfe*$^{-/-}$ mice, the levels of GM-CSF, IFN-γ, IL-1b, IL-6, IL-10, MCP-1 and TNF-α were, although not significantly, augmented in *Nrf2*$^{-/-}$ serum. These data show us that *Nrf2*$^{-/-}$ mice present slightly higher levels of pro-inflammatory cytokines and chemokines than the mice of the other genotypes. Lobular inflammation was assessed in H&E stained liver sections and no significant differences were found, which indicates that the low levels of inflammation seen in the livers of the four genotypes must be a

consequence of the advanced age of the model rather than a consequence of the genotype.

Steatosis is commonly observed in HFE-related iron-overload disorders, like HH, and current evidence suggests a causal link between iron and steatosis (Tan et al., 2011). Excessive iron causes oxidative stress that leads to mitochondrial dysfunction, impaired fatty acid (FA) oxidation and subsequent development of steatosis (Rector et al., 2010). In this study, steatosis was significantly augmented in *Hfe*$^{-/-}$ livers when compared to WT and *Nrf2*$^{-/-}$ livers. Tan et al., 2011 have already reported an augment of steatosis degree in *Hfe*$^{-/-}$ mice when compared to WT mice (Tan et al., 2011). Steatosis was not observed, however, in *Nrf2/Hfe*$^{-/-}$ mice, possibly as a consequence of their low body weight/condition.

7. *Hfe* and *Nrf2* genes and liver damage

Oxidative stress affects liver function, induces hepatocyte cell death and disturbs the regeneration process after injury (Fausto, 2000), so NRF2 is essential to protect the liver against possible injuries caused by oxidative stress. It was reported that pharmacological activation of *Nrf2*, for example, by synthetic triterpenoids or avicins, could be a promising new strategy to improve regeneration in patients with acute or chronic liver damage (Hanausek et al., 2001; Hyer et al., 2005; Liby et al., 2005). In the current study, ALT activity in serum, a marker of liver damage, was not augmented in *Nrf2*$^{-/-}$ and *Nrf2/Hfe*$^{-/-}$ mice. However, the number of TUNEL-positive cells and the degree of necrosis were significantly increased in *Nrf2/Hfe*$^{-/-}$ livers, indicating that double knockout mice had more hepatic cell death. This study showed that the suppression of NRF2 leads to spontaneous liver damage in the mouse model of HH (*Hfe*$^{-/-}$), which suggests that NRF2 may also play an important hepatoprotectant role in HH patients.

Human study

It is known that oxidative stress may aggravate the clinical expression of HH (Pietrangelo, 2010). NRF2 is one key transcription factor involved in the antioxidant defense and there are strong associations between *NRF2* sequence variations and disease risks (Cho, 2013). In this work we aimed to determine if SNPs in the promoter region of *NRF2* gene could influence the severity of HH. For that purpose we estimated allele frequencies of known SNPs in the *NRF2* promoter region in a large cohort of clinically well characterized HH patients and analysed both allele and genotype frequencies in relation to a set of clinical relevant variables.

Patients in our study presented elevated levels of ferritin and transferrin saturation, typical features of HH patients (Beutler, 2006) that are indicative of systemic iron overload. The severity of the iron overload ranged from moderate to severe. In terms of clinical manifestations, skin pigmentation was the most common one (17.9%), followed by cirrhosis (21.4%), arthropathy (16.4%), diabetes (4.5%) and hypogonadism (1.5%).

When comparing the frequencies of Rs35652124, Rs6706649, Rs150648896 and Rs6721961 SNPs between the total 97 DNA samples from unrelated subjects and the ones reported in Ensembl for the European population, no statistically significant differences were observed. Moreover, when comparing the frequency of each SNP in patients clinically well characterized (n = 57) according to the expression of the disease, also no significant differences were found indicating that, in general, none of the studied SNPs *per se* prompts the patients to develop a specific clinical manifestation. Nevertheless, the frequency of the allele T in Rs35652124 SNP was increased in patients with cirrhosis and in symptomatic patients in general, when compared to patients without cirrhosis and without any clinical manifestations. To further clarify this question, we compared genotypes homozygous for the allele T in Rs35652124 SNP (Total TT) and genotypes homozygous/heterozygous for the allele C in Rs35652124 SNP (Total with C) in a subgroup of patients (n = 36) more strictly selected in terms of clinical variables. We then observed that frequency of cirrhosis was significantly increased in Total TT when compared to Total with CC genotypes and, although not statistically significant, symptomatic patients in general were also more common in Total TT genotypes. One should note that TBIS were also significantly increased in Total TT genotypes, therefore at this stage we cannot distinguish the relative impact of genotype and/or iron overload in the frequency of cirrhosis. Further extended studies, with a larger sample of patients, are needed to clarify that question. We can exclude, however, the impact of CD8+ T lymphocyte numbers on the results observed. It is known that low numbers of CD8+ T-lymphocytes are associated with a more severe iron overload and clinical expression in HH patients (Cruz et al., 2006). Since no significant differences were found in the CD8 phenotype between Total TT and Total with C genotypes, we can exclude CD8+ T-lymphocytes as the origin of the different clinical manifestation between the two groups.

It is worth noting that the Rs35652124 T allele, which was found here associated with a more severe clinical expression, is the most frequent in the normal European population. If natural selection favored this allele in normal populations, we would not expect it have appeared as a particularly deleterious genotype in patients with HH, where it is also naturally more common. On the contrary, we hypothesize that the rarer allele C

in Rs35652124 SNP may act as a putative protective allele in HH, since, in our cohort, patients with this genotype had a less severe clinical picture. The Rs35652124 SNP has been previously reported to be a functional SNP predicted to affect *Nrf2* myeloid zinc finger 1 (MZF1) promoter binding site. More specifically, the Rs35652124 C allele was shown to reduce the transcription activity of *Nrf2* in a Luciferase activity assay (Marzec et al., 2007), presumably resulting in decreased *Nrf2*-dependent gene transcription. Interestingly, a study by von Otter et al., 2014 implicated Rs35652124 SNP in the progression of Parkinson's disease showing that the Rs35652124 T allele was part of a protective haplotype that was associated with decreased risk and later onset of Parkinson's disease (von Otter et al., 2014). How could differences in the transcription activity of *NRF2* affect iron metabolism and the clinical consequences of HH, this is certainly a subject of great interest for future research in the iron biology field.

Study limitations

We acknowledge that the human study has two important limitations. One is the small sample size. More patients must be recruited in future in order to gain statistical power and hence augment the chances of finding significant associations between *NRF2* SNPs and the clinical manifestation of HH. We should stress, however, that the reduction in the sample size from the original total number of patients genotyped was done with the objective of maintaining highly rigorous and strict clinical criteria. The second limitation of the study was the fact that we have only analyzed SNPs present in the promoter region of the *NRF2* gene. Even though there is evidence in the literature linking Rs35652124, Rs6706649, Rs150648896 and Rs6721961 SNPs to phenotype-variants of certain diseases, it would be interesting to also study polymorphisms in the coding region of the *NRF2* gene, by TaqMan Allelic Discrimination Assay, a multiplexed end-point assay that detects variants of a single nucleic acid sequence, or by sequencing the exons and exon-flanking regions.

Conclusions

In this study, *Hfe*$^{-/-}$ mice were used as a model of HH, mimicking what happens in patients homozygous for the *HFE* C282Y mutation. It is known that the lack of the *Hfe* gene leads to iron overload. The liver is capable of accumulating high amounts of iron and, in turn, iron is capable of generating ROS, leading to oxidative stress. Oxidative stress, in the absence of proper antioxidant defense, can lead to liver damage. NRF2 is the key transcription factor that regulates the antioxidant defense. *Nrf2/Hfe*$^{-/-}$ mice thus represent what happens to HH patients in the absence of an appropriate antioxidant defense.

In our study, *Nrf2/Hfe*$^{-/-}$ mice were mildly anemic. Even if we could not determine the exact source of the anemia, we suppose that the lack of both *Nrf2* and *Hfe* genes may have contributed to this finding, as *Hfe* gene is essential to balance the iron uptake by RBC and *Nrf2* gene is necessary to increase RBC survival in the presence of ROS. *Nrf2/Hfe*$^{-/-}$ mice were also hypoglycemic. We hypothesized that the hypoglycemia at starvation could be a consequence of the worse body condition of *Nrf2/Hfe*$^{-/-}$ mice, as they presented the lowest weight.

Nrf2/Hfe$^{-/-}$ mice presented lower levels of serum iron and transferrin saturation than *Hfe*$^{-/-}$ mice. The lack of NRF2 seems to have no influence on these parameters, since identical values were observed in *Nrf2*$^{-/-}$ and WT mice. The low serum iron and transferrin saturation of *Nrf2/Hfe*$^{-/-}$ mice were possibly a consequence of the anemia, as a decrease in erythrophagocytosis would be expected to decrease iron liberation into the bloodstream. An increase in bone marrow iron demand would also be expected to diminish the iron in circulation. In *Nrf2/Hfe*$^{-/-}$ mice, iron deposits were observed in the sinusoidal cells, contrary to the exclusive iron deposition in the liver parenchyma in *Hfe*$^{-/-}$ mice. NRF2 thus seems to modulate iron metabolism in *Hfe*$^{-/-}$ mice, by shifting iron deposition from the liver parenchyma to the sinusoidal cells.

Nrf2$^{-/-}$ and *Nrf2/Hfe*$^{-/-}$ livers presented significantly decreased transcript levels of *Nqo1* when compared to WT and *Hfe*$^{-/-}$ mice, confirming that the NRF2 signaling pathway was not being activated, due to the lack of functional NRF2 in these animals. Besides, the GSH/GSSG ratio was significantly decreased in *Nrf2*$^{-/-}$ livers when compared to *Hfe*$^{-/-}$ livers. These data indicate that *Nrf2*$^{-/-}$ mice are under more oxidative stress than *Hfe*$^{-/-}$ mice, which reinforces the importance of NRF2 in the antioxidant defense. It is worth noting that MDA concentration of the four genotypes was not statistically different, suggesting that the occurrence of lipid peroxidation may be a consequence of the late age of the model, as the markers of lipid peroxidation tend to augment with age.

Mild liver inflammation was detected in mice of the four genotypes, with no significant differences between the experimental groups. The low levels of inflammation are thus

likely to be a consequence of the advanced age of the model rather than a consequence of the genotype. On the other hand, steatosis was significantly augmented in *Hfe*$^{-/-}$ livers, but not in *Nrf2/Hfe*$^{-/-}$ livers, when compared to WT and *Nrf2*$^{-/-}$ livers. We speculate that the absence of steatosis in *Nrf2/Hfe*$^{-/-}$ mice may be a consequence of their low body weight/condition.

The amount of non-heme Fe present in the livers of *Hfe*$^{-/-}$ and *Nrf2/Hfe*$^{-/-}$ mice was very similar, but markers of liver fibrosis and the degree of liver fibrosis were augmented only in *Nrf2/Hfe*$^{-/-}$ livers. Likewise, the number of TUNEL-positive cells and the degree of necrosis were significantly increased only in *Nrf2/Hfe*$^{-/-}$ livers, indicating increased hepatic cell death. Overall, we conclude that the suppression of NRF2 leads to spontaneous liver damage in *Hfe*$^{-/-}$ mice, the mouse model of HH. Based on this evidence, we hypothesize that NRF2 may also play an important role in HH patients, protecting hepatic cells from the damage caused by excessive iron.

To address that hypothesis, we asked if some SNP variants in the *NRF2* promoter region could prompt HH patients to develop a more severe phenotype of the disease. Our results indicate that none of the SNPs alone prompts the patients to develop a specific clinical manifestation, but it showed that patients carrying the allele C in Rs35652124 SNP are somehow protected from clinical manifestations of HH. Further studies are required to overcome the present sample limitations and to determine if the here observed effect is the result of a lower accumulation of iron in allele C carriers or from an enhanced antioxidant response in these subjects.

In conclusion, the current study shows that NRF2 has an important hepatoprotective role in the animal model of HH and suggests that gene variants may be also implicated in the clinical course of the human disease. The possibility that SNPs in the *NRF2* gene may modify HH penetrance warrants further investigation.

Future perspectives

Concerning the animal study, the anemia and hypoglycemia at starvation of the *Nrf2/Hfe*$^{-/-}$ mice need to be clarified. The low body weight/condition of *Nrf2/Hfe*$^{-/-}$ mice also needs to be investigated, to determine if the lack of both *Nrf2* and *Hfe* genes combined with the advanced age of the model is by itself the origin of this poor condition. The role of NRF2 as a modulator of iron distribution in *Hfe*$^{-/-}$ mice and the mechanisms how NRF2 protects these mice against liver damage also need to be clarified. In what concerns the human study, more SNPs should be studied (including coding regions of the NRF2 gene) and the sample size should be increased, in order to determine if there is an association between NRF2 genetic variants and clinical manifestations of HH.

Publications

Chambel, S.S., Santos-Goncalves, A., and Duarte, T.L. (2015). The Dual Role of *Nrf2* in Nonalcoholic Fatty Liver Disease: Regulation of Antioxidant Defenses and Hepatic Lipid Metabolism. BioMed research international *2015*, 597134.

References

Abboud, S., and Haile, D.J. (2000). A novel mammalian iron-regulated protein involved in intracellular iron metabolism. The Journal of biological chemistry *275*, 19906-19912.
Ahmad, K.A., Ahmann, J.R., Migas, M.C., Waheed, A., Britton, R.S., Bacon, B.R., Sly, W.S., and Fleming, R.E. (2002). Decreased liver hepcidin expression in the Hfe knockout mouse. Blood cells, molecules & diseases *29*, 361-366.
Aisen, P. (2004). Transferrin receptor 1. The international journal of biochemistry & cell biology *36*, 2137-2143.
Andrews, N.C. (1999). Disorders of iron metabolism. The New England journal of medicine *341*, 1986-1995.
Andrews, N.C., and Schmidt, P.J. (2007). Iron homeostasis. Annual review of physiology *69*, 69-85.
Aronoff, S.L., Berkowitz, K., Shreiner, B., and Want, L. (2004). Glucose metabolism and regulation: beyond insulin and glucagon. Diabetes Spectrum *17*, 183-190.
Aslinia, F., Mazza, J.J., and Yale, S.H. (2006). Megaloblastic Anemia and Other Causes of Macrocytosis. Clinical Medicine and Research *4*, 236-241.
Austyn, J.M., and Gordon, S. (1981). F4/80, a monoclonal antibody directed specifically against the mouse macrophage. European journal of immunology *11*, 805-815.
Ayonrinde, O.T., Milward, E.A., Chua, A.C., Trinder, D., and Olynyk, J.K. (2008). Clinical perspectives on hereditary hemochromatosis. Critical reviews in clinical laboratory sciences *45*, 451-484.
Bacon, B.R. (1997). Diagnosis and management of hemochromatosis. Gastroenterology *113*, 995-999.
Bahram, S., Gilfillan, S., Kuhn, L.C., Moret, R., Schulze, J.B., Lebeau, A., and Schumann, K. (1999). Experimental hemochromatosis due to MHC class I HFE deficiency: immune status and iron metabolism. Proceedings of the National Academy of Sciences of the United States of America *96*, 13312-13317.
Barbero-Becerra, V.J., Giraudi, P.J., Chavez-Tapia, N.C., Uribe, M., Tiribelli, C., and Rosso, N. (2015). The interplay between hepatic stellate cells and hepatocytes in an in vitro model of NASH. Toxicology in vitro : an international journal published in association with BIBRA *29*, 1753-1758.
Barton, J.C., Bertoli, L.F., and Rothenberg, B.E. (2000). Peripheral blood erythrocyte parameters in hemochromatosis: evidence for increased erythrocyte hemoglobin content. The Journal of laboratory and clinical medicine *135*, 96-104.
Bataller, R., and Brenner, D.A. (2005). Liver fibrosis. The Journal of clinical investigation *115*, 209-218.
Beguin, Y., Clemons, G.K., Pootrakul, P., and Fillet, G. (1993). Quantitative assessment of erythropoiesis and functional classification of anemia based on measurements of serum transferrin receptor and erythropoietin. Blood *81*, 1067-1076.
Bernard, J. (1991). The erythroblastic island: past and future. Blood cells *17*, 5-10; discussion 10-14.
Beutler, E. (2006). Hemochromatosis: genetics and pathophysiology. Annual review of medicine *57*, 331-347.
Bioulac-Sage, P., and Lebail B. Balabaud, C. (2007). Liver and biliary tract histology. In Textbook of hepatology: from basic science to clinical practice (Malden: Wiley-Blackwell Publishing).
Brown, P.J., and Johnson, P.M. (1981). Isolation of a transferrin receptor structure from sodium deoxycholate-solubilized human placental syncytiotrophoblast plasma membrane. Placenta *2*, 1-10.

Cabiscol, E., Tamarit, J., and Ros, J. (2000). Oxidative stress in bacteria and protein damage by reactive oxygen species. International microbiology : the official journal of the Spanish Society for Microbiology *3*, 3-8.
Camaschella, C., Roetto, A., Cali, A., De Gobbi, M., Garozzo, G., Carella, M., Majorano, N., Totaro, A., and Gasparini, P. (2000). The gene TFR2 is mutated in a new type of haemochromatosis mapping to 7q22. Nature genetics *25*, 14-15.
Canonne-Hergaux, F., Donovan, A., Delaby, C., Wang, H.J., and Gros, P. (2006). Comparative studies of duodenal and macrophage ferroportin proteins. American journal of physiology Gastrointestinal and liver physiology *290*, G156-163.
Cartwright, G. (1966). The anemia of chronic disorders. Paper presented at: Seminars in hematology.
Casanovas, G., Mleczko-Sanecka, K., Altamura, S., Hentze, M.W., and Muckenthaler, M.U. (2009). Bone morphogenetic protein (BMP)-responsive elements located in the proximal and distal hepcidin promoter are critical for its response to HJV/BMP/SMAD. Journal of molecular medicine (Berlin, Germany) *87*, 471-480.
Caza, M., and Kronstad, J.W. (2013). Shared and distinct mechanisms of iron acquisition by bacterial and fungal pathogens of humans. Frontiers in cellular and infection microbiology *3*, 80.
Chai, Y.C., Ashraf, S.S., Rokutan, K., Johnston, R.B., Jr., and Thomas, J.A. (1994). S-thiolation of individual human neutrophil proteins including actin by stimulation of the respiratory burst: evidence against a role for glutathione disulfide. Archives of biochemistry and biophysics *310*, 273-281.
Chalasani, N., Wilson, L., Kleiner, D.E., Cummings, O.W., Brunt, E.M., and Unalp, A. (2008). Relationship of steatosis grade and zonal location to histological features of steatohepatitis in adult patients with non-alcoholic fatty liver disease. Journal of hepatology *48*, 829-834.
Chateauvieux, S., Grigorakaki, C., Morceau, F., Dicato, M., and Diederich, M. (2011). Erythropoietin, erythropoiesis and beyond. Biochemical pharmacology *82*, 1291-1303.
Cho, H.Y. (2013). Genomic structure and variation of nuclear factor (erythroid-derived 2)-like 2. Oxidative medicine and cellular longevity *2013*, 286524.
Cohen, L.A., Gutierrez, L., Weiss, A., Leichtmann-Bardoogo, Y., Zhang, D.L., Crooks, D.R., Sougrat, R., Morgenstern, A., Galy, B., Hentze, M.W.*, et al.* (2010). Serum ferritin is derived primarily from macrophages through a nonclassical secretory pathway. Blood *116*, 1574-1584.
Cooksey, R.C., Jouihan, H.A., Ajioka, R.S., Hazel, M.W., Jones, D.L., Kushner, J.P., and McClain, D.A. (2004). Oxidative stress, beta-cell apoptosis, and decreased insulin secretory capacity in mouse models of hemochromatosis. Endocrinology *145*, 5305-5312.
Cruz, E., Melo, G., Lacerda, R., Almeida, S., and Porto, G. (2006). The CD8+ T-lymphocyte profile as a modifier of iron overload in HFE hemochromatosis: an update of clinical and immunological data from 70 C282Y homozygous subjects. Blood cells, molecules & diseases *37*, 33-39.
Delaby, C., Rondeau, C., Pouzet, C., Willemetz, A., Pilard, N., Desjardins, M., and Canonne-Hergaux, F. (2012). Subcellular localization of iron and heme metabolism related proteins at early stages of erythrophagocytosis. PloS one *7*, e42199.
Deugnier, Y.M., Turlin, B., Powell, L.W., Summers, K.M., Moirand, R., Fletcher, L., Loreal, O., Brissot, P., and Halliday, J.W. (1993). Differentiation between heterozygotes and homozygotes in genetic hemochromatosis by means of a histological hepatic iron index: a study of 192 cases. Hepatology (Baltimore, Md) *17*, 30-34.
Donovan, A., Brownlie, A., Zhou, Y., Shepard, J., Pratt, S.J., Moynihan, J., Paw, B.H., Drejer, A., Barut, B., Zapata, A.*, et al.* (2000). Positional cloning of zebrafish ferroportin1 identifies a conserved vertebrate iron exporter. Nature *403*, 776-781.
Dunn, L.L., Suryo Rahmanto, Y., and Richardson, D.R. (2007). Iron uptake and metabolism in the new millennium. Trends in cell biology *17*, 93-100.

Evstatiev, R., and Gasche, C. (2012). Iron sensing and signalling. Gut *61*, 933-952.
Fausto, N. (2000). Liver regeneration. Journal of hepatology *32*, 19-31.
Feeney, G.P., Carter, K., Masters, G.S., Jackson, H.A., Cavil, I., and Worwood, M. (2005). Changes in erythropoiesis in hereditary hemochromatosis are not mediated by HFE expression in nucleated red cells. Haematologica *90*, 180-187.
Fernandez-Real, J.M., Lopez-Bermejo, A., and Ricart, W. (2002). Cross-talk between iron metabolism and diabetes. Diabetes *51*, 2348-2354.
Fleming, R.E., Ahmann, J.R., Migas, M.C., Waheed, A., Koeffler, H.P., Kawabata, H., Britton, R.S., Bacon, B.R., and Sly, W.S. (2002). Targeted mutagenesis of the murine transferrin receptor-2 gene produces hemochromatosis. Proceedings of the National Academy of Sciences of the United States of America *99*, 10653-10658.
Fleming, R.E., and Ponka, P. (2012). Iron overload in human disease. The New England journal of medicine *366*, 348-359.
Ford, E.S., and Cogswell, M.E. (1999). Diabetes and serum ferritin concentration among U.S. adults. Diabetes care *22*, 1978-1983.
Forouhi, N.G., Harding, A.H., Allison, M., Sandhu, M.S., Welch, A., Luben, R., Bingham, S., Khaw, K.T., and Wareham, N.J. (2007). Elevated serum ferritin levels predict new-onset type 2 diabetes: results from the EPIC-Norfolk prospective study. Diabetologia *50*, 949-956.
Fowell, A.J., Collins, J.E., Duncombe, D.R., Pickering, J.A., Rosenberg, W.M., and Benyon, R.C. (2011). Silencing tissue inhibitors of metalloproteinases (TIMPs) with short interfering RNA reveals a role for TIMP-1 in hepatic stellate cell proliferation. Biochemical and biophysical research communications *407*, 277-282.
Fraser, S.T., Midwinter, R.G., Berger, B.S., and Stocker, R. (2011). Heme Oxygenase-1: A Critical Link between Iron Metabolism, Erythropoiesis, and Development. Advances in hematology *2011*, 473709.
Ganz, T. (2013). Systemic iron homeostasis. Physiological reviews *93*, 1721-1741.
Ganz, T., and Nemeth, E. (2012). Hepcidin and iron homeostasis. Biochimica et biophysica acta *1823*, 1434-1443.
Gao, J., Chen, J., Kramer, M., Tsukamoto, H., Zhang, A.S., and Enns, C.A. (2009). Interaction of the hereditary hemochromatosis protein HFE with transferrin receptor 2 is required for transferrin-induced hepcidin expression. Cell metabolism *9*, 217-227.
Gkouvatsos, K., Papanikolaou, G., and Pantopoulos, K. (2012). Regulation of iron transport and the role of transferrin. Biochimica et biophysica acta *1820*, 188-202.
Gordon, S., and Taylor, P.R. (2005). Monocyte and macrophage heterogeneity. Nature reviews Immunology *5*, 953-964.
Gunshin, H., Mackenzie, B., Berger, U.V., Gunshin, Y., Romero, M.F., Boron, W.F., Nussberger, S., Gollan, J.L., and Hediger, M.A. (1997). Cloning and characterization of a mammalian proton-coupled metal-ion transporter. Nature *388*, 482-488.
Gunshin, H., Starr, C.N., Direnzo, C., Fleming, M.D., Jin, J., Greer, E.L., Sellers, V.M., Galica, S.M., and Andrews, N.C. (2005). Cybrd1 (duodenal cytochrome b) is not necessary for dietary iron absorption in mice. Blood *106*, 2879-2883.
Halliwell, B., and Gutteridge, J.M. (1990). Role of free radicals and catalytic metal ions in human disease: an overview. Methods in enzymology *186*, 1-85.
Hanausek, M., Ganesh, P., Walaszek, Z., Arntzen, C.J., Slaga, T.J., and Gutterman, J.U. (2001). Avicins, a family of triterpenoid saponins from Acacia victoriae (Bentham), suppress H-ras mutations and aneuploidy in a murine skin carcinogenesis model. Proceedings of the National Academy of Sciences of the United States of America *98*, 11551-11556.
Hayes, J.D., and Dinkova-Kostova, A.T. (2014). The Nrf2 regulatory network provides an interface between redox and intermediary metabolism. Trends in biochemical sciences *39*, 199-218.

Healy, J., and Tipton, K. (2007). Ceruloplasmin and what it might do. Journal of neural transmission (Vienna, Austria : 1996) *114*, 777-781.
Hentze, M.W., Muckenthaler, M.U., and Andrews, N.C. (2004). Balancing acts: molecular control of mammalian iron metabolism. Cell *117*, 285-297.
Hentze, M.W., Muckenthaler, M.U., Galy, B., and Camaschella, C. (2010). Two to tango: regulation of Mammalian iron metabolism. Cell *142*, 24-38.
Hider, R.C. (2002). Nature of nontransferrin-bound iron. European journal of clinical investigation *32 Suppl 1*, 50-54.
Huang, J., Jones, D., Luo, B., Sanderson, M., Soto, J., Abel, E.D., Cooksey, R.C., and McClain, D.A. (2011). Iron overload and diabetes risk: a shift from glucose to Fatty Acid oxidation and increased hepatic glucose production in a mouse model of hereditary hemochromatosis. Diabetes *60*, 80-87.
Hvidberg, V., Maniecki, M.B., Jacobsen, C., Hojrup, P., Moller, H.J., and Moestrup, S.K. (2005). Identification of the receptor scavenging hemopexin-heme complexes. Blood *106*, 2572-2579.
Hyer, M.L., Croxton, R., Krajewska, M., Krajewski, S., Kress, C.L., Lu, M., Suh, N., Sporn, M.B., Cryns, V.L., Zapata, J.M.*, et al.* (2005). Synthetic triterpenoids cooperate with tumor necrosis factor-related apoptosis-inducing ligand to induce apoptosis of breast cancer cells. Cancer research *65*, 4799-4808.
Ilyin, G., Courselaud, B., Troadec, M.B., Pigeon, C., Alizadeh, M., Leroyer, P., Brissot, P., and Loreal, O. (2003). Comparative analysis of mouse hepcidin 1 and 2 genes: evidence for different patterns of expression and co-inducibility during iron overload. FEBS letters *542*, 22-26.
Itoh, K., Chiba, T., Takahashi, S., Ishii, T., Igarashi, K., Katoh, Y., Oyake, T., Hayashi, N., Satoh, K., Hatayama, I.*, et al.* (1997). An Nrf2/small Maf heterodimer mediates the induction of phase II detoxifying enzyme genes through antioxidant response elements. Biochemical and biophysical research communications *236*, 313-322.
Kahn, C.M. (2010). The Merck Veterinary Manual. In The Merck Veterinary Manual, C.M. Kahn, ed. (Merck & Co., Inc.).
Kansanen, E., Jyrkkanen, H.K., and Levonen, A.L. (2012). Activation of stress signaling pathways by electrophilic oxidized and nitrated lipids. Free radical biology & medicine *52*, 973-982.
Kartikasari, A.E., Wagener, F.A., Yachie, A., Wiegerinck, E.T., Kemna, E.H., and Swinkels, D.W. (2009). Hepcidin suppression and defective iron recycling account for dysregulation of iron homeostasis in heme oxygenase-1 deficiency. Journal of cellular and molecular medicine *13*, 3091-3102.
Kato, G.J., McGowan, V., Machado, R.F., Little, J.A., Taylor, J.t., Morris, C.R., Nichols, J.S., Wang, X., Poljakovic, M., Morris, S.M., Jr.*, et al.* (2006). Lactate dehydrogenase as a biomarker of hemolysis-associated nitric oxide resistance, priapism, leg ulceration, pulmonary hypertension, and death in patients with sickle cell disease. Blood *107*, 2279-2285.
Kautz, L., Jung, G., Valore, E.V., Rivella, S., Nemeth, E., and Ganz, T. (2014). Identification of erythroferrone as an erythroid regulator of iron metabolism. Nature genetics *46*, 678-684.
Kautz, L., Meynard, D., Monnier, A., Darnaud, V., Bouvet, R., Wang, R.H., Deng, C., Vaulont, S., Mosser, J., Coppin, H.*, et al.* (2008). Iron regulates phosphorylation of Smad1/5/8 and gene expression of Bmp6, Smad7, Id1, and Atoh8 in the mouse liver. Blood *112*, 1503-1509.
Kawabata, H., Yang, R., Hirama, T., Vuong, P.T., Kawano, S., Gombart, A.F., and Koeffler, H.P. (1999). Molecular cloning of transferrin receptor 2. A new member of the transferrin receptor-like family. The Journal of biological chemistry *274*, 20826-20832.
Kawatani, Y., Suzuki, T., Shimizu, R., Kelly, V.P., and Yamamoto, M. (2011). Nrf2 and selenoproteins are essential for maintaining oxidative homeostasis in erythrocytes and protecting against hemolytic anemia. Blood *117*, 986-996.

Kensler, T.W., Wakabayashi, N., and Biswal, S. (2007). Cell survival responses to environmental stresses via the Keap1-Nrf2-ARE pathway. Annual review of pharmacology and toxicology *47*, 89-116.
Khan, A.A., and Quigley, J.G. (2011). Control of intracellular heme levels: heme transporters and heme oxygenases. Biochimica et biophysica acta *1813*, 668-682.
Klaassen, C.D., and Reisman, S.A. (2010). Nrf2 the rescue: effects of the antioxidative/electrophilic response on the liver. Toxicology and applied pharmacology *244*, 57-65.
Kleiner, D.E., Brunt, E.M., Van Natta, M., Behling, C., Contos, M.J., Cummings, O.W., Ferrell, L.D., Liu, Y.C., Torbenson, M.S., Unalp-Arida, A.*, et al.* (2005). Design and validation of a histological scoring system for nonalcoholic fatty liver disease. Hepatology (Baltimore, Md) *41*, 1313-1321.
Knutson, M., and Wessling-Resnick, M. (2003). Iron metabolism in the reticuloendothelial system. Critical reviews in biochemistry and molecular biology *38*, 61-88.
Kovtunovych, G., Eckhaus, M.A., Ghosh, M.C., Ollivierre-Wilson, H., and Rouault, T.A. (2010). Dysfunction of the heme recycling system in heme oxygenase 1-deficient mice: effects on macrophage viability and tissue iron distribution. Blood *116*, 6054-6062.
Kristiansen, M., Graversen, J.H., Jacobsen, C., Sonne, O., Hoffman, H.J., Law, S.K., and Moestrup, S.K. (2001). Identification of the haemoglobin scavenger receptor. Nature *409*, 198-201.
Laftah, A.H., Latunde-Dada, G.O., Fakih, S., Hider, R.C., Simpson, R.J., and McKie, A.T. (2009). Haem and folate transport by proton-coupled folate transporter/haem carrier protein 1 (SLC46A1). The British journal of nutrition *101*, 1150-1156.
Lane, D.J., Merlot, A.M., Huang, M.L., Bae, D.H., Jansson, P.J., Sahni, S., Kalinowski, D.S., and Richardson, D.R. (2015). Cellular iron uptake, trafficking and metabolism: Key molecules and mechanisms and their roles in disease. Biochimica et biophysica acta *1853*, 1130-1144.
LeCluyse, E.L., Witek, R.P., Andersen, M.E., and Powers, M.J. (2012). Organotypic liver culture models: meeting current challenges in toxicity testing. Critical reviews in toxicology *42*, 501-548.
Lee, J.M., Calkins, M.J., Chan, K., Kan, Y.W., and Johnson, J.A. (2003). Identification of the NF-E2-related factor-2-dependent genes conferring protection against oxidative stress in primary cortical astrocytes using oligonucleotide microarray analysis. The Journal of biological chemistry *278*, 12029-12038.
Levi, S., Corsi, B., Bosisio, M., Invernizzi, R., Volz, A., Sanford, D., Arosio, P., and Drysdale, J. (2001). A human mitochondrial ferritin encoded by an intronless gene. The Journal of biological chemistry *276*, 24437-24440.
Liaskou, E., Wilson, D.V., and Oo, Y.H. (2012). Innate immune cells in liver inflammation. Mediators of inflammation *2012*, 949157.
Liby, K., Hock, T., Yore, M.M., Suh, N., Place, A.E., Risingsong, R., Williams, C.R., Royce, D.B., Honda, T., Honda, Y.*, et al.* (2005). The synthetic triterpenoids, CDDO and CDDO-imidazolide, are potent inducers of heme oxygenase-1 and Nrf2/ARE signaling. Cancer research *65*, 4789-4798.
Lim, J.E., Jin, O., Bennett, C., Morgan, K., Wang, F., Trenor, C.C., 3rd, Fleming, M.D., and Andrews, N.C. (2005). A mutation in Sec15l1 causes anemia in hemoglobin deficit (hbd) mice. Nature genetics *37*, 1270-1273.
Liuzzi, J.P., Aydemir, F., Nam, H., Knutson, M.D., and Cousins, R.J. (2006). Zip14 (Slc39a14) mediates non-transferrin-bound iron uptake into cells. Proceedings of the National Academy of Sciences of the United States of America *103*, 13612-13617.
Mackenzie, B., Shawki, A., Kim, R., Anthony, S.R., Knight, P.B., Bradford, E.M., and Shull, G.E. (2011). Intestinal brush-border Na+/H+ exchangers are required for iron homeostasis in the mouse. The FASEB Journal *25*, 238.231.

Marzec, J.M., Christie, J.D., Reddy, S.P., Jedlicka, A.E., Vuong, H., Lanken, P.N., Aplenc, R., Yamamoto, T., Yamamoto, M., Cho, H.Y*., et al.* (2007). Functional polymorphisms in the transcription factor NRF2 in humans increase the risk of acute lung injury. FASEB journal : official publication of the Federation of American Societies for Experimental Biology *21*, 2237-2246.
McCord, J.M., and Fridovich, I. (1969). Superoxide dismutase. An enzymic function for erythrocuprein (hemocuprein). The Journal of biological chemistry *244*, 6049-6055.
McKie, A.T., Barrow, D., Latunde-Dada, G.O., Rolfs, A., Sager, G., Mudaly, E., Mudaly, M., Richardson, C., Barlow, D., Bomford, A*., et al.* (2001). An iron-regulated ferric reductase associated with the absorption of dietary iron. Science (New York, NY) *291*, 1755-1759.
McKie, A.T., Marciani, P., Rolfs, A., Brennan, K., Wehr, K., Barrow, D., Miret, S., Bomford, A., Peters, T.J., Farzaneh, F*., et al.* (2000). A novel duodenal iron-regulated transporter, IREG1, implicated in the basolateral transfer of iron to the circulation. Molecular cell *5*, 299-309.
McLaren, C.E., Barton, J.C., Gordeuk, V.R., Wu, L., Adams, P.C., Reboussin, D.M., Speechley, M., Chang, H., Acton, R.T., Harris, E.L*., et al.* (2007). Determinants and characteristics of mean corpuscular volume and hemoglobin concentration in white HFE C282Y homozygotes in the hemochromatosis and iron overload screening study. American journal of hematology *82*, 898-905.
Muckenthaler, M.U. (2014). How mutant HFE causes hereditary hemochromatosis. Blood *124*, 1212-1213.
Muckenthaler, M.U., Galy, B., and Hentze, M.W. (2008). Systemic iron homeostasis and the iron-responsive element/iron-regulatory protein (IRE/IRP) regulatory network. Annual review of nutrition *28*, 197-213.
Murphy, F.R., Issa, R., Zhou, X., Ratnarajah, S., Nagase, H., Arthur, M.J., Benyon, C., and Iredale, J.P. (2002). Inhibition of apoptosis of activated hepatic stellate cells by tissue inhibitor of metalloproteinase-1 is mediated via effects on matrix metalloproteinase inhibition: implications for reversibility of liver fibrosis. The Journal of biological chemistry *277*, 11069-11076.
Naigamwalla, D.Z., Webb, J.A., and Giger, U. (2012). Iron deficiency anemia. The Canadian Veterinary Journal *53*, 250-256.
Nemeth, E., Tuttle, M.S., Powelson, J., Vaughn, M.B., Donovan, A., Ward, D.M., Ganz, T., and Kaplan, J. (2004). Hepcidin regulates cellular iron efflux by binding to ferroportin and inducing its internalization. Science (New York, NY) *306*, 2090-2093.
Neuman, R.E., and Logan, M.A. (1950). The determination of hydroxyproline. The Journal of biological chemistry *184*, 299-306.
Nguyen, T., Sherratt, P.J., and Pickett, C.B. (2003). Regulatory mechanisms controlling gene expression mediated by the antioxidant response element. Annual review of pharmacology and toxicology *43*, 233-260.
Nordberg, J., and Arner, E.S. (2001). Reactive oxygen species, antioxidants, and the mammalian thioredoxin system. Free radical biology and medicine *31*, 1287-1312.
Oh, C.J., Kim, J.Y., Min, A.K., Park, K.G., Harris, R.A., Kim, H.J., and Lee, I.K. (2012). Sulforaphane attenuates hepatic fibrosis via NF-E2-related factor 2-mediated inhibition of transforming growth factor-beta/Smad signaling. Free radical biology & medicine *52*, 671-682.
Ohgami, R.S., Campagna, D.R., McDonald, A., and Fleming, M.D. (2006). The Steap proteins are metalloreductases. Blood *108*, 1388-1394.
Papanikolaou, G., and Pantopoulos, K. (2005). Iron metabolism and toxicity. Toxicology and applied pharmacology *202*, 199-211.
Paradkar, P.N., Zumbrennen, K.B., Paw, B.H., Ward, D.M., and Kaplan, J. (2009). Regulation of mitochondrial iron import through differential turnover of mitoferrin 1 and mitoferrin 2. Molecular and cellular biology *29*, 1007-1016.

Park, C.H., Valore, E.V., Waring, A.J., and Ganz, T. (2001). Hepcidin, a urinary antimicrobial peptide synthesized in the liver. The Journal of biological chemistry *276*, 7806-7810.
Parola, M., and Robino, G. (2001). Oxidative stress-related molecules and liver fibrosis. Journal of hepatology *35*, 297-306.
Pietrangelo, A. (2005). Non-HFE hemochromatosis. Seminars in liver disease *25*, 450-460.
Pietrangelo, A. (2010). Hereditary hemochromatosis: pathogenesis, diagnosis, and treatment. Gastroenterology *139*, 393-408, 408.e391-392.
Pinto, J.P., Ribeiro, S., Pontes, H., Thowfeequ, S., Tosh, D., Carvalho, F., and Porto, G. (2008). Erythropoietin mediates hepcidin expression in hepatocytes through EPOR signaling and regulation of C/EBPalpha. Blood *111*, 5727-5733.
Poli, G., and Parola, M. (1997). Oxidative damage and fibrogenesis. Free radical biology & medicine *22*, 287-305.
Poss, K.D., and Tonegawa, S. (1997). Heme oxygenase 1 is required for mammalian iron reutilization. Proceedings of the National Academy of Sciences of the United States of America *94*, 10919-10924.
Rajagopal, A., Rao, A.U., Amigo, J., Tian, M., Upadhyay, S.K., Hall, C., Uhm, S., Mathew, M.K., Fleming, M.D., Paw, B.H.*, et al.* (2008). Haem homeostasis is regulated by the conserved and concerted functions of HRG-1 proteins. Nature *453*, 1127-1131.
Ramey, G., Deschemin, J.C., Durel, B., Canonne-Hergaux, F., Nicolas, G., and Vaulont, S. (2010). Hepcidin targets ferroportin for degradation in hepatocytes. Haematologica *95*, 501-504.
Ramos, P., Guy, E., Chen, N., Proenca, C.C., Gardenghi, S., Casu, C., Follenzi, A., Van Rooijen, N., Grady, R.W., de Sousa, M.*, et al.* (2011). Enhanced erythropoiesis in Hfe-KO mice indicates a role for Hfe in the modulation of erythroid iron homeostasis. Blood *117*, 1379-1389.
Rappaport, A.M. (1977). Microcirculatory units in the mammalian liver. Their arterial and portal components. Bibliotheca anatomica, 116-120.
Rector, R.S., Thyfault, J.P., Uptergrove, G.M., Morris, E.M., Naples, S.P., Borengasser, S.J., Mikus, C.R., Laye, M.J., Laughlin, M.H., Booth, F.W.*, et al.* (2010). Mitochondrial dysfunction precedes insulin resistance and hepatic steatosis and contributes to the natural history of non-alcoholic fatty liver disease in an obese rodent model. Journal of hepatology *52*, 727-736.
Rhee, S.G., Chae, H.Z., and Kim, K. (2005). Peroxiredoxins: a historical overview and speculative preview of novel mechanisms and emerging concepts in cell signaling. Free radical biology & medicine *38*, 1543-1552.
Richardson, D.R., Huang, M.L., Whitnall, M., Becker, E.M., Ponka, P., and Suryo Rahmanto, Y. (2010). The ins and outs of mitochondrial iron-loading: the metabolic defect in Friedreich's ataxia. Journal of molecular medicine (Berlin, Germany) *88*, 323-329.
Robb, A.D., Ericsson, M., and Wessling-Resnick, M. (2004). Transferrin receptor 2 mediates a biphasic pattern of transferrin uptake associated with ligand delivery to multivesicular bodies. American journal of physiology Cell physiology *287*, C1769-1775.
Roetto, A., Papanikolaou, G., Politou, M., Alberti, F., Girelli, D., Christakis, J., Loukopoulos, D., and Camaschella, C. (2003). Mutant antimicrobial peptide hepcidin is associated with severe juvenile hemochromatosis. Nature genetics *33*, 21-22.
Roy, C.N. (2010). Anemia of inflammation. Hematology / the Education Program of the American Society of Hematology American Society of Hematology Education Program *2010*, 276-280.
Rozen, S., and Skaletsky, H. (2000). Primer3 on the WWW for general users and for biologist programmers. Methods in molecular biology (Clifton, NJ) *132*, 365-386.
Sadahira, Y., and Mori, M. (1999). Role of the macrophage in erythropoiesis. Pathology international *49*, 841-848.
Samuel, V.T., Beddow, S.A., Iwasaki, T., Zhang, X.-M., Chu, X., Still, C.D., Gerhard, G.S., and Shulman, G.I. (2009). Fasting hyperglycemia is not associated with increased expression of

PEPCK or G6Pc in patients with Type 2 Diabetes. Proceedings of the National Academy of Sciences *106*, 12121-12126.
Sharp, P.A. (2010). Intestinal iron absorption: regulation by dietary & systemic factors. International journal for vitamin and nutrition research Internationale Zeitschrift fur Vitamin- und Ernahrungsforschung Journal international de vitaminologie et de nutrition *80*, 231-242.
Shaw, G.C., Cope, J.J., Li, L., Corson, K., Hersey, C., Ackermann, G.E., Gwynn, B., Lambert, A.J., Wingert, R.A., Traver, D*., et al.* (2006). Mitoferrin is essential for erythroid iron assimilation. Nature *440*, 96-100.
Shayeghi, M., Latunde-Dada, G.O., Oakhill, J.S., Laftah, A.H., Takeuchi, K., Halliday, N., Khan, Y., Warley, A., McCann, F.E., Hider, R.C*., et al.* (2005). Identification of an intestinal heme transporter. Cell *122*, 789-801.
Shi, H., Bencze, K.Z., Stemmler, T.L., and Philpott, C.C. (2008). A cytosolic iron chaperone that delivers iron to ferritin. Science (New York, NY) *320*, 1207-1210.
Shih, P.H., and Yen, G.C. (2007). Differential expressions of antioxidant status in aging rats: the role of transcriptional factor Nrf2 and MAPK signaling pathway. Biogerontology *8*, 71-80.
Shimoyama, Y., Mitsuda, Y., Hamajima, N., and Niwa, T. (2014). Polymorphisms of Nrf2, an antioxidative gene, are associated with blood pressure in Japanese. Nagoya journal of medical science *76*, 113-120.
Silva-Gomes, S., Santos, A.G., Caldas, C., Silva, C.M., Neves, J.V., Lopes, J., Carneiro, F., Rodrigues, P.N., and Duarte, T.L. (2014). Transcription factor NRF2 protects mice against dietary iron-induced liver injury by preventing hepatocytic cell death. Journal of hepatology *60*, 354-361.
Silva, B., and Faustino, P. (2015). An overview of molecular basis of iron metabolism regulation and the associated pathologies. Biochimica et biophysica acta *1852*, 1347-1359.
Stadtman, E.R. (1993). Oxidation of free amino acids and amino acid residues in proteins by radiolysis and by metal-catalyzed reactions. Annual review of biochemistry *62*, 797-821.
Suh, J.H., Shenvi, S.V., Dixon, B.M., Liu, H., Jaiswal, A.K., Liu, R.M., and Hagen, T.M. (2004). Decline in transcriptional activity of Nrf2 causes age-related loss of glutathione synthesis, which is reversible with lipoic acid. Proceedings of the National Academy of Sciences of the United States of America *101*, 3381-3386.
Suzuki, T., Motohashi, H., and Yamamoto, M. (2013). Toward clinical application of the Keap1-Nrf2 pathway. Trends in pharmacological sciences *34*, 340-346.
Tamarit, J., Cabiscol, E., and Ros, J. (1998). Identification of the major oxidatively damaged proteins inEscherichia coli cells exposed to oxidative stress. Journal of Biological Chemistry *273*, 3027-3032.
Tan, T.C., Crawford, D.H., Jaskowski, L.A., Murphy, T.M., Heritage, M.L., Subramaniam, V.N., Clouston, A.D., Anderson, G.J., and Fletcher, L.M. (2011). Altered lipid metabolism in Hfe-knockout mice promotes severe NAFLD and early fibrosis. American journal of physiology Gastrointestinal and liver physiology *301*, G865-876.
Tolosano, E., Fagoonee, S., Morello, N., Vinchi, F., and Fiorito, V. (2010). Heme scavenging and the other facets of hemopexin. Antioxidants & redox signaling *12*, 305-320.
Tong, K.I., Kobayashi, A., Katsuoka, F., and Yamamoto, M. (2006). Two-site substrate recognition model for the Keap1-Nrf2 system: a hinge and latch mechanism. Biological chemistry *387*, 1311-1320.
Torrence, J.D., and Bothwell, T.H. (1980). Tissue iron stores. In Methods of Haematology, C. JD, ed. (New York: Churchill Livingstone), pp. 104-109.
Van Gorp, H., Delputte, P.L., and Nauwynck, H.J. (2010). Scavenger receptor CD163, a Jack-of-all-trades and potential target for cell-directed therapy. Molecular immunology *47*, 1650-1660.
Velasco-Rodriguez, D., Alonso-Dominguez, J.M., Gonzalez-Fernandez, F.A., Villarrubia, J., Sopena, M., Abalo, L., Ropero, P., Martinez-Nieto, J., de la Fuente Gonzalo, F., and Cava, F.

(2015). Reticulocyte parameters of delta beta thalassaemia trait, beta thalassaemia trait and iron deficiency anaemia. Journal of clinical pathology.
von Otter, M., Bergstrom, P., Quattrone, A., De Marco, E.V., Annesi, G., Soderkvist, P., Wettinger, S.B., Drozdzik, M., Bialecka, M., Nissbrandt, H.*, et al.* (2014). Genetic associations of Nrf2-encoding NFE2L2 variants with Parkinson's disease - a multicenter study. BMC medical genetics *15*, 131.
Vulpe, C.D., Kuo, Y.M., Murphy, T.L., Cowley, L., Askwith, C., Libina, N., Gitschier, J., and Anderson, G.J. (1999). Hephaestin, a ceruloplasmin homologue implicated in intestinal iron transport, is defective in the sla mouse. Nature genetics *21*, 195-199.
Wan, J., Benkdane, M., Teixeira-Clerc, F., Bonnafous, S., Louvet, A., Lafdil, F., Pecker, F., Tran, A., Gual, P., Mallat, A.*, et al.* (2014). M2 Kupffer cells promote M1 Kupffer cell apoptosis: a protective mechanism against alcoholic and nonalcoholic fatty liver disease. Hepatology (Baltimore, Md) *59*, 130-142.
Weiss, G. (2009). Iron metabolism in the anemia of chronic disease. Biochimica et biophysica acta *1790*, 682-693.
Weiss, G., and Goodnough, L.T. (2005). Anemia of chronic disease. New England Journal of Medicine *352*, 1011-1023.
Wessling-Resnick, M. (2010). Iron homeostasis and the inflammatory response. Annual review of nutrition *30*, 105-122.
Wood, M.J., Powell, L.W., Dixon, J.L., and Ramm, G.A. (2012). Clinical cofactors and hepatic fibrosis in hereditary hemochromatosis: the role of diabetes mellitus. Hepatology (Baltimore, Md) *56*, 904-911.
Wrighting, D.M., and Andrews, N.C. (2006). Interleukin-6 induces hepcidin expression through STAT3. Blood *108*, 3204-3209.
Wyllie, J.C., and Kaufman, N. (1982). An electron microscopic study of heme uptake by rat duodenum. Laboratory investigation; a journal of technical methods and pathology *47*, 471-476.
Yachie, A., Niida, Y., Wada, T., Igarashi, N., Kaneda, H., Toma, T., Ohta, K., Kasahara, Y., and Koizumi, S. (1999). Oxidative stress causes enhanced endothelial cell injury in human heme oxygenase-1 deficiency. Journal of Clinical Investigation *103*, 129.
Yoon, J.C., Puigserver, P., Chen, G., Donovan, J., Wu, Z., Rhee, J., Adelmant, G., Stafford, J., Kahn, C.R., and Granner, D.K. (2001). Control of hepatic gluconeogenesis through the transcriptional coactivator PGC-1. Nature *413*, 131-138.
Young, S., and Bomford, A. (1984). Transferrin and cellular iron exchange. Clinical science (London, England : 1979) *67*, 273-278.
Yun, S., and Vincelette, N.D. (2015). Update on iron metabolism and molecular perspective of common genetic and acquired disorder, hemochromatosis. Critical reviews in oncology/hematology *95*, 12-25.
Zhong, L., Arner, E.S., and Holmgren, A. (2000). Structure and mechanism of mammalian thioredoxin reductase: the active site is a redox-active selenolthiol/selenenylsulfide formed from the conserved cysteine-selenocysteine sequence. Proceedings of the National Academy of Sciences of the United States of America *97*, 5854-5859.
Zitka, O., Skalickova, S., Gumulec, J., Masarik, M., Adam, V., Hubalek, J., Trnkova, L., Kruseova, J., Eckschlager, T., and Kizek, R. (2012). Redox status expressed as GSH:GSSG ratio as a marker for oxidative stress in paediatric tumour patients. Oncology letters *4*, 1247-1253.